

ABSTRACT

Title of Dissertation: EXAMINATION OF THE
PHOTOCHEMISTRY AND MESOSCALE
METEOROLOGY ASSOCIATED WITH
POOR AIR QUALITY IN THE U.S.

Gina Marie Mazzuca, Doctor of Philosophy,
2018

Dissertation directed by: Professor Russell Dickerson, Department of
Atmospheric and Oceanic Science
Research Professor Kenneth Pickering,
Department of Atmospheric and Oceanic
Science

Mesoscale meteorological processes including advection, vertical mixing, thermally-direct circulations (sea/bay breezes) combined with chemical processes and deposition dominate boundary-layer ozone (O_3). While bay breezes (BBs) transport higher O_3 over land on polluted days, they also advect humid air and induce low-level convergence, which can lead to haze and deep convection. Thunderstorms can vent pollution out of the boundary layer and entrain cleaner, mid-tropospheric air into it, reducing surface pollutant concentrations. Here, the net local effect of these two mesoscale forcings (BBs and thunderstorms) on O_3 concentrations are quantified. First, case studies using vertical profiles and surface observations during the 2011 MD and the 2013 TX deployments of DISCOVER-AQ show the severity of bay/gulf

breeze exacerbation of pollution. Next is a BB and thunderstorm climatology for a Chesapeake Bay coastal site (summer 2011-2016). BBs are identified by a data-driven automated detection algorithm customized for the complex coastline. Thunderstorm vs. non-thunderstorm days are analyzed using gridded lightning data within an influential radius of the site. These meteorological classifications are compared with O₃ exceedance days. While the highest conditional mean O₃ was on BB days and the lowest on thunderstorm only days, thunderstorms do not always terminate an O₃ event, especially in combination with a BB. To further understand the dynamical mechanisms responsible for changes in O₃ from BBs and thunderstorms, the Weather Research and Forecasting (WRF) model is run at fine resolution with water vapor nudging to capture air-mass thunderstorms forced by the BB in MD. The model compared well with DISCOVER-AQ observations and radar reflectivity. Finally, an observation-constrained box model was used to study photochemical processes along the flight track during the 2013 TX DISCOVER-AQ deployment. O₃ production and its sensitivity to NO_x and VOCs were calculated at different locations and times of day. Results indicate controlling NO_x emissions will benefit the Houston area overall, but select areas will also benefit from controlling VOC emissions. These studies, which can also be applied to particulate matter, uncover how meteorology and photochemistry come together to generate smog events at coastal cities, and can help develop efficient, high resolution policies for cleaner air.

EXAMINATION OF THE PHOTOCHEMISTRY AND MESOSCALE
METEOROLOGY ASSOCIATED WITH POOR AIR QUALITY IN THE U.S.

by

Gina Marie Mazzuca

Dissertation submitted to the Faculty of the Graduate School of the
University of Maryland, College Park, in partial fulfillment
of the requirements for the degree of
Doctor of Philosophy
2018

Advisory Committee:

Professor Russell Dickerson, Chair/Advisor

Research Professor Kenneth Pickering, Co-Chair/Co-Advisor

Professor Ross Salawitch

Associate Research Professor Timothy Canty

Research Scientist Xinrong Ren

Dean Steve Fetter, Dean's Representative

© Copyright by
Gina Marie Mazzuca
2018

Dedication

My thesis is dedicated to my parents, Georgia and Michael Mazzuca, and my brother, Marcus Mazzuca for their support, encouragement, and realization of my potential throughout my life, and especially, throughout my academic endeavors.

My mom encouraged and stimulated my brain at such a young age by taking me to historical landmarks, touring, providing support for my many music lessons (violin, piano, clarinet), and supporting my book collection (many weather books). As a little girl, she would always answer my constant, annoying question of, “What’s that?” and encourage that curiosity throughout my life. She taught me organization (while I will never be as organized as she is), priorities, and how to be charming. She also taught by example to always be sweet to strangers and realize that people might not be as lucky as others. I owe my values, my character, and my genuine interest in helping humanity through science to my mother.

My dad is known for taking care of everyone he knows - especially his children. His life lessons and wisdom have been instrumental to my success. He always helps me to realize that being fortunate in life with health, family, friends, and an education is a privilege, and that I should always give back to the community as best I can. Building his own business from the ground up, I admire his determination in achieving his goals and setting the stage for mine. He taught me that relationships with people are vital to life and how to diffuse a situation. I owe my determination and diplomacy to my father.

My scientific curiosity was fueled the most by my brother, Marcus. Being the brilliant math and science wiz that he was (is), I too wanted to learn how the world worked. His books on science, space, and technology that he grew out of were now mine to peruse. When he moved on to different toys, I would play for hours with his building blocks and mini cars. When he got a new gaming system, I was playing Nintendo and Sega Genesis. While I also played with Barbie™, I found myself splitting time between “girly toys” and trying to build a tree house, roller blading in the basement, or playing video games, like he did. I owe my curiosity, critical thinking, and scientific inspiration to my brother, Marcus.

I always had unique interests – both traditional and non-traditional for a young female. My family always supported me to have the unique interests I had and to ultimately, just be me. This drove my confidence and self-awareness that led me to become a woman in science, and to know that I am an equal among my male scientist counterparts.

My thesis is also dedicated to David New for all of his support throughout my time in graduate school. Never before had I met a person so brilliant, humble, and genuine to himself and others. He truly inspires me every day, and I am very lucky to have him in my life.

Lastly, this work is also dedicated to my kitty, my dear Loki Long-cat. Not only serving as instant blood pressure medication, he has given me support in ways he will never know.

Acknowledgements

I would first like to thank my advisors, Drs. Ken Pickering and Russ Dickerson, for their support, encouragement, and dedication to my graduate studies. They had always been supportive of my educational curiosity and showed me the path to gain the knowledge and skills I desired. I am very lucky to have been able to work with such brilliant, caring, and resourceful advisors.

I am also forever indebted to the atmospheric chemistry group in AOSC, especially Drs. Ross Salawitch and Tim Canty, for serving on my committee, and more generally, for their support, teachings, and help throughout my graduate career. I would also like to thank the rest of my Ph.D. committee, Dr. Xinrong Ren for choosing me to work on a research grant with him, and Dr. Steve Fetter for serving as my Dean's Representative. A thank you is extended to Dr. Daryl T. Kleist, who served on my prospectus committee, for his help, support, and friendship.

They say that everyone should find a mentor – whether it be for personal or career goals. I am beyond lucky to have so many amazing mentors in my life, especially the following amazing men: Rich Clark, Bill Murtagh, and Bruce Doddridge.

I met Rich when I was a freshman in college at 17 years old. At 19, he took a chance on me and invited me to participate in the NASA DISCOVER-AQ project. Working on projects, teaching me the necessities of meteorology, and showing me how to build a shed out of 2x4s and particle board, he had a monumental role in shaping my career and my life.

Bill and I met when I went to a space weather workshop as a junior at Millersville. I later had the privilege to work with him as an intern in the White House Office of Science and Technology Policy (OSTP) during the Obama Administration. He truly does attract the best people to him with his wonderful personality and work ethic.

I was introduced to Bruce during the DISCOVER-AQ mission when I was a sophomore at Millersville. Bruce not only helped to shape my career, introduce me to great people, and get me a flight on the P-3B, he was also the supportive voice I needed before each of my most nerve-racking presentations and gave me so many valuable lessons about life, beyond just academia.

I would also like to thank DISCOVER-AQ, the Texas Air Quality Research Program (AQRP), and the Maryland Department of the Environment (MDE) for the funds to carry out the research in this dissertation, as well as the National Center for Atmospheric Research (NCAR) for supporting my computational needs with access to their super computer. Thanks also to Dr. Jim Crawford and Dr. Ryan Stauffer, the incredible staff and interns I had the privilege to work with while at OSTP, Dr. Bill Hooke and the AMS policy group, and the countless professionals who took time out of their day to grab coffee and chat with me about life and career decisions. Whether many of you knew it or not, you had helped me in ways I can never repay you for, so I will make it my goal to pay it forward. Lastly, I would like to thank my friends from UMD, Millersville, and Pottsville, as you have been such an important source of support for so many years. I love you all!

Table of Contents

Dedication.....	ii
Acknowledgements.....	iii
Table of Contents.....	iv
List of Tables.....	vii
List of Figures.....	ix
List of Abbreviations and Acronyms.....	xviii
Chapter 1: Introduction.....	1
1.1 Boundary-layer O ₃ Formation, Sensitivity, and Emissions Controls.....	2
1.1.1 Tropospheric O ₃ Production.....	2
1.1.2 O ₃ Production Sensitivity.....	4
1.1.3 Emissions Control.....	6
1.2 The Role of Meteorology in Modulating Surface Pollution.....	7
1.2.1 Thermally-direct Mesoscale Circulations due to the Land-water Interface (Bay Breezes and Thunderstorms) and Surface Pollution.....	8
1.2.2 Thermally-direct Mesoscale Circulations due to Topography (Mountain Breezes and Thunderstorms) and Surface Pollution.....	10
1.3 Overview of NASA’s DISCOVER-AQ Field Project (2011-2014).....	11
1.4 Objectives of this Research.....	16
Chapter 2: Extreme Events: Bay and Gulf Breeze Case Studies in Maryland and Texas (published as Mazzuca et al., 2017).....	21
2.1 Introduction.....	21
2.2 Measurements.....	23
2.2.1 P-3B Aircraft.....	24
2.2.2 Edgewood, MD Ground Site.....	25
2.2.3 Smith Point, TX Ground Site.....	27
2.3 Bay Breeze Case Study: Edgewood, MD 29 July 2011.....	29
2.4 Gulf and Bay Breeze Case Study: Smith Point, TX 25 September 2013.....	39
2.4.1 Synoptic Conditions, Local Winds, and Air Quality Observation Overview	40
2.4.2 Transport to Smith Point from Major Sources.....	42
2.4.3 Recirculation from Bay and Gulf Breezes.....	51
2.5 Discussion and Conclusions.....	55
2.5.1 Discussion.....	55
2.5.2 Conclusions.....	59
Chapter 3: Overall Impacts of Bay Breeze and Thunderstorm Circulations on Surface O ₃ at a Site along the Chesapeake Bay from 2011-2016 (Mazzuca et al., 2018 – in review).....	61
3.1 Introduction.....	61
3.2 Data and Methodology.....	63
3.2.1 Observations and Characterization of the Analysis Site – Edgewood, MD	63
3.2.2 The Bay-breeze Identification Algorithm (BIA).....	70

3.2.3 Thunderstorm Detection Criteria	73
3.3 Results	74
3.3.1 Bay Breeze Detection	74
3.3.2 The Role of Bay Breezes and Thunderstorms on Surface O ₃ Concentrations	80
3.3.3 The Relationship between Days with Extreme O ₃ (O ₃ Exceedances / High O ₃ Events) and Days with a Mesoscale Circulation (Bay Breezes, Thunderstorms, or Both).....	89
3.4 Discussion	94
3.5 Conclusions	97
Chapter 4: Observations and Modeling of Thermally-direct Circulations and Implications for Trace Gases (Maryland and Colorado)	100
4.1 Introduction	100
4.2 Methods	101
4.2.1 Observational Network	101
4.2.2 The Weather Research and Forecasting (WRF) Model Simulation	101
4.3 Results	105
4.3.1 Observations: 22 July 2011 Bay Breeze and Thunderstorm Case Study in Maryland	105
4.3.2 WRF Modeling: 22 July 2011 Combined Bay Breeze and Thunderstorm Case Study in Maryland	112
4.3.3 Observations: 29 July 2014 Mountain Breeze and Thunderstorm Case Study in Colorado	119
4.4 Discussion	124
4.5 Summary and Future Work	126
Chapter 5: Ozone Production and Its Sensitivity to NO _x and VOCs: Results from the DISCOVER-AQ Field Experiment, Houston 2013 (published as Mazzuca et al., 2016)	128
5.1 Introduction	128
5.2 Methods	132
5.2.1 O ₃ Production and Sensitivity	132
5.2.2 Box Model Simulations	133
5.2.3 WRF-CMAQ Model Simulations	135
5.3 Results	138
5.3.1 Photochemical O ₃ Production Rate, Sensitivity, and Diurnal Variations	138
5.3.2 O ₃ Production Efficiency	146
5.4 Discussion and Conclusions	154
Chapter 6: Concluding Remarks and Future Work	157
6.1 – Concluding Remarks	157
6.2 – Future Work	161
Bibliography	164

List of Tables

Table 2.1 provides a summary of measurements used for the Edgewood, MD and Smith Point, TX studies.....22

Table 2.2 Conditions during bay breezes observed on 7/29/2011 at Edgewood, MD.....31

Table 3.1 EPA monitor-level design values calculated as the 3-year average of the annual 4th highest daily maximum 8-hour O₃ concentration (ppbv) at each O₃ monitor in Maryland (source: <https://www.epa.gov/air-trends/air-quality-design-values>). The colored boxes represent the highest design value (red), the second-highest design value (orange), and the third-highest design value (yellow) for each time bin. It should be noted that table does not account for the 2016 exceptional events in its design values.....60-61

Table 3.2 Validation of the Bay-breeze Identification Algorithm (BIA) against bay breezes identified in Stauffer et al., 2015a. In the two columns labeled Stauffer et al. 2015a and BIA-data: **yellow shading**: Stauffer does not match BIA-data, **green shading**: Stauffer bay breeze matches BIA-data. In the column labeled BIA-RTMA: **yellow letter**: BIA-RTMA matches Stauffer analysis, but not BIA-data, **red letter**: BIA-RTMA does not match either of the other two other columns, **green letter**: BIA-RTMA bay breeze matches the BIA-data bay breeze. Plain black letter: techniques match each other on non-bay breeze days.....68

Table 3.3 Validation of BIA-RTMA by comparison with the Stauffer et al. analysis and BIA with 1-minute data (BIA-data) for the month of July, 2011 over the analysis time period (11:00-19:00 EST)72

Table 3.4 Conditional probabilities of an OE or H-O₃ given the occurrence of a bay breeze, thunderstorm, or both for June, July, and August 2011-2016. Top: percentage of days with a 2008 EPA-defined O₃ exceedance event (OE; 8-hr max O₃ higher than 75 ppbv) given the occurrence of thunderstorm only (TS), a bay breeze only (BB), or both (TS&BB); Bottom: Percentage of days with daily mean O₃ exceeding the yearly mean O₃ + 1 stdev (H-O₃) given the occurrence of a thunderstorm only (TS), a bay breeze only (BB), or both (TS&BB)84

Table 3.5 Left: Years with the highest proportion of an O₃ exceedance (8-hr max > 75 ppbv) given the occurrence of a bay breeze, thunderstorm or both; Right: the years with the highest proportion of daily mean O₃ exceeding the yearly mean + 1 stdev given these mesoscale events

.....85

Table 4.1 Model Parametrization Options for WRF run94

Table 5.1 WRF and CMAQ model options that were used in both the original and improved modeling scenarios126

List of Figures

- Figure 1.1:** (Figure from Jacob 1999; Fig 12-4) O₃ concentration (ppbv) simulated by a regional photochemical model as a function of NO_x and VOC emissions where the thick black line delineates the NO_x-sensitive (top left) and the VOC-sensitive (bottom right) regimes.....5
- Figure 2.1** 07/29/2011 Edgewood MARAF site wind direction with height derived from SODAR wind profiler (colors) and labeled surface trace gases: O₃ (dark green), NO_x (blue), SO₂ (pink), and CO (olive green). Note WSW winds starting at 8:30 EDT as the nocturnal PBL broke up and concentrations of primary pollutants CO and NO_x increased. This is followed by inflow of more O₃ rich air from over the Chesapeake Bay in a shallow (~100m; see also Figures 2.2 and 2.3) layer, shifting to generally SSW winds with sustained high O₃ concentrations by 16:30 EDT.....29
- Figure 2.2** 07/29/2011 Edgewood MARAF site wind speed with height derived from SODAR (colors) and 4-meter vertical eddy momentum flux (black line).....30
- Figure 2.3** 07/29/2011 Millersville tethersonde profiles of O₃ concentration, water vapor mixing ratio, potential temperature, and wind speed from the surface to ~340 m. The first sounding (blue) is from the surface to maximum altitude (08:20 – 08:42 EDT) and the second sounding (pink) is down from maximum altitude (08:42 – 09:07 EDT). Profiles indicate higher O₃ concentration and water vapor mixing ratio layer aloft during first sounding and mixing down (weaker vertical gradient) by the second sounding.....31
- Figure 2.4** 07/29/2011 Midday blended profile of the first circuit P-3B spiral over Edgewood (orange) and the corresponding Millersville tethersonde sounding (blue) of O₃ concentration, water vapor mixing ratio, and potential temperature from the surface to ~5000 m; surface O₃ concentration (pink dot; at maximum surface O₃ concentration). The shallow bay breeze passage is observed in the tethersonde profile and the surface, but not by the P-3B due its extremely shallow depth.....33
- Figure 2.5** 07/29/2011 MARAF surface O₃ concentration (black line), 4-m temperature (orange line) and 4-m flux tower specific humidity (blue line). Spikes that positively correlate between O₃ concentration and specific humidity and negatively correlate to temperature observed (13:30, 16:15, 18:00 EDT) indicate two small-scale bay breeze passages and then a larger scale passage from 16:00 to 19:00 EDT.....34

Figure 2.6 07/29/2011 Late afternoon blended profile of the third circuit P-3B spiral over Edgewood (orange) and the corresponding Millersville tethersonde sounding (blue) of O₃ concentration, water vapor mixing ratio, and potential temperature from the surface to ~4000 m; surface O₃ concentration (pink dot). The tethersonde profile was taken ~25 minutes before the P-3B spiral, resulting in somewhat greater disparity between platforms.....35

Figure 2.7 09/25/2013 Smith Point, TX MARAF site wind direction with height derived from SODAR (colors) and NATIVE surface trace gases: O₃ (purple) and NO_y (green). Note: consistent buildup of O₃ under NW winds was followed by a spike as winds shifted to SW around 17:00 EDT, which brought photochemically aged smog to the site.....37

Figure 2.8 09/25/2013 (a) CH₂O, (b) CO, and (c) NO_y concentrations measured on the P-3B flight track during the first circuit. Black square is location of Deer Park and white square is location of Facilities at Baytown.....40

Figure 2.9 09/25/2013 (a) CH₂O, (b) CO, and (c) NO_y concentrations measured on the P-3B flight track during the second circuit42

Figure 2.10 09/25/2013 Blended profile of the second circuit P-3B spiral over Smith Point (orange) and the corresponding Millersville tethersonde sounding (blue) of O₃ concentration, NO_y concentration (NO_x with interferences from other reactive nitrogen species on tethersonde), water vapor mixing ratio, and potential temperature from the surface to ~4000 m. The P-3B measured a NO_y plume at ~100 m that the tethersonde did not due to temporal and spatial differences between the soundings.....43

Figure 2.11 09/25/2013 Tethersonde soundings of O₃ concentration, potential temperature, and water vapor mixing ratio at Smith Point from 12:56 – 13:49 CDT from the surface to 500 m.....44

Figure 2.12 Six-hour WRF back trajectories at six initialization altitudes (2 m, 100 m, 200 m, 300 m, 400 m, 500 m) from the location of the tethersonde at Smith Point. (a) Initialized at 12:56 CDT (b) Initialized at 13:14 CDT46

Figure 2.13 09/25/2013 Tethersonde soundings of O₃ concentration, water vapor mixing ratio, and potential temperature at Smith Point from (a) 14:31 – 15:42 CDT, (b) 16:00 – 17:11 CDT, (c) 17:31- 18:42 CDT from the surface to 500 m49

Figure 2.14 09/25/2013 Houston/Galveston, TX (KHGX) radar reflectivity in dBZ of the bay and Gulf breezes at 22:30 UTC (17:30 CDT) passing over Smith Point.....50

Figure 2.15 09/25/2013 surface WeatherPak observations of temperature, water vapor mixing ratio, wind speed, and wind direction from MARAF platform at Smith Point..51

Figure 3.1 Location of the Edgewood, MD O₃ monitor and meteorological site (white circle) and its relative distance from the Chesapeake Bay, rivers, and a major urban area (Baltimore, MD).....60

Figure 3.2 10-m wind climatology at Edgewood, MD from 2011-2016. Top: Vectoral wind direction with notable SSW-SW wind direction during peak heating times (09:00 – 17:00 EST) during June, July, and August. Bottom: Wind steadiness with peak steadiness in July – August from ~13:00 – 17:00 EST, likely associated with bay breezes and other mesoscale circulations.....63

Figure 3.3 O₃ concentration (ppbv) vs. temperature (°C) in 3°C bins from 15 – 37°C with the colored lines representing the 5th, 25th, 50th, 75th, and 95th percentiles of the 1-hr averaged O₃ concentration (gray dots) between 07:00 – 19:00 EST at Edgewood, MD. A higher slope is observed on the left pane (2011-2016) than the right (2013-2016) demonstrating the higher O₃ concentrations and temperatures observed in 2011 and 2012 compared to the other years of the analysis and the efficacy of abatement measures.....64

Figure 3.4 WRF WPS land-mask variable at 300 x 300 m resolution grid spacing where black is the land, white is the water (Chesapeake Bay and its associated estuaries), and the pink circle is the user specified search radius for land and water flags centered around Edgewood, MD.....66

Figure 3.5 Meteorological and O₃ 1-minute observations at the MDE site at Edgewood, MD on 29 July 2011. Top panel: dots: raw wind data, thin black line: the faster varying wind signal, red line: the slower varying wind signal, thick black line: times when BIA detects a bay breeze. 2nd panel (orange): temperature (°C), 3rd panel (blue): water vapor mixing ratio (g/kg), 4th panel (black): O₃ concentration (ppbv), bottom panel (red): wind speed (m/s).....71

Figure 3.6 Bay breeze day on 29 July 2011 at Edgewood, MD Left: BIA-data (bay breeze identification using 1-minute data) where the black dots are the raw minute data, the red line is the diurnal + synoptic signal, and the blue dots are where BIA-data detect a bay breeze. Right: BIA-RTMA where the black line is the 1-hrly model

output, the red line is the diurnal + synoptic signal, and the blue dots are where BIA-RTMA detects a bay breeze.....74

Figure 3.7 Pie chart of the percent of days and number of days that exhibit the four different meteorological categories (yellow: neither bay breeze nor thunderstorm, blue: bay breeze only, tan: thunderstorm only, gray: both a bay breeze and a thunderstorm) during the analysis time period. In red: the average of the daily mean O₃ concentrations for each meteorological category, and in blue: the average of the daily 1-hr avg. max O₃ concentrations for each meteorological category in ppbv.....75

Figure 3.8 Bar chart of the average of daily mean O₃ concentrations for bay breeze days (light blue), days without a bay breeze (brown), and the difference in O₃ concentration between bay breeze and no bay breeze (gray) during the analysis time period for each year and all years. Top: average of the daily mean O₃ concentration (11-19 EST) for each year (June, July, August) for bay breeze days, no bay breeze days, and the difference. Bottom: Average of the daily 1-hr average max O₃ concentrations for bay breeze days, no bay breeze days, and the difference.....77

Figure 3.9 Bar chart of the average daily mean O₃ concentrations for thunderstorm days (yellow), days without a thunderstorm (brown), and the difference in O₃ concentration between thunderstorm days and no thunderstorm days (gray) during the analysis time period for each year and all years. Top: average of the daily mean O₃ concentration (11-19 EST) for each year (June, July, August) for thunderstorm days, no thunderstorm days, and the difference. Bottom: Average of the daily 1-hr average max O₃ concentrations for thunderstorm days, no thunderstorm days, and the difference. The numbers on the gray bars (difference) are colored by red (positive difference between TS-noTS) and blue (negative difference between TS-noTS).....79

Figure 3.10 Bar chart of the average daily mean O₃ concentrations for thunderstorm days (dark gray, yellow, light gray) and no thunderstorm days (pink), where the thunderstorm days are separated by when the thunderstorm had occurred (early: 11-14 EST; late: 14-19 EST; both: storms either spanned through both time periods or there was more than one storm that occurred in both time periods). Overall, the difference in O₃ concentration on thunderstorm days with either a thunderstorm in early afternoon or a thunderstorm in late afternoon is not significantly different from days with no thunderstorm.....80

Figure 3.11 Bar chart of O₃ concentration on days with frontal thunderstorms in comparison to days with non-frontal, or, thunderstorms not associated with forcing by a synoptic-scale front (e.g., pop-up thunderstorm by bay breeze convergence) during the analysis time period (11:00 – 19:00 EST, June-August, 2011-2016) at Edgewood,

MD. Light blue: # of days for each meteorological category (BB: bay breeze days, NoBB: no bay breeze days); Dark blue: Daily mean O₃ concentration (ppbv) for the days that exhibit each meteorological category. Days with frontal thunderstorms were more than double the number of days with non-frontal thunderstorms during this analysis time period. Non-frontal thunderstorms were generally associated with higher daily average O₃ concentrations.....82

Figure 3.12 Pie charts of the % of days with an O₃ exceedance (OE; left) and % of days with a H-O₃ event (H-O₃; right) that had also exhibited at bay breeze (BB; light blue), thunderstorm (TS; yellow), both (BB & TS; hatched yellow and blue), and neither (neither BB or TS; gray) for June, July, and August 2011-2016 between 11-19 EST at Edgewood, MD.....84

Figure 3.13 Distribution of daily mean O₃ concentration (ppbv) at Edgewood, MD from 2011-2016 during the analysis time period (11:00 – 19:00 EST) for all days (top row), days without a bay breeze or thunderstorm (2nd row), days with a thunderstorm only (3rd row), days with both a bay breeze and a thunderstorm (4th row), and days with a bay breeze only (last row). From the 3rd row down (days with a mesoscale circulation), the y-axis (frequency) is scaled to clarify the relative contribution of each mesoscale event on the less-frequent tail-end of the O₃ distributions.....87

Figure 4.1 WRF model domain set up: 1km grid spacing for d01 (outer domain; black square) and 333m grid spacing for d02 (inner domain; white square).....95

Figure 4.2 07/22/2011 Edgewood, MD site. Top: 2-m specific humidity (g/kg). Bottom: wind direction with height derived from SODAR wind profiler (colors) and labeled surface trace gases: ozone (dark green), NO_x (blue), SO₂ (pink), and CO (olive green). Steep decrease in trace gas concentrations after local noon as a result of pop-up thunderstorms.....99

Figure 4.3 Radar reflectivity (dBz) at 17:01 UTC (13:01 EDT) of the storms of interest. White line: line of the vertical cross-section slice as shown in the lower panel. The vertical cross-section shows the altitude of the storms reaching around 50 kft (15.2 km) during the time of this cross-section, likely near or overshooting the tropopause. The storm reached a maximum altitude of ~60 kft (18.3 km) during its peak.....100

Figure 4.4 P-3B profiles (orange), tethered balloon profiles (blue), and surface O₃ (pink square) for the second spiral of the day (first spiral after the storm; top) and the third spiral of the day (bottom). First panel: O₃ concentration (ppb)with height in AGL; Second panel: water vapor mixing ratio (g/kg) with height, and potential temperature (K) with height.....101

Figure 4.5 HYSPLIT back trajectory initialized by the North American Mesoscale (NAM) model at 18Z (14:00 EDT) at Edgewood, MD. Blue line: trajectory at 200m; red line: trajectory at 100m. Dots on the trajectories represent the location at the given time (10:00 EDT). These trajectories indicate that the air transported to Edgewood, MD after the thunderstorms had passed through the Baltimore metropolitan area at the end of rush hour and is likely the source of the high O₃ and precursor concentrations observed at the Edgewood site in the afternoon after a temporary reduction in concentrations.....102

Figure 4.6 Left: Surface O₃ concentration (ppbv) at Aldino, Edgewood, Essex, and Fairhill, MD. Right: Site locations and composite radar reflectivity (dBZ) from Sterling, VA (KLWX) demonstrating the relative thunderstorm extent and sites directly affected (Edgewood and Essex) for three different stages of the thunderstorms. The shaded box on the left indicates the time during the time series of O₃ concentration that corresponds to the radar reflectivity on the right. Note that the eastern cell dies out first.103

Figure 4.7 Locations of the Millersville University site (MU; blue), the Maryland Department of the Environment site (MDE; green), and the middle grid point from the WRF simulation between the two sites (WRF; red). Line: cross-section used in Figure 4.10.....105

Figure 4.8 Surface water vapor mixing ratio (g/kg) observations at the MU site (blue) and the MDE site (green), and 2m WRF output (red). The observations are hourly averaged. The MU and MDE sites were ~2.7 km away from each other with the MU site closer to the bay with more influence from the bay breeze and the thermal internal boundary layer.....106

Figure 4.9 2-m WRF water vapor mixing ratio (g/kg) and the observations at MDE monitors in the domain (colored circles). MDE observations are the 15 minute average from 14:45 – 15:00 UTC.....107

Figure 4.10 Vertical cross-section of WRF water vapor mixing ratio with height across the slice denoted in Figure 4.6 at the times that matched the observations best within a 30 minute window. The timing for the P-3B spiral was between 15:30-15:49 UTC (11:30 – 11:49 EDT) and the tethersonde profile was taken between 15:30 – 16:04 UTC (11:30 – 12:04 EDT) for the first combined profile (top panel) and the P-3B spiral was between 17:35 – 17:54 UTC (13:35 – 13:54 EDT) and the tethersonde profile was taken between 18:20 – 18:40 UTC (14:20 – 14:40 EDT) for the second

combined profile (bottom panel). Dashed lines are modeled potential temperature (K).....108

Figure 4.11 Left: Observed composite radar reflectivity from NEXRAD KLWX (Sterling, VA) in dBZ and right: modeled composite radar reflectivity from the WRF simulation using the LDA technique during the dissipation stage of cell near Edgewood and the peak intensity of the cell over Essex.....109

Figure 4.12 Vertical cross-section of radar reflectivity (left) in dBZ and water vapor mixing ratio (right) in g/kg from the slice denoted by the black line in Figure 4.11 (right). This is around the time of maximum reflectivity for the western-most cell while the eastern-most cell is in its dissipation stage. In the water vapor cross-section, there is notable water vapor present in upper-altitudes and above the boundary layer demonstrating vertical transport, however, it is also notable that the boundary layer is not effected by the drier mid-tropospheric downdraft air.....110

Figure 4.13 Terrain map of the area referred to as the Front Range of Colorado, as well as Golden, CO, one of the surface and spiral sites during the DISCOVER-AQ deployment in July-August 2014 and the site chosen for the case study described in this section.....111

Figure 4.14 Normalized probability distribution of Convective Available Potential Energy (CAPE) in J/kg for July and August, 2014 at Golden, CO at 18Z (12 MDT).112

Figure 4.15 Hourly averaged O₃ concentration vs. time (UTC; where MDT is UTC-6) during the DISCOVER-AQ CO deployment (07/17/14 – 08/10/2014). Top: O₃ vs. time of day for July and Bottom: O₃ vs. time for August. Blue lines are days that did not exhibit a thunderstorm and thunderstorm and black lines are days that had a thunderstorm from the examination radar reflectivity.....113

Figure 4.16 Top: Hourly averaged O₃ concentration on 29 Jul 2014 in UTC (where MDT is UTC-6). Bottom: 1-minute avg. wind direction (0-360°), color coated by the direction from which the winds are blowing (yellow: NE, blue: SE, green: SW, red: NW) from bottom to top.....114

Figure 4.17 Radar reflectivity at 1.3° tilt from the Denver International Airport (KFTG) on JUL 29 2014 at 14:15 MDT (20:15 UTC). The white dot is the location of the site (Golden, CO) and the circled storm is the one that directly influenced the site. Outflow was also observed at the site from the larger system to the east.....115

Figure 5.1 O₃ production empirical kinetic modeling approach (EKMA) diagram using a box model results with NO_x levels varying from 0-20 ppbv and VOC levels from 0-200 ppbv while the mean concentrations of other species and the speciation of NO_x and VOCs observed during DISCOVER-AQ in Houston in 2013 were used to constrain the box model. This diagram clearly shows the sensitivity of O₃ production to NO_x and VOCs in Houston.....120

Figure 5.2 DISCOVER-AQ ground and spiral sites (yellow dots) during the September 2013 Houston campaign.....122

Figure 5.3 36, 12, and 4 km CMAQ modeling domains (top); 4 and 1 km CMAQ modeling domains. The red dots show the NASA P-3B aircraft spiral locations (bottom).....126

Figure 5.4 Net O₃ production rate (net P(O₃)) calculated from the box model results along the P-3B flight track during DISCOVER-AQ in Houston in 2013. The size of dots is proportional to P(O₃).....130

Figure 5.5 O₃ production sensitivity indicator, L_N/Q, along the P-3B flight track during DISCOVER-AQ in Houston in 2013. P(O₃) is VOC-sensitive when L_N/Q > 0.5, and NO_x-sensitive when L_N/Q < 0.5.....131

Figure 5.6 Vertical profiles of O₃ production rate (left), O₃ loss rate (middle), and net O₃ production rate (right) during DISCOVER-AQ in Houston in 2013.....132

Figure 5.7 Diurnal variation of O₃ production rate colored with the indicator L_N/Q on ten flight days during DISCOVER-AQ in Houston in 2013. The solid red circles represent the median values in hourly bins of P(O₃). Data are limited with the pressure altitude less than 1000 m to represent the boundary layer.....132

Figure 5.8 Diurnal variations of the indicator L_N/Q of O₃ production rate sensitivity colored with O₃ production rate and median hourly bins of L_N/Q shown in solid red circles (left) and median hourly NO and NO₂ concentrations (pptv) (right) below 1000 m during DISCOVER-AQ in Houston in 2013.....133

Figure 5.9 Diurnal variations of O₃ production rate at eight individual spiral locations. Individual points are 1-min data colored with L_N/Q and the linked red circles represent the median values in hourly bins of P(O₃). Data are limited with the pressure altitude less than 1000 m to represent the boundary layer.....134

Figure 5.10 O₃ production as a function of NO mixing ratio. Individual data points are the 1-minute averages and are colored with the production rate of HO_x (= OH + HO₂) during DISCOVER-AQ in Houston in 2013. The linked solid red circles represent the median values in [NO] bins. Note a log scale is used for the x-axis.....135

Figure 5.11. Diurnal variations of the indicator of O₃ production sensitivity to NO_x and VOCs, L_N/Q, at the individual spiral locations during DISCOVER-AQ in Houston in 2013. Individual points are 1-min data colored by P(O₃) and the linked red circles represent the median values in hourly bins of P(O₃). Data are limited with the pressure altitude less than 1000 m to approximately represent the boundary layer.....136

Figure 5.12 Photochemical oxidant, Ox (=O₃+NO₂) as a function of NO_z (=NO_y+NO_x) during DISCOVER-AQ in Houston in 2013. Red dots are the data collected on September 25 and 26, 2013 when high ambient O₃ concentrations were observed. Blue circles are the data collected during other flights. Data are limited with the pressure altitude less than 1000 m to represent the concentrations in the boundary layer.....137

Figure 5.13 O₃ production efficiency (OPE) versus NO_x in the box model (blue circles) and CMAQ model (pink dots) results. The linked blue circles show the median OPE values binned by NO_x concentration in the box model, the linked red triangles show the median OPE values binned by NO_x concentration in the CMAQ model. OPE is calculated according to its definition as the net O₃ formation rate divided by of the formation rate of NO_z.....139

Figure 5.14 CO versus NO_y and linear regression on September 25 and 26 at different times of the day: (a) 07:00-17:00 (all data), (b) 07:00-09:00, (c) 09:00-11:00, (d) 11:00-13:00, (e) 13:00-15:00, and (f) 15:00-17:00 (CST).....140

Figure 5.15 O₃ production efficiency (OPE) along the P-3B flight track during DISCOVER-AQ in Houston in 2013. OPE was calculated using the box model results as the ratio of net O₃ formation rate to the formation rate of NO_z.....142

List of Abbreviations and Acronyms

AGL	Above Ground Level
AOD	Aerosol Optical Depth
APG	Aberdeen Proving Grounds
AQRP	Air Quality Research Program
BB	Bay Breeze
BIA	Bay-breeze Identification Algorithm
CAMx	Comprehensive Air-Quality Model with Extensions
CAPE	Convective Available Potential Energy
CDT	Central Daylight Time
CH ₂ O	Formaldehyde
CMAQ	Community Multiscale Air Quality
CO	Carbon Monoxide
DCVZ	Denver Convergence Vorticity Zone
DISCOVER-AQ	Deriving Information on Surface conditions from Column and Vertically Resolved Observations Relevant to Air Quality
EDT	Eastern Daylight Time
ENTLN	Earth Networks Total Lightning Network
EPA	Environmental Protection Agency
EST	Eastern Standard Time
H-O ₃	High O ₃
HO ₂	Hydrogen Dioxide
KNMI	Royal Netherlands Meteorological Institute
LDA	Lightning Data Assimilation
LES	Large-eddy Simulation
Lidar	Light Detection and Ranging
MARAF	Millersville Atmospheric Research and Aerostat Facility
MDE	Maryland Department of the Environment
MDT	Mountain Daylight Time
MU	Millersville University
NAA	Non-Attainment Area
NAAQS	National Ambient Air Quality Standard
NARR	North American Regional Reanalysis

NASA	National Aeronautics and Space Administration
NATIVE	Nittany Atmospheric Trailer and Integrated Validation Experiment
NCAR	National Center for Atmospheric Research
NCEP	National Centers for Environmental Prediction
NEI	National Emissions Inventory
NO	Nitric Oxide
NO ₂	Nitrogen Dioxide
NoBB	No Bay Breeze
NoTS	No Thunderstorm
NO _x	Nitrogen Oxides
PM	Particulate Matter
O ₃	Ozone
OE	Ozone Exceedance
OPE	Ozone Production Efficiency
ppb(v)	parts per billion (by volume)
Q _s	Saturation water vapor mixing ratio
Q _v	Water vapor mixing ratio
RO ₂	Organic peroxy radical
RTMA	Real-Time Mesoscale Analysis
SIP	State Implementation Plan
SODAR	SONic Detection and Ranging
SSA	Single Scattering Albedo
TCEQ	Texas Commission on Environmental Quality
TIBL	Thermal Internal Boundary Layer
TS	Thunderstorm
UTC	Coordinated Universal Time
UV	Ultraviolet
VOCs	Volatile Organic Compounds
WPC	Weather Prediction Center
WPS	WRF Preprocessing System
WRF	Weather Research and Forecasting

Chapter 1: Introduction

A byproduct of global industrialization and development is the release of trace gases and particulate matter into the atmosphere. Emissions as a result of human activities (anthropogenic emissions) pose serious threats to human life and health. “Diseases caused by pollution were responsible for an estimated 9 million premature deaths in 2015—16% of all deaths worldwide—three times more deaths than from AIDS, tuberculosis, and malaria combined and 15 times more than from all wars and other forms of violence...” (Landrigan et al., 2017). Severe pollution episodes, which typically occur from a combination of emissions and meteorology, need to be addressed with urgency. In order to provide solutions for reducing anthropogenic air pollution appropriately, there needs to be a better understanding of the role that meteorology plays in exacerbating or alleviating the pollution, and this understanding must be integrated into solutions that are fiscally realistic in the global economic arena. Hooke (2014) emphasizes the serious economic and societal costs to making policy decisions without understanding how some natural phenomena works. Getting the information wrong, being ignorant, or moving on to the next step before adequately researching an issue comes with huge risks. Therefore, the focus of this work is to gain a better understanding of the role that meteorology plays in modulating one form of air pollution in the United States, boundary-layer ozone (O₃), such that policy decisions for a broad array of pollutants can be made with an understanding of its natural variability.

1.1 Boundary-layer O₃ Formation, Sensitivity, and Emissions Controls

Boundary-layer O₃ is a secondary photochemical pollutant formed by a reaction mechanism involving nitrogen oxides (NO_x = NO + NO₂), volatile organic compounds (VOCs), carbon monoxide (CO), and sunlight (UV radiation). Since O₃ is harmful to both the human respiratory system and the photosynthetic processes of vegetation, the United States Environmental Protection Agency (EPA) has implemented air quality standards for O₃ as a criteria pollutant (Krupa and Manning 1988; Burnett et al., 1997). Surface O₃ is regulated according to the current primary National Ambient Air Quality Standard (NAAQS) of 70 parts per billion by volume (ppbv), calculated as the daily maximum of an eight-hour running mean.

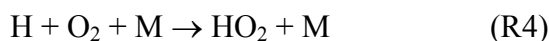
1.1.1 Tropospheric O₃ Production

Since O₃ is not emitted directly, it is important to understand the mechanisms through which O₃ precursors, namely NO_x, VOCs, and CO, are emitted or created. Sources of NO_x (as NO) include fossil fuel combustion and biomass burning (as NO) and the photochemical production of NO₂ through NO + O₃, or NO + RO₂, or NO + HO₂ (R5). Sources of VOCs include natural emissions from trees and other vegetation as well as anthropogenic emissions from fossil fuel evaporation, solvents, and heavy industry. Some sources of CO are fossil fuel combustion and biomass burning. OH (the hydroxyl radical) reacts very rapidly with non-radical species and is even more reactive with molecules that contain H. The production of OH is shown below (Jacob, 1999):

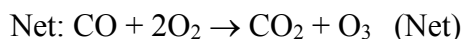




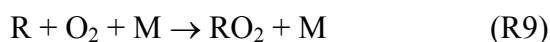
The oxidation of CO by OH then goes on to produce O₃ by the following reactions:



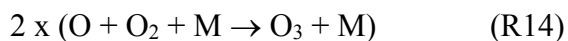
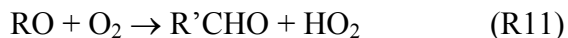
The resulting reaction is:



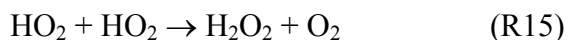
Aerosols with a high single scattering albedo can increase UV flux and accelerate R6, therefore increasing the amount of O₃ production (e.g., Dickerson et al., 1997). It is important to note that R5 is considered to be the rate-limiting step for O₃ production, as NO can also react with O₃ to form NO₂, thus depleting O₃. If NO is converted to NO₂ through the reaction with HO₂, then there is net production of O₃. As noted above, O₃ is also produced by oxidation of VOCs. In the following reactions, the simplified notation R represents organic groups and RH is the simplified notation for VOCs.



From this point, the NO₂ produced will photolyze to produce O₃. However, the RO radical has several paths forward, where an HO₂ radical is produced. Following the same notation, the following reactions occur (Jacob, 1999):



An example of RH and R'CHO for the reaction chain above are methane (CH₄) and formaldehyde (CH₂O). The loss of HO_x radicals, and thus the termination of the chain, can happen in two ways that are dependent upon the concentration of NO_x. At relatively low NO_x or in remote areas, HO₂ is terminated via reaction with itself:



However, in areas with high concentrations of NO_x, the major sink of HO_x is through NO₂ oxidation by OH:



The path through which radicals are terminated has important implications for the production of O₃.

1.1.2 O₃ Production Sensitivity

The production of O₃ is nonlinear with respect to its precursors, NO_x and VOCs. Understanding this nonlinear chemistry and how it varies in time and space has important policy implications for emissions control strategies. The production of O₃ can be NO_x-sensitive or VOC-sensitive, depending upon the concentrations of each of these precursors. In the case of low NO_x concentrations, O₃ production varies

with the concentration of NO and is relatively independent of VOCs. In this scenario, O₃ production is considered to be NO_x-sensitive in that the production of O₃ is sensitive to (or limited by) the ambient concentrations of NO_x.

In the case of high NO_x concentrations, O₃ production rates increase with rising VOC concentrations and decrease with NO_x concentrations. In this scenario, O₃ production is considered to be VOC-sensitive since the production of O₃ limited by the ambient VOC concentrations (although total ozone production nearly always goes up with increasing NO_x emissions). Figure 1.1 demonstrates a model calculation of the two regimes, NO_x and VOC sensitive, simulated over the U.S. as depicted in Jacob, 1999. To properly address the air pollution problem, it is critical to obtain knowledge of the regime for O₃ production in the area of interest.

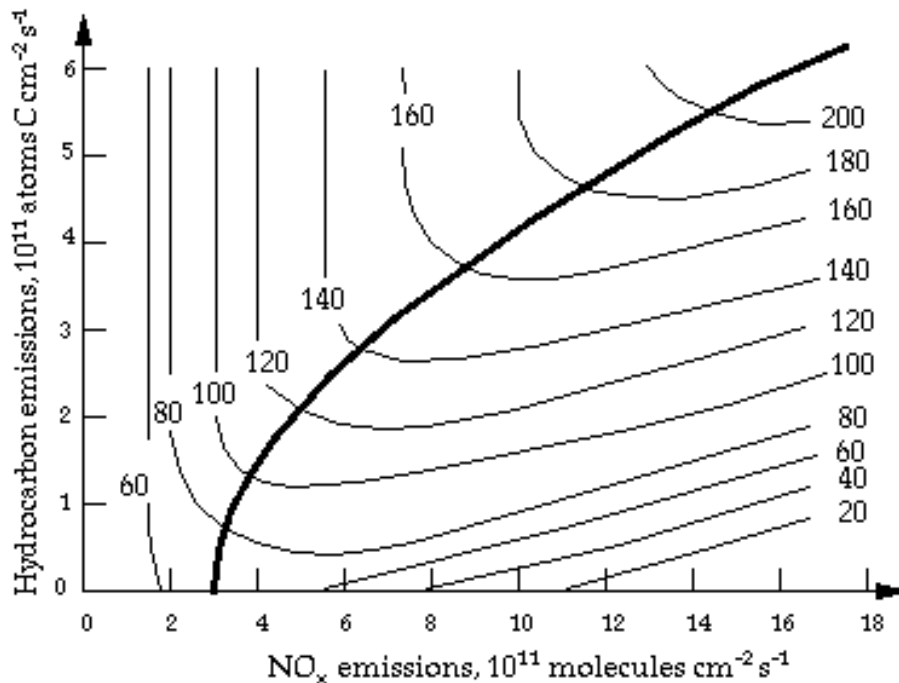


Figure 1.1: (Figure from Jacob 1999; Fig 12-4) O₃ concentration (ppbv) simulated by a regional photochemical model as a function of NO_x and VOC emissions where

the thick black line delineates the NO_x-sensitive (top left) and the VOC-sensitive (bottom right) regimes.

Since the effectiveness of O₃ reduction is contingent upon an accurate understanding of how O₃ responds to the reduction of NO_x or VOCs emissions in a given area or time of day, simulations from air quality models are an important part of emissions control strategies.

1.1.3 Emissions Control

O₃ is one of the six criteria pollutants identified in the Clean Air Act and monitored by the EPA. NAAQS were implemented for each of the six criteria pollutants: carbon monoxide (CO), lead (Pb), nitrogen dioxide (NO₂), O₃, sulfur dioxide (SO₂), and particulate matter (PM). The EPA designates areas in the U.S. as places of attainment or nonattainment of the NAAQS. Individual states make an air quality plan, called a State Implementation Plan (SIP), which describes the actions needed for areas that are not in attainment to meet the standards. The NAAQS for O₃ is a specified maximum concentration allowed in the ambient outdoor air. In 2015, the EPA updated the O₃ standard from 75 ppbv (in 2008) to 70 ppbv. There have been significant reductions in O₃ concentrations over the last three decades, especially in the Eastern U.S., accomplished by controlling emissions of O₃ precursors (e.g., the removal of NO_x from power plants and the reduction of vehicular NO_x with more efficient catalytic converters). However, while there have been marked improvements in the O₃ problem in the U.S. due to the application of a blanket of emissions reductions, there are many monitors still out of attainment during summer months,

especially along the coast in the NE U.S. In order to understand and identify the individual situations that lead to nonattainment, a deeper investigation needs to be performed by coupling anthropogenic emissions and meteorology and informing policy around known sources of variability.

1.2 The Role of Meteorology in Modulating Surface Pollution

The concentration of O₃ at or near the surface is also contingent upon meteorological conditions such as the synoptic-scale circulation, boundary-layer height and turbulence, advection, incoming solar radiation, temperature, and humidity (Seaman and Michelson, 2000; Hegarty et al., 2007). Areas most commonly affected by high O₃ concentrations are downwind of power plants or metropolitan centers. Coastal regions are also frequently subject to poor air quality due to bay or sea breezes that can effectively recirculate pollution in the lower boundary layer (Banta et al., 2005; Loughner et al., 2011; 2014).

During NASA'S 2011 DISCOVER-AQ (Deriving Information on Surface conditions from Column and Vertically Resolved Observations Relevant to Air Quality) field campaign in the Baltimore/Washington DC area (detailed in Section 1.3 of this chapter), days that experienced high humidity (relative humidity above 60%) contributed significantly to the variability of regional and diurnal aerosol optical extinction (Beyersdorf et al., 2016); changes in aerosol optical depth (AOD) can be strongly influenced by spatial and temporal variations in humidity. During 2011 DISCOVER-AQ, AOD was shown to increase significantly from morning to late afternoon, especially in correspondence to cumulus cloud formation (Eck et al., 2014), demonstrating that AOD would also be sensitive to bay breezes and cumulus

formation by these breezes. Higher humidity can increase AOD and single scattering albedo (SSA), enhancing the UV flux and increasing the production of O₃ (Dickerson et al., 1997). Since OH from O₃ photolysis can aid in oxidation of SO₂ and VOCs to form PM, bay breezes can increase the aerosol loading and AOD over coastal areas, and should be investigated further, although this is beyond the scope of this dissertation.

1.2.1 Thermally-direct Mesoscale Circulations due to the Land-water Interface (Bay Breezes and Thunderstorms) and Surface Pollution

Thermally direct circulations (circulations with ascending motion in an area of relatively high temperature and descending motion in an area of relatively low temperature) that are the result of a temperature differential across the land-water interface are a common summer-time phenomenon for areas near a body of water during the day, with cooler surface temperatures over the water than the adjacent land. The breeze is named by the body of water from which it is derived (e.g., sea breezes are from the ocean, bay breezes are from the bay, etc.). The land-water temperature difference leads to horizontal pressure gradients, which cause shallow, but significant, breezes to form. The sea breeze (herein referred to by the context of the bulk of this study, “bay breeze”) is a relatively cool wind that blows from the water to the land in synoptic regimes susceptible to these breezes (weak geostrophic flow, few clouds, significant day-time heating) and which, if sustained, contain a return flow aloft (from land to water). The bay breeze is marked by a cool leading edge that is similar to, but weaker than, that of an advancing cold front. If enough moisture is present, this leading edge can trigger moist convection, such as a line of

fair-weather cumulus clouds over the land, and can also trigger deep convection if the air is convectively unstable (Wallace and Hobbs, 2006). A shallow, internal boundary layer forms (Thermal Internal Boundary Layer; TIBL) from the cool air advected from the water, modifying the surface heat flux and growing in depth with the square root of distance from the coast (Wallace and Hobbs, 2006). In this layer, pollutants can be trapped near the source and accumulate.

The same meteorological conditions that yield thermally direct circulations, such as bay breezes, can also lead to O₃ and other pollution events in the right chemical regime: weak winds, warm temperatures, intense solar radiation, and subsidence inversions. Pollutants accumulate under these atmospheric conditions, leading to O₃ formation and allowing these mesoscale circulations to compete with synoptic forcing. These pollutants are transported from the land to the water in the synoptic-scale flow prior to bay breeze development. Pressure gradients that develop due to differential heating force the air near the surface to move from water (high pressure) to land (low pressure) during the day. The reversal of this occurs at night when the land cools much more quickly than the water and causes a pressure gradient force in the opposite direction. This sequence forces early morning emissions over land to be transported over the adjacent body of water, and then re-circulated back to the land in the afternoon (Wang et al., 2001). NASA's DISCOVER-AQ field campaign provided data and analysis that demonstrated the enhancement of pollution over the land near the Chesapeake Bay coastline as a result of higher concentrations over the bay (Goldberg et al., 2014) being transported landward from the bay breeze (Stauffer et al., 2015a; 2015b; Loughner et al., 2014, Mazzuca et al., 2017). Since

many of the world's most populated cities reside along coastal regions (Small and Nicholls, 2003) and are therefore prone to air quality recirculation events, it is important to evaluate and understand the impacts of anthropogenic emissions and naturally-induced circulations on local air quality.

Along with high O₃ concentrations, the bay breeze also transports higher concentrations of water vapor over the land which, in combination with low-level convergence, can develop deep convection. Deep convective storms can transport polluted air from the boundary layer into the free troposphere (Dickerson et al., 1987), where O₃ production can increase (Pickering et al., 1992). Storms can be triggered as a result of upward vertical transport of water vapor associated with the rising branch of the land-sea overturning circulation, as well as by surface convergence between synoptic westerlies/south-westerlies and easterly/south-easterly bay breeze. Thunderstorm initiation by the land-sea contrast has been recognized for some time (Byers and Rodebush, 1948), and has been further investigated in complex land-water regimes such as rivers (Zhong et al., 1991). As a bay breeze propagates inland, small bodies of water such as rivers can enhance the convergence zone for thunderstorm initiation (Laird et al., 1995).

1.2.2 Thermally-direct Mesoscale Circulations due to Topography (Mountain Breezes and Thunderstorms) and Surface Pollution

The Denver area, along the Front Range in Colorado, is subject to complex meteorological features that can exacerbate air pollution and make for a challenging modeling situations for surface O₃. Similar to the bay breeze, by afternoon on fair-

weather days, the air over the mountains (especially those facing the sun) is heated more quickly than the adjacent air at the same altitude, creating low pressure over the mountains and initiating an upslope breeze. Favored during times of weak synoptic flow, upslope winds reverse direction at nighttime. This results in downslope winds that can recirculate the polluted air that was advected over the mountains with the upslope flow during the daytime, and reduce the transport of pollution away from the urban sources (Reddy et al., 2016). In addition, during daytime the air that rises over the mountains may enter a solenoid circulation in which the synoptic-scale flow recirculates pollution eastward above the Planetary Boundary Layer (PBL) to the plains. There, the air descends and recirculates pollutants to the Front Range urban corridor (Reddy et al., 2016).

Upslope winds can trigger deep convection from surface heating at the leading edge of the mountain breeze given a moist, unstable atmosphere. In addition to the storms triggered as a result of daytime heating in CO, an area called the Denver Convergence Vorticity Zone (DCVZ, or “Denver Cyclone”) where potential severe weather is initiated when SE flow from the Gulf of Mexico interacts with NW flow and with plateaus (such as the Palmer Divide), can add to the chemical transport complexity.

1.3 Overview of NASA’s DISCOVER-AQ Field Project (2011-2014)

While surface trace gas monitors are in place around the U.S., it remains a challenge to accurately detect and resolve near-surface pollution with Earth

observations from space (Liu et al., 2005; Fishman et al., 2008; Martin 2008; Chatfield and Esswein 2012). DISCOVER-AQ, a five-year NASA Earth Venture campaign, was designed to advance satellite observation capabilities by investigating the relationship between column-integrated trace gas quantities and pollution in the near-surface environment (<http://discover-aq.larc.nasa.gov>). Goals of DISCOVER-AQ include assessing uncertainties in column versus surface trace gas and aerosol observation correlations, characterizing the diurnal variation of the column and surface observations, and investigating how much horizontal variability can be captured in satellite retrievals and model calculations. The P-3B aircraft provided profiling of meteorological, trace gas, and aerosol variables centered over surface air quality sites, and the B200 aircraft provided remote sensing of trace gases and aerosols.

The ability to understand and predict air pollution events has been limited in part by the lack of vertical meteorological and chemical profile observations. With this unprecedented DISCOVER-AQ data set, the spatial-temporal variability of air pollution can be better addressed in terms of horizontal, vertical, and temporal coverage. Understanding the varying meteorology at each of the campaign locations is crucial when trying to better understand air pollution. Each deployment has a common link: to understand air pollution near urban centers, polluted corridors, and areas of heavy industry. However, what makes each site distinctly different from one another lies in the mesoscale meteorological phenomena and unique topography in each region.

The first deployment was in the Baltimore-Washington Metropolitan area in July 2011, during the second hottest July on record (79.6°F average) in Maryland (<https://www.ncdc.noaa.gov>). One focus of this deployment was to characterize O₃ and NO₂ along the I-95 corridor and the metropolitan area. During this deployment, there was a notable stagnation episode (Bermuda high setup) and associated heat wave with record high temperatures and poor air quality from July 18 – July 23, 2011 (He et al., 2014). This campaign was subject to Chesapeake Bay influences at some of the surface monitors and lowest aircraft spiral altitudes. On days with bay breezes, under weak synoptic flow, air that is already polluted is transported to the Maryland sites from the Ohio River Valley, Pennsylvania, and western Maryland. These pollutants move with the mean flow over the bay, where mixing in a slightly shallower and potentially more polluted marine boundary-layer occurs and can accumulate more O₃. This air is then advected back over land with the bay breeze.

The second deployment took place in San Joaquin Valley, California during January and February 2013. The focus of this deployment was on particulate matter from agriculture as well as NO_x from mobile emissions in the Fresno and Bakersfield area. The meteorology in the San Joaquin Valley during the deployment consisted of periods of strong stagnation, which trapped the pollutants in the valley.

The third deployment occurred in the Houston, Texas metropolitan area in September 2013. In this region, ground-based measurement sites were subject to high water vapor mixing ratios and deep convection. Due to the geographic location of the Houston area with respect to the Bermuda High, cleaner maritime air is typically advected from the south and southeast to the Houston area in the summer months.

When this pattern breaks, usually in September, the surrounding areas are subject to high concentrations of O₃ precursors transported from the urban center and shipping docks (NO_x), and petrochemical facilities (VOCs). On September 25, 2013, one of the worst-case scenarios occurred wherein high concentrations of VOCs were emitted by petrochemical facilities and high concentrations of NO_x were measured. After these chemicals were carried to the Gulf and Galveston Bay by northwesterly synoptic-scale flow behind a cold front, a recirculation event occurred from both a gulf breeze and a bay breeze, leading to dangerously high O₃ concentrations observed at the surface and aloft at sites around the Houston area.

The fourth deployment took place along the Front Range in the Denver, Colorado area in July and August 2014. This area is subject to complex meteorology from upslope and downslope mountain flow, solenoidal circulations, pop-up mountain thunderstorms, and severe weather from the DCVZ. The chemistry that occurs in this area is driven by high NO_x concentrations from mobile sources and VOCs from the oil and gas industry as well as feedlot operations.

The DISCOVER-AQ project yielded several important publications addressing the coupling of meteorology and emissions, as well as over-arching goals of the field mission. Highlighted here are some works where analyses and modeling studies were conducted using the dense network of DISCOVER-AQ meteorological and chemical observing sites. Some papers demonstrate the importance of understanding how O₃ concentrations vary along the land-water interface (Goldberg et al., 2014), how bay/gulf breezes can further complicate the transport of emissions and O₃ concentration at sites along the bay during the Maryland and Texas

deployments (Loughner et al., 2014; Stauffer et al., 2015; Mazzuca et al., 2017), and can aid in fair-weather cumulus cloud formation and venting (Loughner et al., 2011). Additionally, He et al. (2014) discuss a situation where an elevated reservoir of pollutants was observed above the PBL, downwind of Baltimore, during a heat wave in the Maryland deployment. The DISCOVER-AQ observations also led to the ability to compare and improve chemical modeling platforms. For example, Anderson et al. (2014) used the DISCOVER-AQ data set to determine that the National Emissions Inventory (NEI), the emissions inventory used for regulatory photochemical modeling, overestimates mobile NO_x emissions by 51-70%. Canty et al. (2015) used observations from DISCOVER-AQ to develop improvements to the Community Multiscale Air Quality (CMAQ) model to better match observations of NO₂, and Goldberg et al., (2016) compared the baseline Comprehensive Air-Quality Model with Extensions (CAMx) simulation with DISCOVER-AQ data and introduced a model framework that better matches the observations in Maryland. In addition, some of the goals of the mission were addressed directly. For example, linear regression analyses were conducted between mixing ratios at the surface and column abundances for O₃ and NO₂ (Flynn et al., 2014), and the variability of profile shapes by use of a hierarchical cluster analysis of O₃ and NO₂ profiles was investigated to better understand times when the column observations are most representative of the surface concentrations (Flynn et al., 2016). Follette-Cook et al. (2015) examined the spatial and temporal variability of trace gases during the DISCOVER-AQ Maryland campaign and determined that the horizontal resolution and precision of future

geostationary atmospheric chemistry satellites will be sufficient to adequately observe pollution episodes.

1.4 Objectives of this Research

The work herein mostly focuses on bridging the gap between air chemistry and meteorology with observational and modeling analyses. Additionally, we investigate the production of O₃ and its sensitivity to NO_x and VOCs during the DISCOVER-AQ field mission with a zero-dimensional box model for emissions control policy implications in the Houston Metro Area. Through this work, we ask the following research questions (numbered) and subsequently discuss the methods through which the research questions are addressed (lettered):

- 1) What are the detailed characteristics of thermally direct land-water breezes (e.g., bay and gulf breezes) and how do these characteristics compare to what is already known about these circulations in areas subject to poor air quality by recirculation?**
 - a. Use the unprecedented DISCOVER-AQ observations, specifically vertical profiles and surface observations, to understand the structure, timing, duration, and extent to which bay and gulf breezes penetrate inland and affect air quality.

- 2) What is the climatology of bay breezes, thunderstorms, and O₃ at a site historically known for having poor air quality along a body of water**

(Edgewood, MD) and how do these mesoscale meteorological phenomena (bay breezes and thunderstorms) affect the O₃ observed at the surface?

a. Create an automated bay breeze and thunderstorm detection algorithm to sort through days and determine if a bay breeze and/or a thunderstorm have occurred in an influential radius of the site. Next, use this statistical model to calculate the conditional probability of an O₃ event given the occurrence of a bay breeze, a thunderstorm, or both in a day, and determine how many O₃ event days were also associated with each, all, or none of these features. This work will:

- i. Aid in understanding the relationship between mesoscale meteorology and O₃
- ii. Quantify the roles of mesoscale meteorological predictors for forecasting O₃ events

3) As discussed in Chapter 3, some storms act to terminate the pollution episode while some do not. That discovery prompted the following individual questions:

- When thunderstorms do not help to clean up the polluted boundary layer air, what are the characteristics of those types of storms and what are the dynamical mechanisms that result in days with both deep convection and poor air quality?
- What are the characteristics of and surface effects from storms that terminate a pollution episode?

- What are the characteristics of storms initiated as a result of topographic forcing?
 - Can small mesoscale events, such as bay breezes and air-mass thunderstorms, be accurately simulated in a dynamical model?
 - a. Perform case study analyses of two air-mass thunderstorms: one that does not terminate the pollution episode and another that does.
 - b. Run the Weather Research and Forecasting (WRF) model (Skamarock et al., 2008) at fine horizontal and vertical resolution to accurately simulate the complex dynamics observed on one of the case study days (July 22, 2011).
 - c. Add tracers to the WRF simulation when an adequate dynamical simulation is acquired for better understanding of boundary layer air distribution and mixing in the storm, determine the altitude of the downdraft, and quantify vertical mass flux.
- 4) In what regime is the production of O₃ (NO_x-sensitive or VOC-sensitive) as a function of time and space around areas of heavy industry and urban pollution, such as the Houston Metro area?**
- a. Using a photochemical box model based on the CB05 chemical mechanism (Yarwood et al., 2005) constrained to DISCOVER-AQ aircraft observations, calculate O₃ production and sensitivity to its precursors, NO_x and VOCs, throughout the analysis time period of DISCOVER-AQ TX using the L_N/Q method (Kleinman et al., 2005).

The thesis is organized in the following manner:

Chapter 2 (Mazzuca et al., 2017) contains the results from two in-depth case studies of bay and gulf breeze circulations during DISCOVER-AQ at Edgewood, MD and Smith Point, TX, and quantifies how these circulations led to extreme O₃ pollution episodes. This work was published in *Atmospheric Environment*.

Chapter 3 (in review: Mazzuca et al., 2018) depicts the results of a statistical modeling effort to quantify and understand the role of mesoscale meteorology and O₃ surface concentrations. An automated detection algorithm was developed to sort through June, July, and August (2011-2016) between the hours of 11-19 EST and to determine days that had: a bay breeze, a thunderstorm, both, or neither. Next, statistics were calculated for O₃ and included the conditional probability of an O₃ event given a bay breeze, thunderstorm, or both, average and maximum concentrations on days with each meteorological category, differences from one year to the next, and the most frequent meteorological events to occur on days with an O₃ event. This work was submitted to *Atmospheric Environment* and is now under review.

Chapter 4 expands upon Chapter 3 by offering an in-depth examination of the complex dynamics that occurred on two case study days during DISCOVER-AQ in Maryland and Colorado, influenced by mesoscale circulations formed by topographic forcing. The observed bay breeze and thunderstorm case study from the Maryland deployment on July 22, 2011 is simulated in WRF using a lightning data assimilation method, and is evaluated using radar reflectivity from Sterling, VA and observations

from the DISCOVER-AQ deployment. WRF is able to reproduce the dynamics observed on that day with fairly good agreement, and can therefore be used to test the physicality of the thunderstorm statistics derived from Chapter 3. Future work will include adding chemical tracers to the dynamical model to better understand the thunderstorm dynamics that resulted in the extreme air pollution episode that was observed on that day. This has led to a paper in preparation to be submitted in the summer of 2018, (journal TBD) (Mazzuca et al., 2018).

For Chapter 5 (Mazzuca et al., 2016), the focus is switched from meteorology to chemical modeling. In this section, an aircraft observation-constrained box model based on the CB05 mechanism is used to better understand the oxidation processes that occur to form O_3 in the Houston Metro area during DISCOVER-AQ. This work demonstrates the nonlinear O_3 production in an area with complex chemical emissions and regimes. The work published in *Atmospheric Chemistry and Physics (ACP)* finds that there are differences in the sensitivity of O_3 production between the spiral sites over the Houston area and differences in time of day. For example, many sites are VOC sensitive in the morning with a transition to NO_x sensitive by later in the day. From this, we conclude that while NO_x control is beneficial in reducing O_3 pollution overall, VOC control is beneficial at select locations and times of day.

Chapter 6, which is the final chapter, provides concluding remarks as well as ideas for future work.

Chapter 2: Extreme Events: Bay and Gulf Breeze Case Studies in Maryland and Texas (published as Mazzuca et al., 2017)

2.1 Introduction

Several studies have shown that sea, bay, and gulf breezes can contribute to poor air quality (Banta et al., 2005; Evtugina et al., 2006; Darby et al., 2007; Loughner et al., 2011). The 2011 DISCOVER-AQ campaign yielded data demonstrating the influence of the Chesapeake Bay breeze as it enhanced pollution inland of the coastline (Stauffer et al., 2015a; 2015b; Loughner et al., 2014). During the July 2011 DISCOVER-AQ campaign, the 2008 8-hour O₃ standard of 75 ppbv was violated at Edgewood, MD on ten days, and a bay breeze was observed on eight of these days (Stauffer et al., 2015a). Studies during the 2011 DISCOVER-AQ campaign showed that concentrations of surface O₃ tended to be higher over the Chesapeake Bay than upwind land areas due to a shallower boundary layer, ship emissions, lower deposition rates, higher photolysis rates, and decreased boundary-layer venting due to a decrease in cloud cover compared to the nearby land (Goldberg et al., 2014).

Concentrations of background O₃ in eastern Texas tend to be higher in late summer and early fall due to the synoptic circulations of northerly and easterly flow transporting continental high O₃ air to the area. Higher background concentrations could contribute to the frequency and magnitude of O₃ episodes (Langford et al., 2009). The Texas Commission on Environmental Quality (TCEQ) uses the background O₃ concentration to estimate the local contribution of O₃ as the difference between the 8-hour maximum background O₃ and the 8-hour maximum measured O₃ (Nielson-Gammon et al., 2005). High O₃ in the Houston area is often a result of small-scale circulations with advection of pollutants from the Houston Ship Channel to the southwestern part of the Houston Metro area (Ngan and Byun, 2011) and in many cases is the result of wind shifts in a postfrontal environment (Rappengluck et al, 2008). When a gulf or Galveston bay breeze sets up after these pollutants are advected over the water behind the front, the Houston Metro area can experience a second dose of pollution.

Studies performed in Houston, TX, showed that O₃ episodes begin when the synoptic-scale winds transport pollutants from the land to water before a bay or gulf breeze sets up (Darby, 2005). As the bay or gulf breeze develops, pollutants are recirculated over the adjacent land adding to the pollution generated locally in these areas. Banta et al. (2005) discussed an O₃ episode where the gulf / bay breeze contributed to surface hourly O₃ concentrations of 200 ppbv.

Similarly in this chapter, we focus on the effects of thermally direct circulations and local meteorology on air quality in Edgewood, MD and Smith Point, TX, as measured during DISCOVER-AQ.

2.2 Measurements

Table 2.1 provides a summary of measurements used for the Edgewood, MD and Smith Point, TX studies

Instrument & Model	Measurement	Platform	Uncertainty/Accuracy
Vaisala, TTS111	Temperature, RH, Pressure	Tethered Balloon	± 0.5 °C, ± 5 %, ± 1.5 hPa
2B Technologies, 205	O ₃	Tethered Balloon	± 2 %
2B Technologies, 401/410	NO/NO ₂	Tethered Balloon (Smith Point only)	± 2 %
KNMI NO2-sonde	NO ₂	Tethered Balloon (Smith Point only)	N/A (TBD)
ScinTec, MFAS SODAR & RAE1 RASS	Vertically Resolved Wind Speed & Direction	MARAF	0.3-0.5 m/s, $\pm 3^\circ$ (<2.0 m/s)
Flux Tower Instruments (denoted by *)	Near-surface Fluxes	MARAF	
CSI 3-D Sonic Anemometer, CSAT3*	u,v,w; Tv	MARAF	U _x ,U _y : ± 8 cm/s U _z : 4 cm/s Direction: $\pm 0.7^\circ$ at 1 m/s Tv: N/A
LI-COR H ₂ O/CO ₂ Gas Analyzer, LI-7500*	H ₂ O/CO ₂ concentration	MARAF	CO ₂ ± 1 % H ₂ O ± 2 %
Vaisala Pressure Sensor, PTB220B*	Pressure (hPa)	MARAF	± 0.25 hPa
Micromet Systems Net Radiometer, Q*7*	Net Radiation (Wm ⁻²)	MARAF	-6% @ 7m/s for positive fluxes, -1% at 7 m/s for negative fluxes
Surface WeatherPak 2000	WxPak Pressure	MARAF	± 1 hPa at 22°C
	WxPak Compass	MARAF	$< \pm 30^\circ$
	WxPak Wind Speed	MARAF	± 0.3 m/s
	WxPak Wind Dir.	MARAF	$\pm 3^\circ$
	WxPak Humidity and Temperature	MARAF	± 0.8 % / ± 0.1 K at 23°C
TECO Inc., 29C	Surface O ₃	NATIVE	± 2 %
TECO Inc., 42C-Y	Surface NO/ NO _y	NATIVE	± 3 %
NCAR 4 Channel Chemiluminescence	O ₃	P-3B	± 5 %
NCAR 4 Channel	NO/NO ₂ /NO _y	P-3B	10-15 %

Chemiluminescence			
General Eastern, 1011B	Temperature	P-3B	±0.2 °C
Rosemount, MADT 2014	Pressure	P-3B	±0.25 hPa
DFGAS	CH ₂ O	P-3B	±4%

2.2.1 P-3B Aircraft

NASA's P-3B aircraft typically spiraled over each ground site three to four times within an operational day at altitudes from 300 to >3000 m AGL. In some DISCOVER-AQ deployments, missed approaches were used to fill this gap between 300 m and the surface, where the P-3B would approach the ground and take off again. In the Maryland deployment, the tethered balloon at Edgewood is used in this study. In the Houston deployment, the Millersville University tethered balloon was used at Smith Point. Onboard the P-3B there was continuous O₃, NO, NO₂, and NO_y measurements made using the National Center for Atmospheric Research (NCAR) 4-Channel Chemiluminescence Instrument with one-second averages with 5% uncertainty for O₃ and NO, 10% for NO₂, and 20% for NO_y. CH₂O measurements were made on the P-3B using the Difference Frequency Generation Absorption Spectrometer (DFGAS) with 30 second averaging and 13% uncertainty (Weibring et al., 2007). Some differences were observed between the P-3B measurements and those of the tethersonde. These differences are likely due to the horizontal distance between the aircraft and the balloon along a convoluted coastline near the Edgewood site, and/or the timing between the flyover and the tethered balloon position. Based on inter-comparisons between the P-3B and the tethersonde, differences due to representativeness (timing and exact location) are likely greater than differences

associated with instrument errors or operations. The timing between the flyover and when the tethered balloon reached the aircraft altitude was sometimes as much as 30 minutes.

2.2.2 Edgewood, MD Ground Site

The Baltimore/Washington metropolitan area is vulnerable to exceeding the 70 ppbv; 2015 (75 ppbv; 2008) EPA O₃ standard due to the abundance of precursor emissions along with meteorological conditions favorable for O₃ production (He et al., 2013). The highest O₃ design value in the Baltimore Non-Attainment Area (NAA) has been consistently measured at the air-monitoring site in Edgewood. This site experienced the highest O₃ measured on the U. S. east coast region for 2011 and was many times the only monitoring station within the NAA that exceeded the O₃ standard of 75 ppbv standard at that time. This is due in part to its location in a bay breeze convergence zone.

Millersville University deployed its mobile lab including a suite of instruments and equipment in support of boundary layer and atmospheric chemistry research (Millersville Atmospheric Research and Aerostat Facility (MARAF; see <http://www.millersville.edu/esci/maraf>). One-hundred sixty-seven tethered balloon soundings captured the temporal and vertical evolution of O₃ on P-3B flight days and some non-flight days throughout the campaign. The continuous soundings provide a useful data set to characterize profile shapes and how they vary as a result of meteorological conditions such as bay breezes, the amount of boundary layer turbulence, and influences of local plumes versus longer-range transport. MARAF was deployed at Eagle Point on the Edgewood side of the Aberdeen Proving Ground

(APG; lat: 39.397N°, lon: 76.271W °) for the first DISCOVER-AQ deployment in July 2011 (Figure S1).

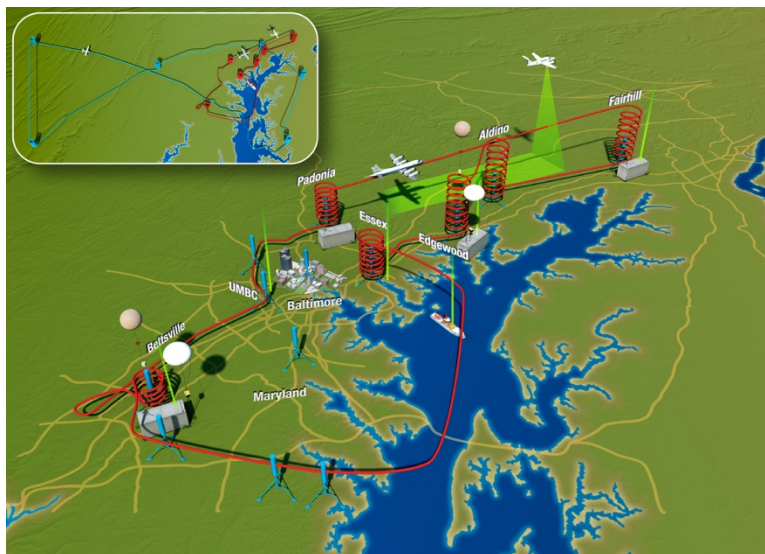


Figure S1. DISCOVER-AQ ground and spiral sites during the July 2011 Baltimore/Washington campaign. Edgewood is where the Millersville Tethersonde/MARAF and NATIVE were located (<http://discover-aq.larc.nasa.gov>).

APG, a U.S. Army facility, is often influenced by transport of O_3 precursors from the Baltimore-Washington Metro area. MARAF includes a 4-meter flux tower, a Sigma Space MicroPulse Lidar (MPL), an acoustic SONic Detection And Ranging (SODAR) with Radio Acoustic Sounding System (RASS) extension, surface trace gases (O_3 , NO_x , SO_2 , and CO), and a 3-wavelength Nephelometer. The tethered balloon system consists of a Vaisala TTS111 system that measures temperature, pressure, relative humidity, wind speed, and wind direction along with a 2B-Technologies Inc. trace gas analyzer for O_3 . Semi-continuous profile measurements were taken in blocks of approximately 1.5 to 2.5 hours depending on available platform battery power, where typically four vertical profiles were measured per charge from the surface to ~500 m AGL. The soundings coincided in time with the P-

3B spirals to fill the gap from the lowest P-3B altitude to the surface. Profiles were also conducted between spirals to capture the temporal evolution of vertical variability throughout the day.

The MARAF site was set up 2.7 km SE of the Edgewood Maryland Department of the Environment monitoring site (MDE) as well as the Nittany Atmospheric Trailer and Integrated Validation Experiment (NATIVE; Martins et al., 2012) for optimal boundary layer sampling immediately on the coast of the bay (Figure S2).



Figure S2. Relative locations of MDE/NATIVE, and MARAF sites, both in Edgewood, MD northeast of Baltimore and surrounded by the Chesapeake Bay and its estuaries.

MDE and NATIVE were collocated platforms for air quality and ground-based in-situ measurements. Chemical measurements included O_3 , NO, NO_y , SO_2 , and CO for NATIVE and O_3 for MDE.

2.2.3 Smith Point, TX Ground Site

Houston, TX has large emissions of O_3 precursors power plants, refineries, and petrochemical industrial plants coupled with meteorological conditions favorable for O_3 production, typically during late summer. Emissions are particularly large

along the Ship Channel and western shore of Galveston Bay (Banta et al., 2005). Aircraft observations from Kleinman et al. (2005a) found that NO_x and light olefins emitted from petrochemical facilities led to the highest O_3 production observed in the study. Smith Point, on a peninsula extending into Galveston bay from the eastern shore, is susceptible to both bay and gulf breeze pollution recirculation. The combination of high emissions and bay and gulf breeze circulations lead to O_3 exceedances.

MARAF was deployed at Smith Point, TX (lat: 29.54N° , lon: 94.76W°) for the third deployment of DISCOVER-AQ in September 2013 (Figure S3) alongside the NATIVE trailer.

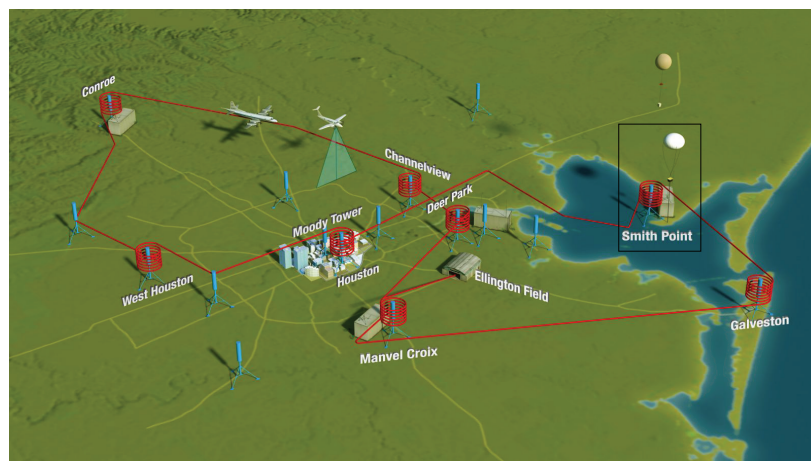


Figure S3. DISCOVER-AQ ground and spiral sites during the September 2013 Houston campaign. Smith Point is where the Millersville Tethersonde/MARAF and NATIVE were co-located (<http://discover-aq.larc.nasa.gov>).

The tethered balloon operation was similar to the Edgewood deployment, but the 2B-Technologies Inc. NO_x analyzer and an NO_2 sonde developed by the Royal Netherlands Meteorological Institute (KNMI) were added for this deployment. The KNMI NO_2 -sonde uses the NO_2 chemiluminescent reaction in a nearly specific to NO_2 aqueous luminol solution (Sluis et al., 2010). Similar surface instruments to the

Maryland deployment were used such as the MPL, SODAR, Nephelometer, and trace gas suite; however, the flux tower experienced technical issues and was not used for this study. A Coastal Environmental WeatherPak 2000 was used in this deployment, which measured surface meteorological constituents such as: pressure, temperature, humidity, wind speed, and wind direction. Again for this campaign, the NATIVE mobile platform for air quality and ground-based in-situ measurements was used, which included surface chemical measurements of O₃, NO, NO_y, SO₂, and CO.

2.3 Bay Breeze Case Study: Edgewood, MD 29 July 2011

During the Baltimore/Washington DISCOVER-AQ campaign, five days exhibited a bay breeze and four days displayed evidence of bay breeze initiation, but were unable to persist due to a thunderstorm or gust front. During this deployment, ten days exceeded the EPA 8-hour 2011 O₃ standard of 75 ppbv at Edgewood - eight of ten were associated with a bay breeze or “interrupted” bay breeze (Stauffer et al., 2015a). On 29 July 2011, surface (Figure 2.1), and tethersonde observations indicated three bay breeze fronts at the Edgewood MARAF site. The morning of the 29 July featured weak synoptic forcing with a surface high pressure and an upper-level ridge in place over the Mid-Atlantic region, typically conducive for both O₃ events and bay breezes. By 12 UTC (08:00 EDT; UTC-4), the synoptic wind pattern over the site was northwesterly (NW) at 850 mb (Figure S4; NCEP Reanalysis data provided by the NOAA/OAR/ESRL PSD, Boulder, Colorado, USA, from their website at <http://www.esrl.noaa.gov/psd/>).

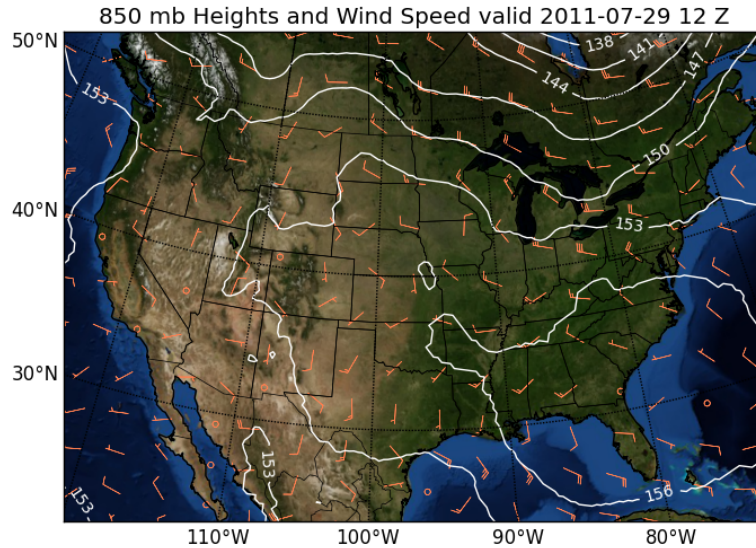


Figure S4. NCEP North American Regional Reanalysis (NARR) 850 mb geopotential heights (white lines) and wind barbs (orange barbs) on 07/29/2011 at 12 UTC (08:00 EDT) over the U.S.

The earliest bay breeze passage of the day (~13:30 EDT) was noted by both the surface observations and a tethersonde profile to be a shallow and brief, but intense boundary between the land environment and the high O₃ air over the bay. Measurements made at the NATIVE trailer only 2.7 km NW of MARAF did not exhibit any effects of the first bay breeze event (Stauffer et al., 2015a). A second bay breeze front passed through the site around 16:15 EDT affecting surface concentrations for about an hour until a wind direction shift brought cleaner air to the research site. By 18:00 EDT, a third bay breeze passage was measured which was sustained until 20:00 EDT when a gust front pushed the O₃ rich marine air off the coast, bringing in cleaner continental air from the thunderstorm outflow. Continuous profiling by the tethersonde captured much of the variability observed on this day. Measurements at the NATIVE trailer were also affected by the second and third bay breeze passages with slightly smaller magnitude fluctuations (Stauffer et al., 2015a).

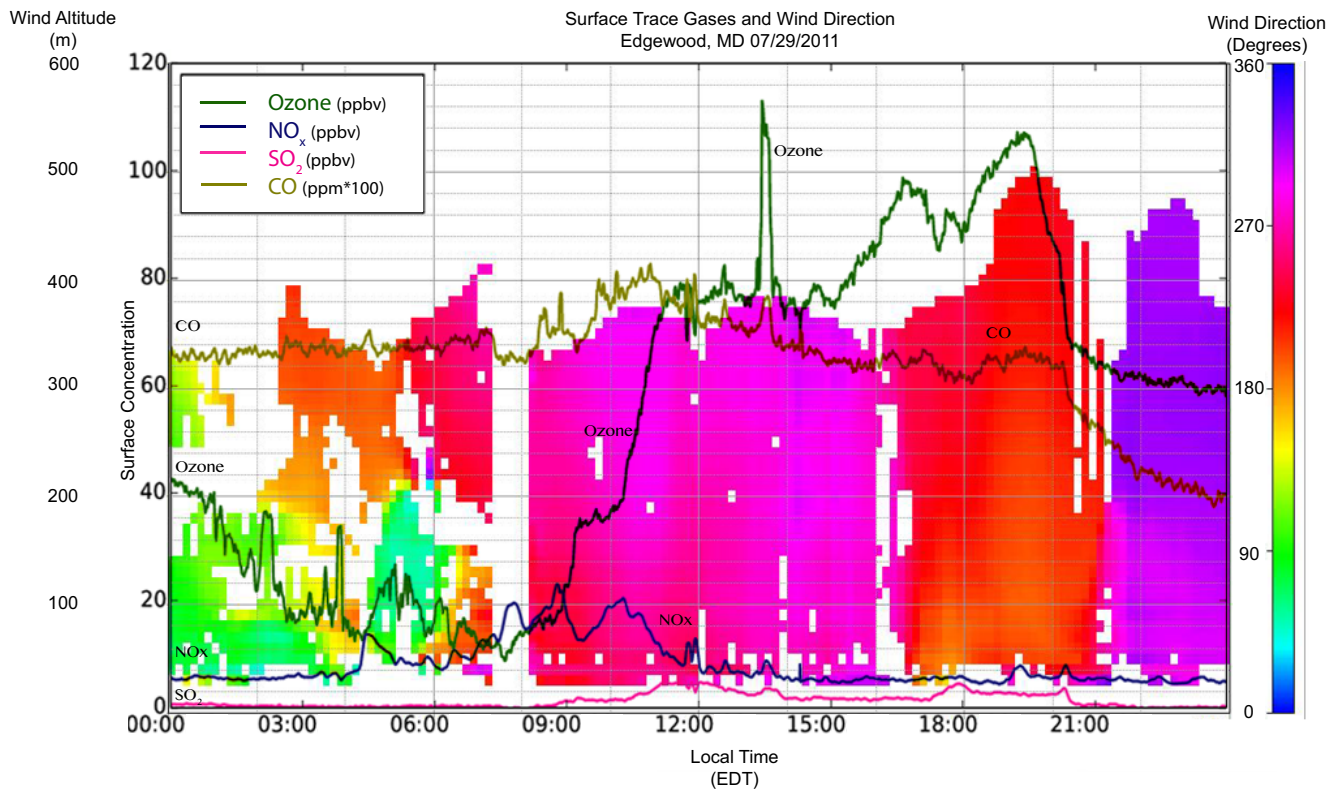


Figure 2.1 07/29/2011 Edgewood MARAF site wind direction with height derived from SODAR wind profiler (colors) and labeled surface trace gases: O₃ (dark green), NO_x (blue), SO₂ (pink), and CO (olive green). Note WSW winds starting at 8:30 EDT as the nocturnal PBL broke up and concentrations of primary pollutants CO and NO_x increased. This is followed by inflow of more O₃ rich air from over the Chesapeake Bay in a shallow (~100m; see also Figures 2.2 and 2.3) layer, shifting to generally SSW winds with sustained high O₃ concentrations by 16:30 EDT.

July 29, 2011 was part of a multi-day ramp up of summertime air pollution as a consequence of the synoptic meteorological conditions. Around 08:30 EDT, a combination of stored O₃ from the (nocturnal) residual layer mixing down to the surface during the growth of the mixed layer and photochemical production led to a rapid increase in surface O₃ from 25 to 75 ppbv within two hours (Figure 2.1). This corresponds to negative vertical eddy momentum flux (downward transport) as

measured by the flux tower, as well as an end to directional wind shear and development of vertical speed shear (Figure 2.2).

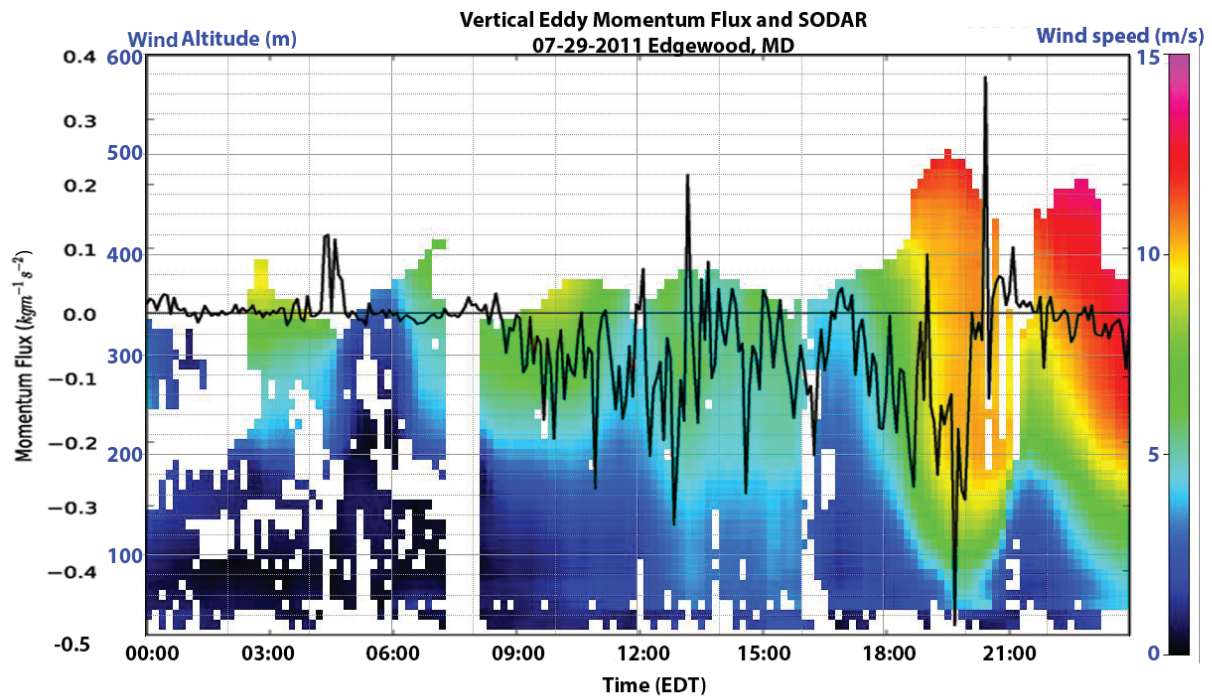


Figure 2.2 07/29/2011 Edgewood MARAF site wind speed with height derived from SODAR (colors) and 4-meter vertical eddy momentum flux (black line).

Tethered balloon soundings between 08:20 and 09:07 EDT (Figure 2.3) show enhanced O_3 concentrations relative to the surface between 150-340 m. The ascending profile (08:20-08:42 EDT) from the surface to 340 m shows increasing O_3 concentration with altitude between 150 – 330 m. The descending profile (08:42 – 09:07 EDT) shows the downward transport of higher O_3 concentrations from aloft to the layer below 200 m. The descending profile indicates a layer (260 – 340 m) of lower water vapor mixing ratio along with higher potential temperature and higher wind speeds than the ascent sounding. From 260 m to the surface, the descending

profile shows fairly well mixed, enhanced water vapor mixing ratio, higher potential temperature, and higher wind speeds than the ascending profile.

Tethersonde Balloon Sounding Edgewood, MD 2011-07-29

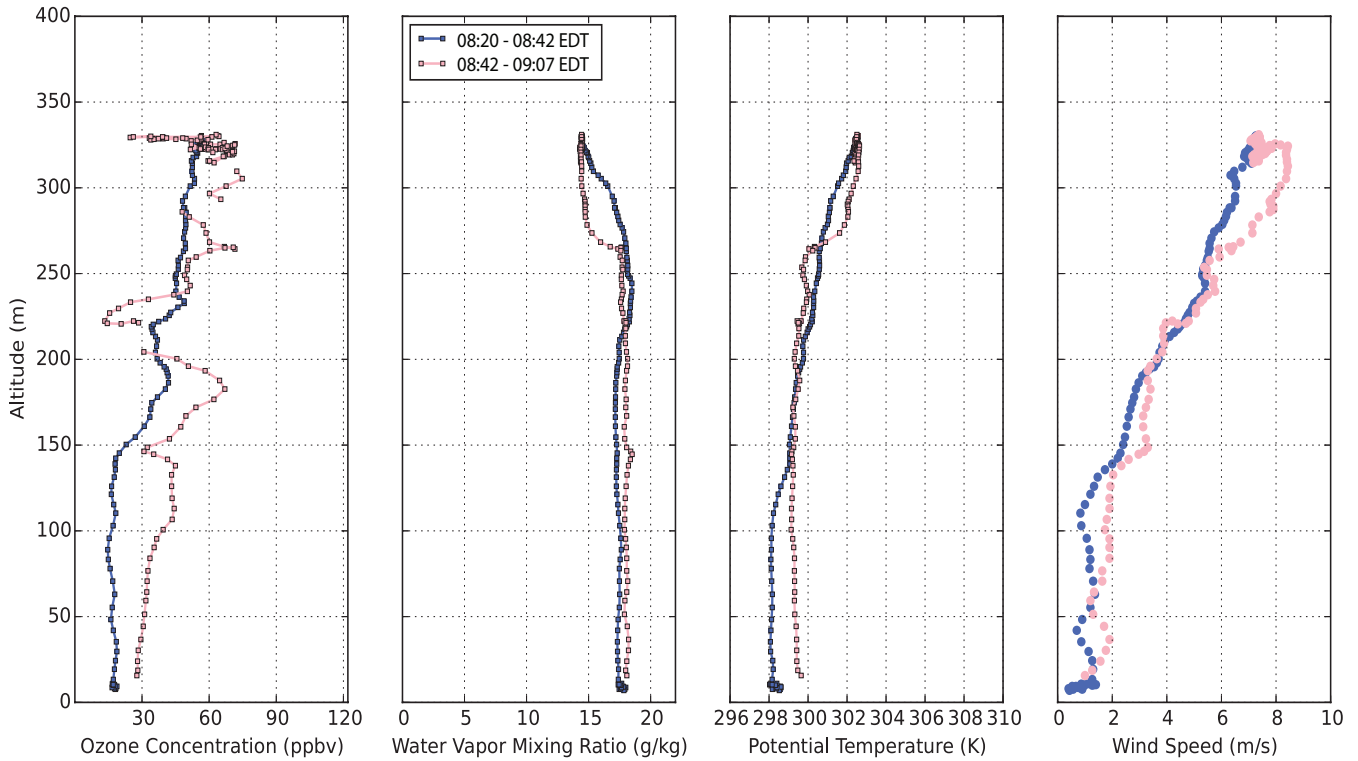


Figure 2.3 07/29/2011 Millersville tethersonde profiles of O₃ concentration, water vapor mixing ratio, potential temperature, and wind speed from the surface to ~340 m. The first sounding (blue) is from the surface to maximum altitude (08:20 – 08:42 EDT) and the second sounding (pink) is down from maximum altitude (08:42 – 09:07 EDT). Profiles indicate higher O₃ concentration and water vapor mixing ratio layer aloft during first sounding and mixing down (weaker vertical gradient) by the second sounding.

Back trajectory analysis calculated for the period six hours prior to these profiles from the Air Resources Laboratory's Hybrid Single-Particle Lagrangian Integrated Trajectory (HYSPLIT) model (Stein et al., 2015; Draxler and Hess, 2004) shows transport from central Pennsylvania at 1000 m and western Pennsylvania at 100 m. Back trajectories from the period one hour before are from eastern Maryland at 1000

m and between Edgewood and Baltimore intersecting I-83 at 100 m. This suggests that some of the enhanced O₃ concentration found in these profiles was due to transport from Pennsylvania cities and Baltimore, MD during early to mid-morning, before the bay breeze.

O₃ concentrations at the surface fluctuated from 75 to 80 ppbv from 11:00 EDT until the first bay breeze passage (~13:30 EDT) that swept through the site in a shallow wedge (<100 m) bringing spikes in O₃ and specific humidity, but a drop in temperature. The combined P-3B and tethersonde profile (Figure 2.4) for the first spiral of the day demonstrates the shallow but intense bay breeze below the P-3B minimum flight altitude (Figure 2.5; Table 2.2).

Table 2.2 Conditions during bay breezes observed on 7/29/2011 at Edgewood, MD

	Time (EDT)	Specific Humidity (g/kg)	Temperature (°C)	O ₃ Concentration (ppbv)
Bay breeze 1	13:30-13:50	15.6 to 18.5	37.8 to 35.8	77 to 113
Bay breeze 2	16:15-17:25	13.6 to 16.5	38.5 to 37.5	84 to 91
Bay breeze 3	18:00-20:00	15.0 to 18.0	37.6 to 36.3	87 to 107

The bay breeze also transported other trace gases during this passage: NO_x increased from 6.5 to 8.8 ppbv, SO₂ increased from 2.7 to 3.6 ppbv, and CO increased from 710 to 760 ppbv (Figure 2.1).

P-3B & Balloon Soundings Edgewood, MD 2011-07-29
1232 - 1329 EDT

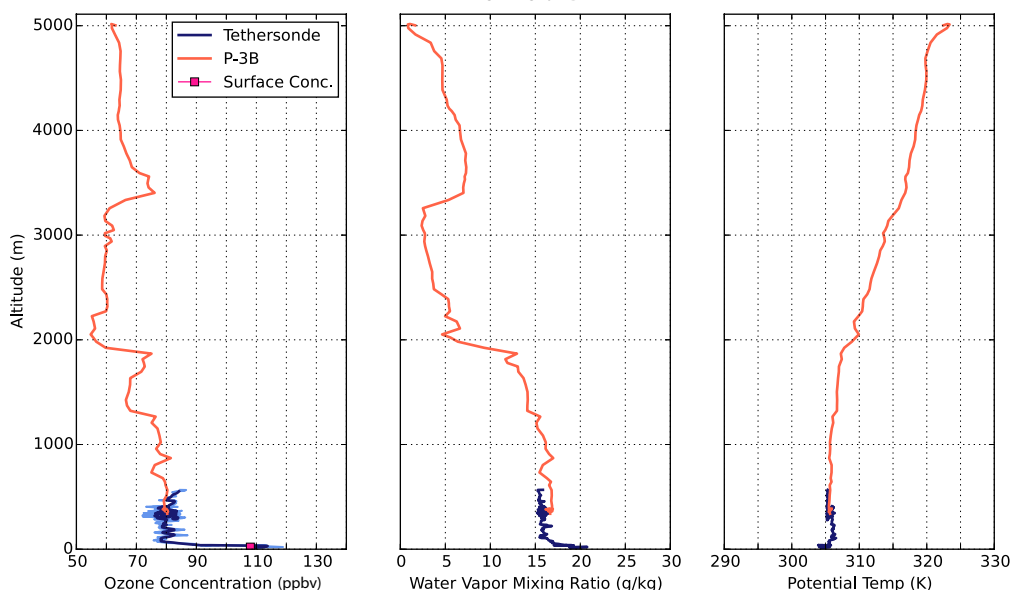


Figure 2.4 07/29/2011 Midday blended profile of the first circuit P-3B spiral over Edgewood (orange) and the corresponding Millersville tethersonde sounding (blue) of O_3 concentration, water vapor mixing ratio, and potential temperature from the surface to ~5000 m; surface O_3 concentration (pink dot; at maximum surface O_3 concentration). The shallow bay breeze passage is observed in the tethersonde profile and the surface, but not by the P-3B due its extremely shallow depth.

This bay breeze was too brief for the 30 minute averaged SODAR wind measurements. However, the tethersonde anemometer measured wind direction in the bay breeze layer to be between 90 and 190 degrees, but fluctuating between 80 and 280 degrees near the surface (Figure S5; wind direction light pink sounding).

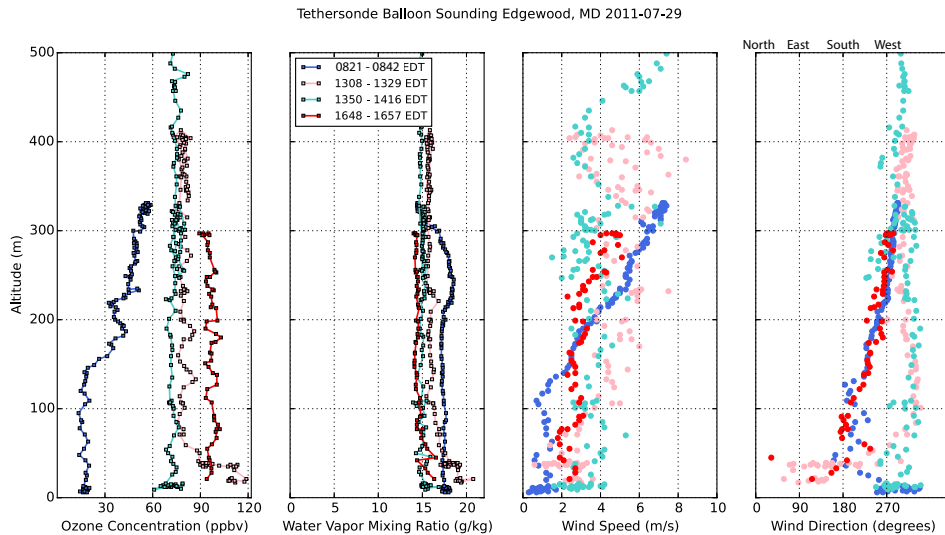


Figure S5. 07/29/2011 Millersville tethered balloon soundings throughout the day capturing temporal variations in concentrations and meteorological parameters at Edgewood. Blue: morning sounding before mixing (08:21-08:42 EDT), light pink: sounding during the first bay breeze (13:30 – 13:29 EDT), green: sounding showing retreated levels of O₃ concentration and water vapor mixing ratio before second bay breeze (13:50 – 14:16 EDT), red: sounding ~30 minutes after second bay breeze passage (16:48- 16:57 EDT).

At 13:50 EDT, trace gas concentrations, specific humidity, and temperature returned to previous levels throughout the vertical profile (Figure S5; green sounding) and at the surface (Figure 2.5). The brevity of this intense yet shallow bay breeze demonstrates the steep, localized gradients at the bay breeze front and the significant impact on surface concentration.

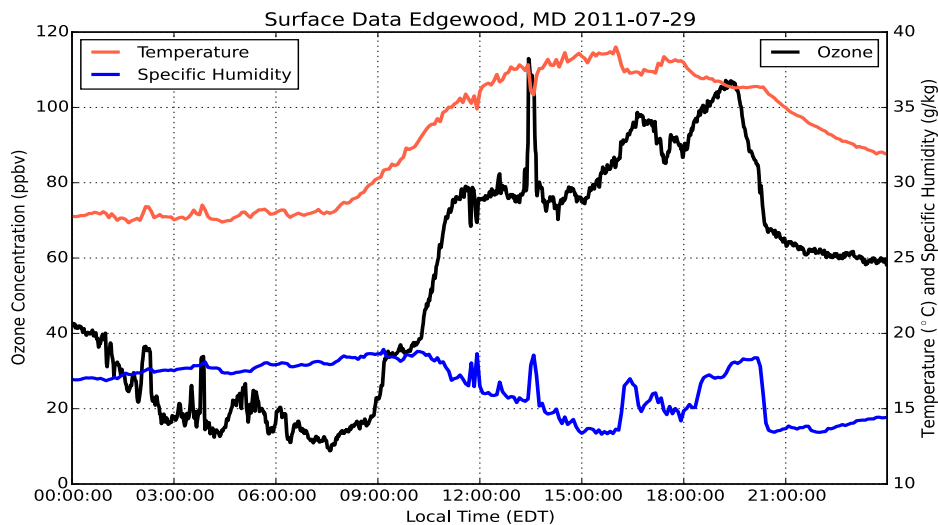


Figure 2.5 07/29/2011 MARAF surface O₃ concentration (black line), 4-m temperature (orange line) and 4-m flux tower specific humidity (blue line). Spikes that positively correlate between O₃ concentration and specific humidity and negatively correlate to temperature observed (13:30, 16:15, 18:00 EDT) indicate two small-scale bay breeze passages and then a larger scale passage from 16:00 to 19:00 EDT.

A second bay breeze frontal passage occurred later in the day around 16:15 EDT (Figure 2.5; Table 2.2). This was associated with a wind shift from NW to SSW with air coming from the Baltimore area and passing over the bay. By 17:25 EDT the wind shifted direction again from SSW to SSE along with a change in surface concentrations. Although this air temporarily passed over the bay, specific humidity decreased to 14.6 g/kg, temperature increased to 38.2 degrees C, and O₃ decreased to 85.3 ppbv (Figure 2.5). A combined P-3B and tethersonde profile was captured during this transition period between wind directional shifts. The tethersonde profile from 16:48 to 16:57 EDT captured the O₃ and water vapor rich air mass from the bay breeze, whereas the P-3B spiraled down 25 minutes later (from 17:24 to 17:36 EDT) over the site measuring the air from the SSE with the previously detailed lower O₃

and specific humidity concentrations along with slightly warmer temperatures (Figure 2.6).

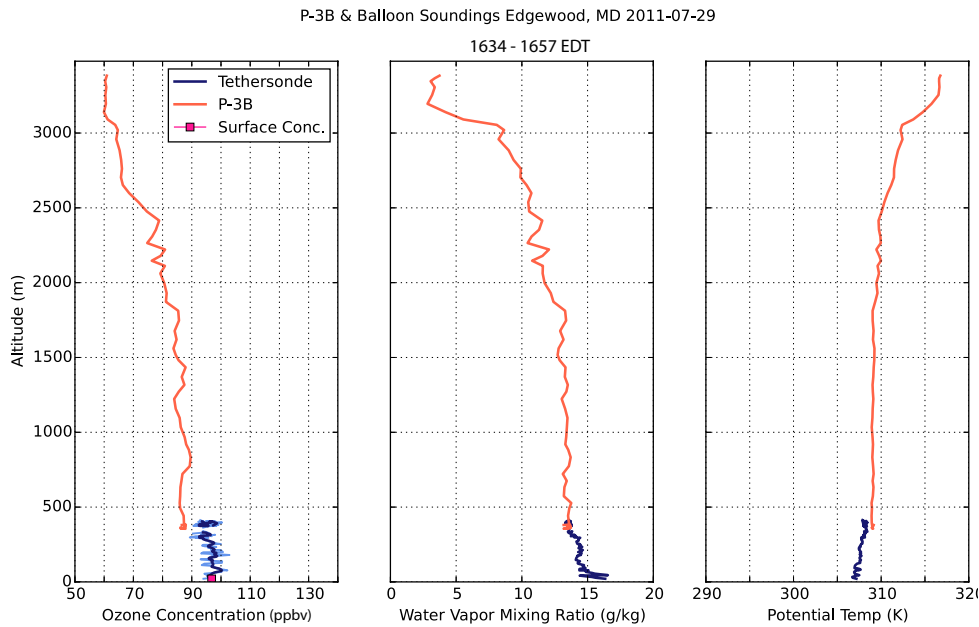


Figure 2.6 07/29/2011 Late afternoon blended profile of the third circuit P-3B spiral over Edgewood (orange) and the corresponding Millersville tethersonde sounding (blue) of O₃ concentration, water vapor mixing ratio, and potential temperature from the surface to ~4000 m; surface O₃ concentration (pink dot). The tethersonde profile was taken ~25 minutes before the P-3B spiral, resulting in somewhat greater disparity between platforms.

By 18:00 EDT, the bay breeze returned and remained for ~2 hours (Figure 2.5; Table 2.2). Around 20:00 EDT, the bay breeze was terminated by NW flow from a gust front heading southeastward from southern Pennsylvania / northern Maryland as shown by the Sterling, VA radar (KLWX) in Figure S6.

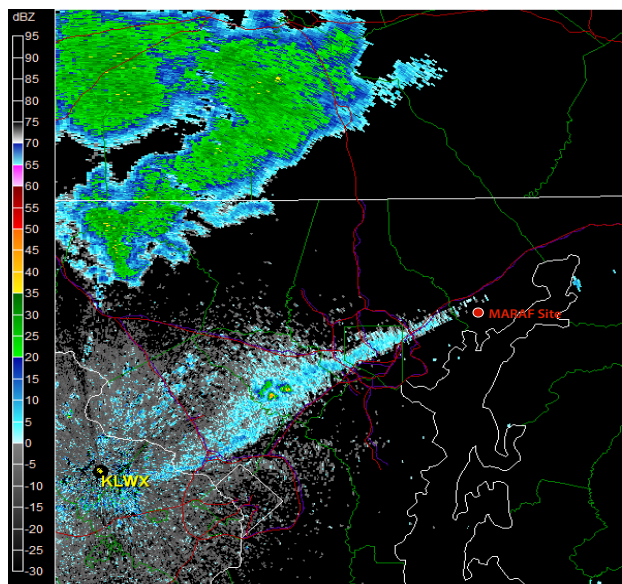


Figure S6. 07/29/2011 Sterling, VA (KLWX) radar reflectivity in dBZ of gust front passage over the MARAF site at 00:03 UTC (20:03 EDT).

With the passage of the gust front, specific humidity decreased from 18.4 to 13.4 g/kg, temperature decreased from 36.4 to 35.6 degrees C, and O₃ concentration dropped from 88 to 67 ppbv (Figure 2.5).

2.4 Gulf and Bay Breeze Case Study: Smith Point, TX 25 September 2013

The effects of local meteorology on this day resulted in the highest instantaneous measured O₃ during all of the DISCOVER-AQ deployments. Leading up to 25 September 2013, and for most of the DISCOVER-AQ Houston deployment, onshore flow dominated at Smith Point. The event on 25 Sep was not part of a ramp up pollution episode or heat wave common to high pollution case study events, but instead, the result of postfrontal and local wind shifts carrying polluted air masses. On this day, the local winds behind the front were northerly and pollution observed at

Smith Point was, largely, a function of the flow from Houston industrial area and chemical plants. The localized Houston pollution that accumulated over the bay and gulf was recirculated back over the research site at Smith Point by the gulf and bay breeze around 17:30 CDT (UTC-5) with O₃ concentrations of 175 ppbv observed at the surface at Smith Point.

2.4.1 Synoptic Conditions, Local Winds, and Air Quality Observation Overview

In the early hours of 25 September 2013, a weak cold front stemming from a low over NW Arkansas moved SE over the Gulf of Mexico. High pressure filled in behind this front and a ridge was in place over much of the south-central United States by 12 UTC (07:00 CDT) featuring subsidence over southeast Texas (Figure S7).

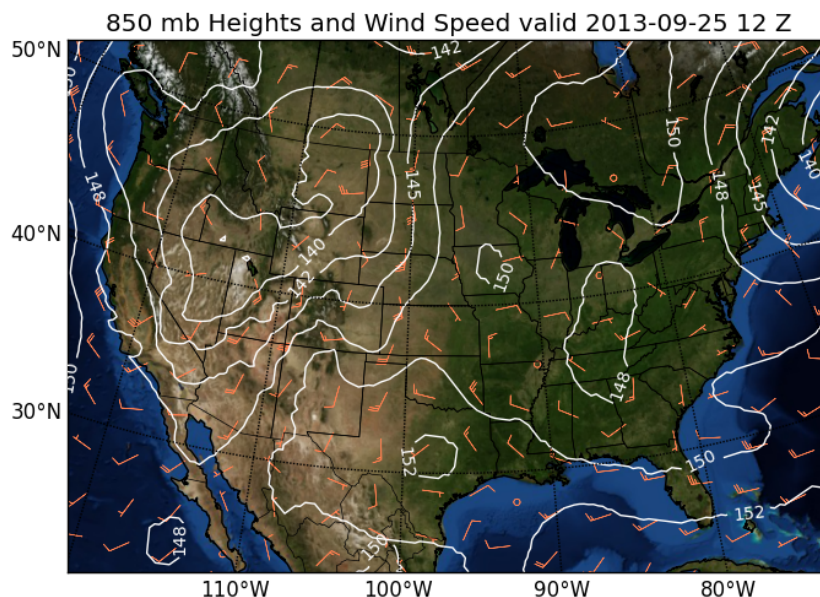


Figure S7. NCEP North American Regional Reanalysis (NARR) 850 mb geopotential heights (white lines) and wind barbs (orange barbs) on 09/25/2013 at 12 UTC (07:00 CDT) over the U.S.

At 10:00 CDT, SODAR (Figure 2.7; colored background) detected a near-surface wind shift from WSW to N bringing higher concentrations of NO_y to Smith Point.

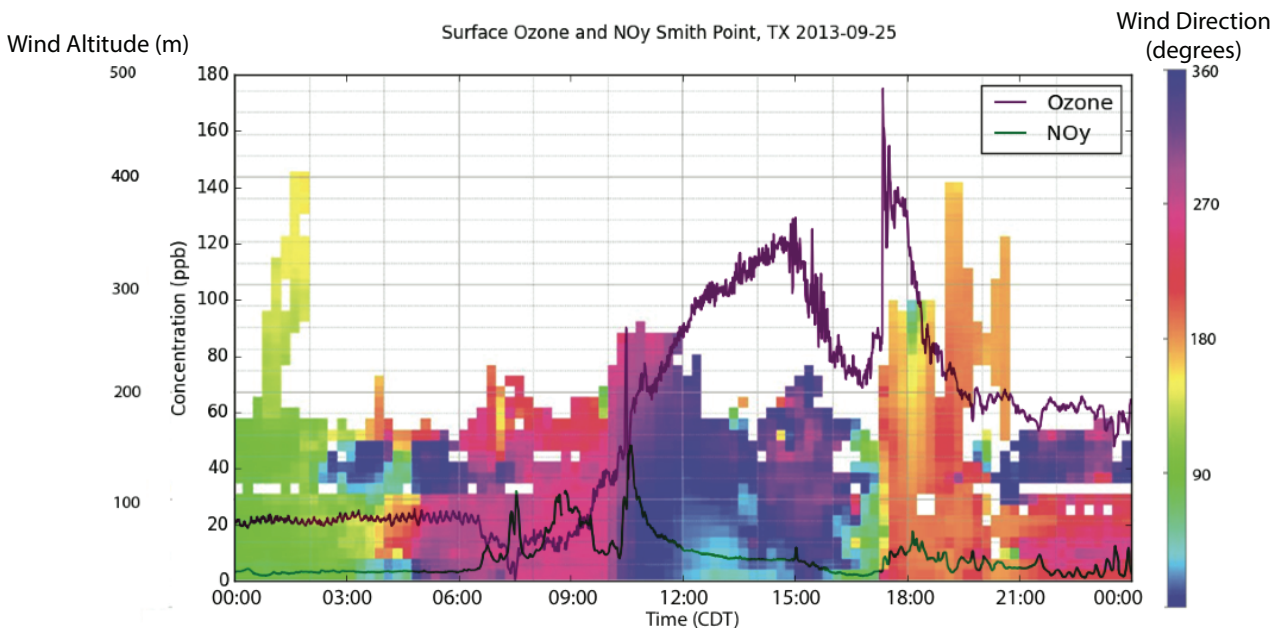


Figure 2.7 09/25/2013 Smith Point, TX MARAF site wind direction with height derived from SODAR (colors) and NATIVE surface trace gases: O_3 (purple) and NO_y (green). Note: consistent buildup of O_3 under NW winds was followed by a spike as winds shifted to SW around 17:00 EDT, which brought photochemically aged smog to the site.

Refineries and chemical plants in Baytown and Deer Park lie to the NW and NNW of Smith Point. While O_3 was increasing since 7:00 CDT, an abrupt jump in O_3 concentration was observed at the surface around 11:00 CDT, most likely due to mixing down of higher concentrations of O_3 and precursors. From 12:00 to 15:00 CDT, surface winds were NNE while winds at 130 m to 200 m were NNW and NW. The NNW and NW winds were associated with the transport of O_3 and precursors of O_3 to Smith Point as shown by the tethered balloon profiles in Figure S8. These profiles, which started at 13:14 CDT, exhibit peaks in O_3 concentration of 220 ppbv

and 200 ppbv with NO_y concentration of 18 ppbv between 100 and 200 m with low NO_2 concentration.

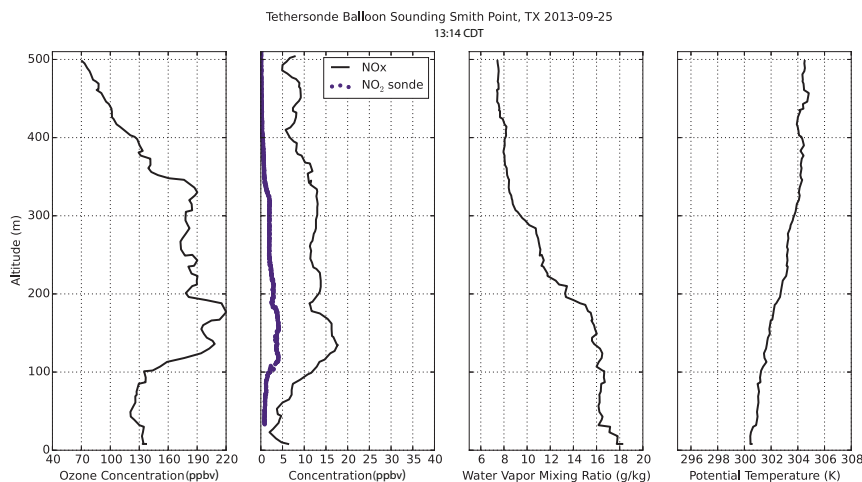


Figure S8. 09/25/2013 Millersville University tethersonde sounding of O_3 , NO_x , NO_2 sonde, water vapor mixing ratio concentration and potential temperature from the surface to 500 m at Smith Point.

O_3 continued to increase at the surface under northwesterly winds until easterly winds at 16:00 CDT brought a brief respite, that lasted until 17:00 CDT. At this time, gulf and bay breezes brought the poorest air quality of the campaign – O_3 concentrations at the surface soared from 70 ppbv to 175 ppbv. By 20:00 CDT, O_3 concentrations retreated between 60 and 70 ppbv (Figure 2.7).

2.4.2 Transport to Smith Point from Major Sources

During the first P-3B circuit of the day at 9:48 CDT, the aircraft flew over the largest petrochemical facility in the U.S. near Baytown (29.741N, 95.010W), and formaldehyde (CH_2O) concentrations rose dramatically (Fried et al. AQRP report, 2016) to 18 – 20 ppbv. CO concentrations were between 500 – 600 ppbv and NO_y

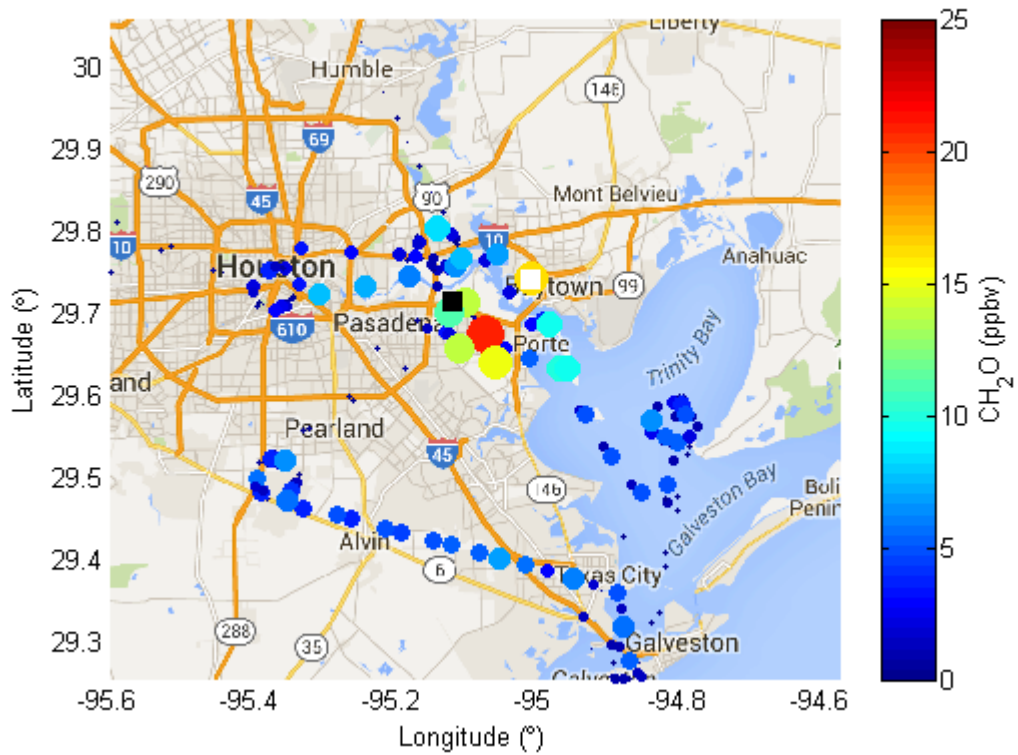
concentrations were between 45 - 50 ppbv (Figure 2.8; concentrations located near the white square).

As the P-3B made its closest approach near Deer Park (29.703, - 95.131) during the first circuit around 11:21 CDT, CH₂O concentrations were between 8-12 ppbv; CO concentrations were between 480 – 520 ppbv and NO_y concentrations between 55-60 ppbv (Figure 2.8; concentrations near the black square).

a)

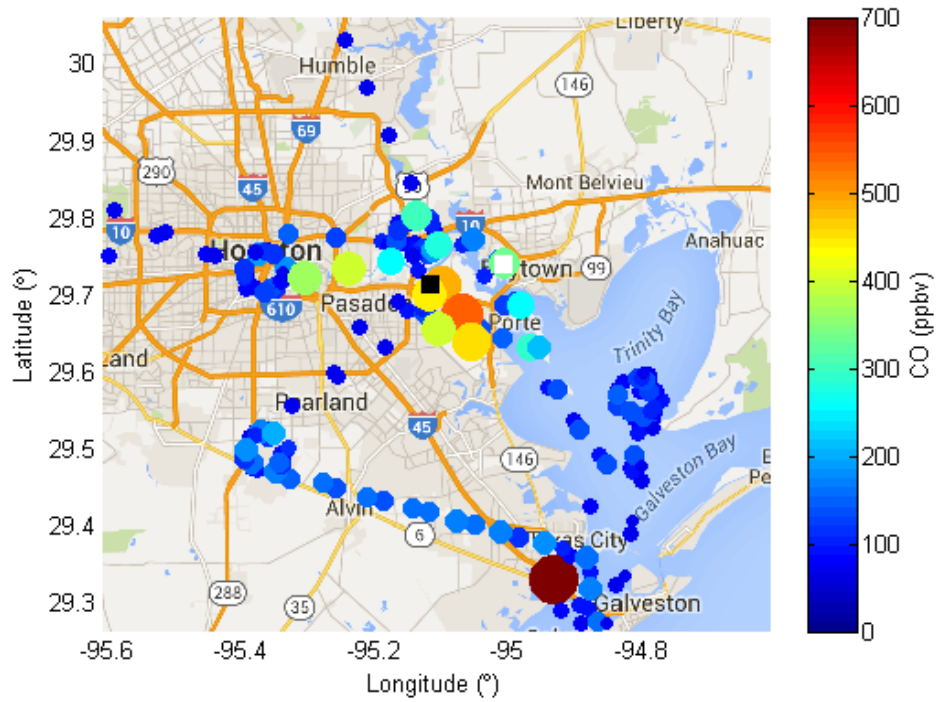
P-3B CH₂O September 25, 2013

Circuit 1



b)

P-3B CO September 25, 2013
Circuit 1



c)

P-3B NO_y September 25, 2013
Circuit 1

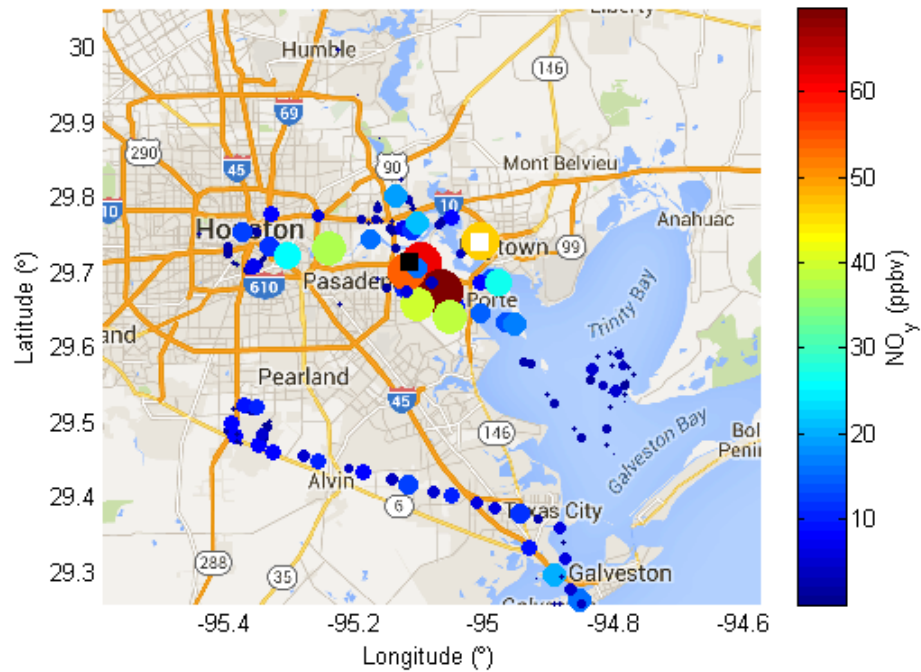
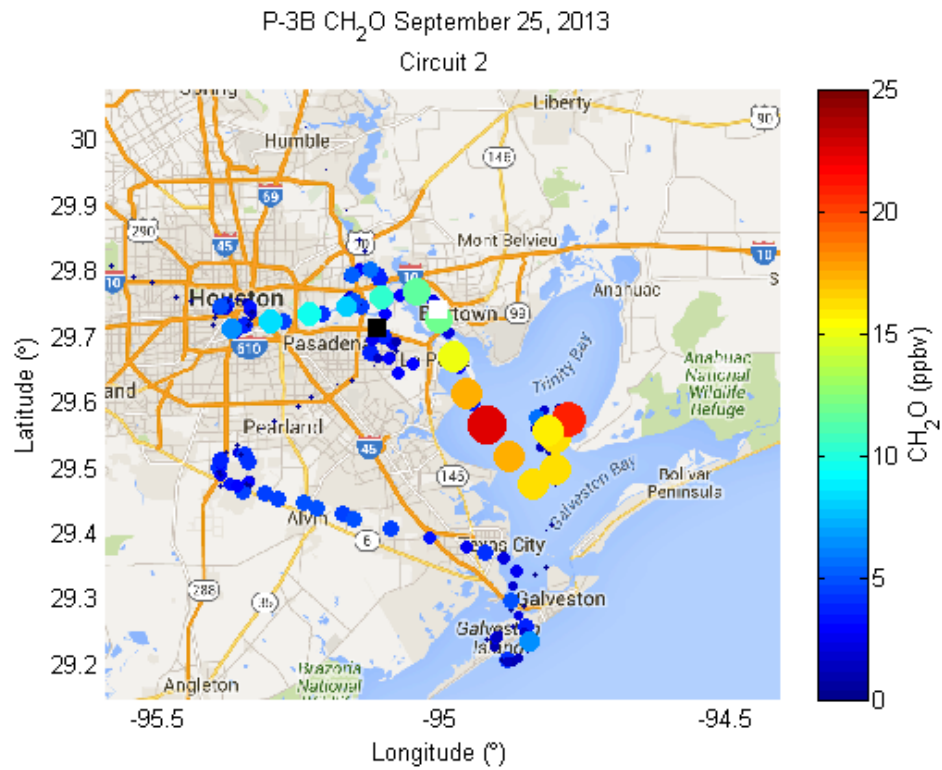


Figure 2.8 09/25/2013 (a) CH₂O, (b) CO, and (c) NO_y concentrations measured on the P-3B flight track during the first circuit. Black square is location of Deer Park and white square is location of Facilities at Baytown.

During the second circuit (12:15 – 12:28 CDT), a polluted air parcel from the Baytown and Deer Park area was observed downwind, over the Galveston Bay and at Smith Point (Figure 2.9).

a)



b)

Figure 2.9 09/25/2013 (a) CH₂O, (b) CO, and (c) NO_y concentrations measured on the P-3B flight track during the second circuit

CH₂O concentrations were between 20-23 ppbv, CO concentrations were 300-400 ppbv, NO_y between 0-5 ppbv, and O₃ 110-145 ppbv. The combined P-3B and tethersonde profile during this spiral shows an elevated layer of O₃ between 400 m. Due to small differences in time and space between the P-3B and the tethersonde, the P-3B measured a NO_y plume at 100 m with an associated decrease in O₃, which was not observed by the balloon. This is likely due to NO titration from a local emission source (Figure 2.10).

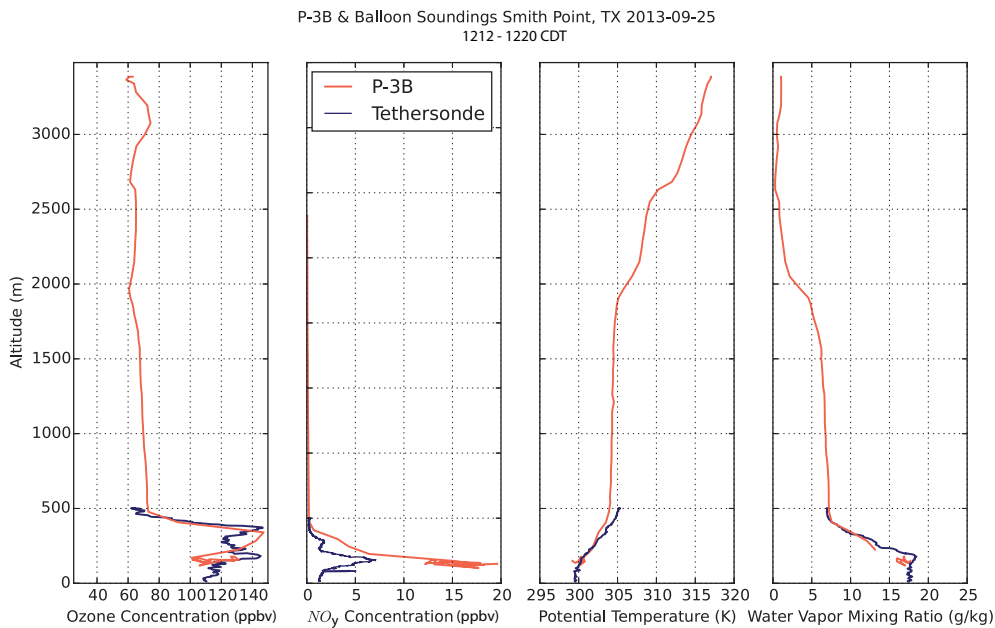


Figure 2.10 09/25/2013 Blended profile of the second circuit P-3B spiral over Smith Point (orange) and the corresponding Millersville tethersonde sounding (blue) of O₃ concentration, NO_y concentration (NO_x with interferences from other reactive nitrogen species on tethersonde), water vapor mixing ratio, and potential temperature from the surface to ~4000 m. The P-3B measured a NO_y plume at ~100 m that the tethersonde did not due to temporal and spatial differences between the soundings.

The tethered balloon continued to profile between the second and third P-3B overpasses. In the next set of tethered balloon profiles from 12:56 to 13:59 CDT, the highest concentration of O_3 was observed within the first 500 m at Smith Point due to photochemistry from significantly elevated precursors emitted upwind (Figure 2.11).

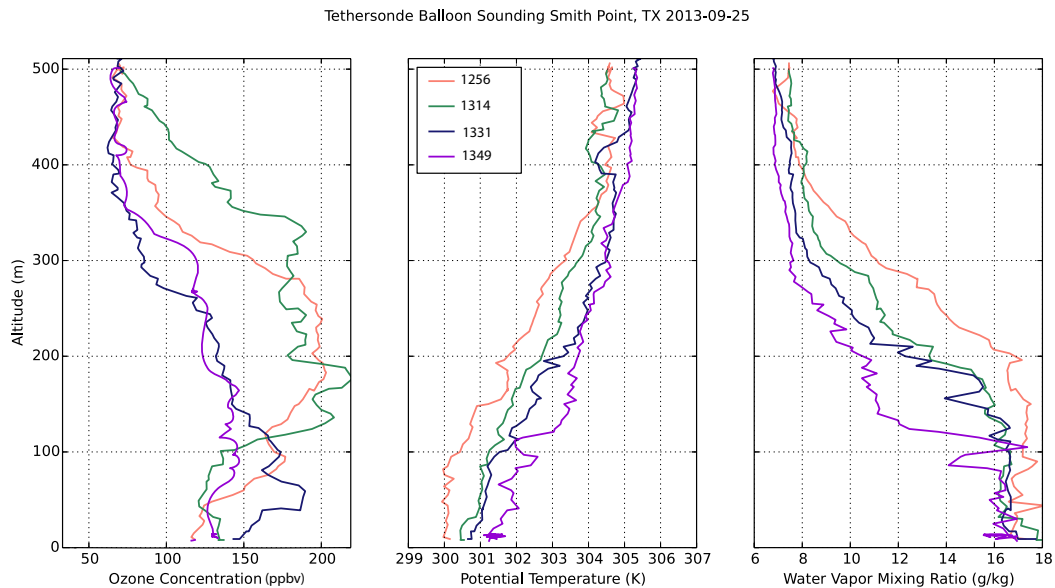
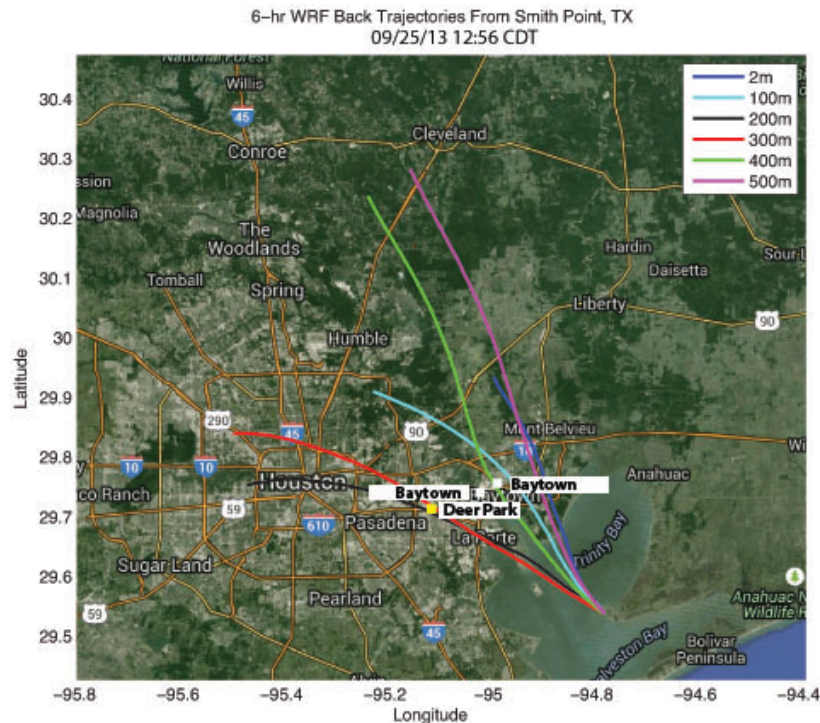


Figure 2.11 09/25/2013 Tethersonde soundings of O_3 concentration, potential temperature, and water vapor mixing ratio at Smith Point from 12:56 – 13:49 CDT from the surface to 500 m.

Six-hour backward trajectories at 1 km horizontal resolution (WRF; Skamarock et al., 2008) were run at six initialization altitudes relevant to the tethered balloon at Smith Point (2, 100, 200, 300, 400, and 500 m). The trajectory and wind directions agree with measured surface wind direction with variations in near-surface vertical wind shear observed by SODAR. The back trajectory from the first profile, which started at 12:56 CDT (Figure 2.12a), shows that air passed over the Deer Park plants between 200 and 300 m altitude. This corresponds to the layer of

highest O₃ concentration from the first sounding in Figure 2.11 (red) in the layer between 125 m and 275 m. At 13:14 CDT, the sounding in Figure 2.11 (green) shows O₃ concentrations of 220 ppbv between 100 and 200 m altitude, which correspond to air coming from the facilities near Baytown at 100 m and air from the Deer Park Plants at 200 m according to the WRF back trajectory (Figure 2.12b). The sounding at 13:31 CDT Figure 2.11 (dark blue) showed that O₃ concentration retreated to mostly below 150 ppbv from 150 m to 500 m and increased to 180 ppbv in a shallow layer between 25 m and 75 m. By 13:49 CDT, the entire tethered sonde profile retreated to O₃ concentrations below 150 ppbv from the surface to 500 m (Figure 2.11; purple sounding).

a)



b)

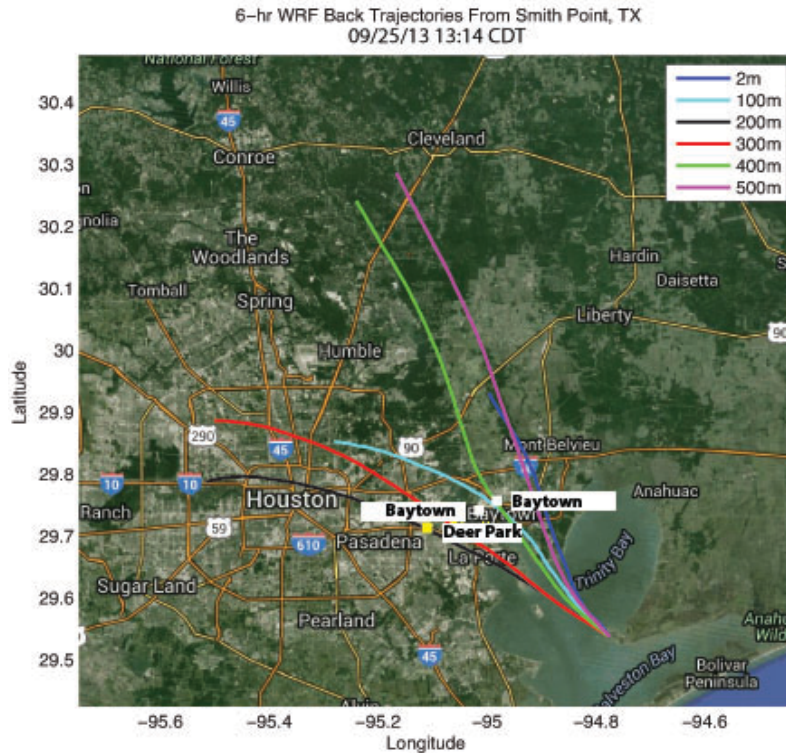


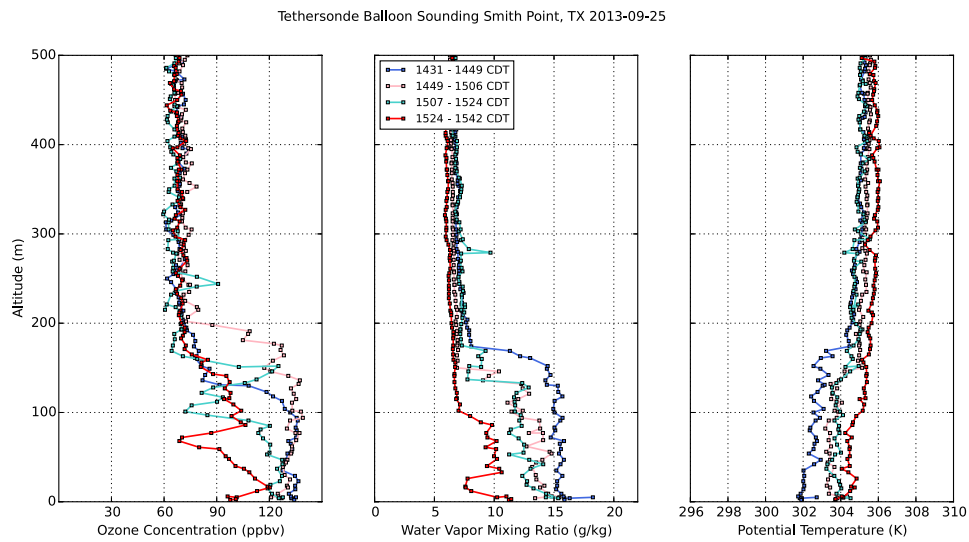
Figure 2.12 Six-hour WRF back trajectories at six initialization altitudes (2 m, 100 m, 200 m, 300 m, 400 m, 500 m) from the location of the tethered sonde at Smith Point. (a) Initialized at 12:56 CDT (b) Initialized at 13:14 CDT

2.4.3 Recirculation from Bay and Gulf Breezes

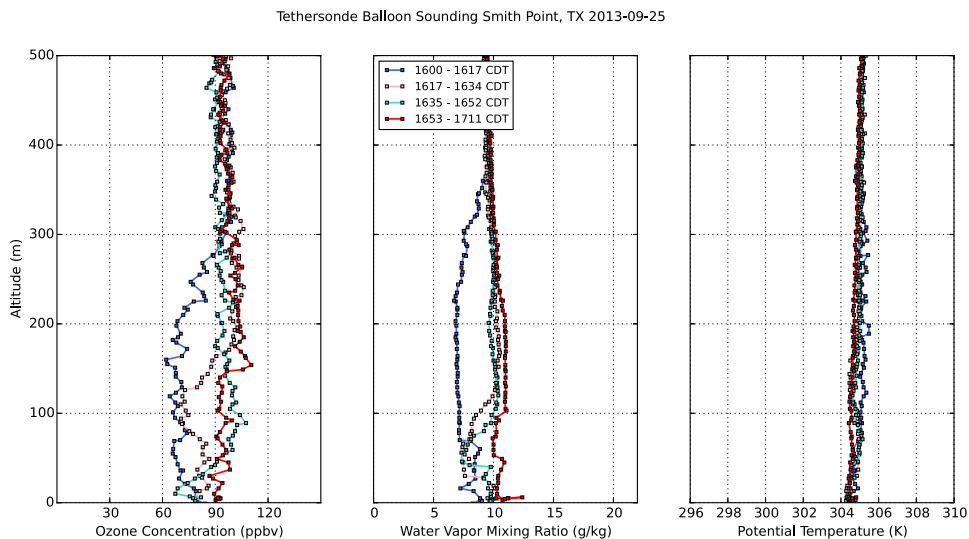
Northwesterly winds throughout the day transported pollutants offshore over the Galveston Bay and the Gulf of Mexico where secondary pollutants formed; these later returned to Smith Point in the strongest episode of the campaign. An intense, O_3 -rich, shallow layer only 200 m deep was observed in the vertical balloon soundings between 14:31 – 15:42 CDT due to the static stability of the air over the relatively cool surface of the bay. In this series of balloon soundings, the shallow marine boundary layer was diluted and warmed by mixing with free tropospheric air from aloft (Figure 2.13a). Around 15:00 CDT, a negatively buoyant thermal that

overshot its neutral level fell down back into the mixed layer, bringing with it drier free tropospheric air. This was also associated with a wind directional change from NNE to NNW at the surface. A combination of this warmer, drier air that entrained into the boundary layer as well as the easterly wind shift observed around 16:00 CDT diluted the amount of O₃ and water vapor observed within the first 200 m above the surface (Figure 2.13b).

a)



b)



c)

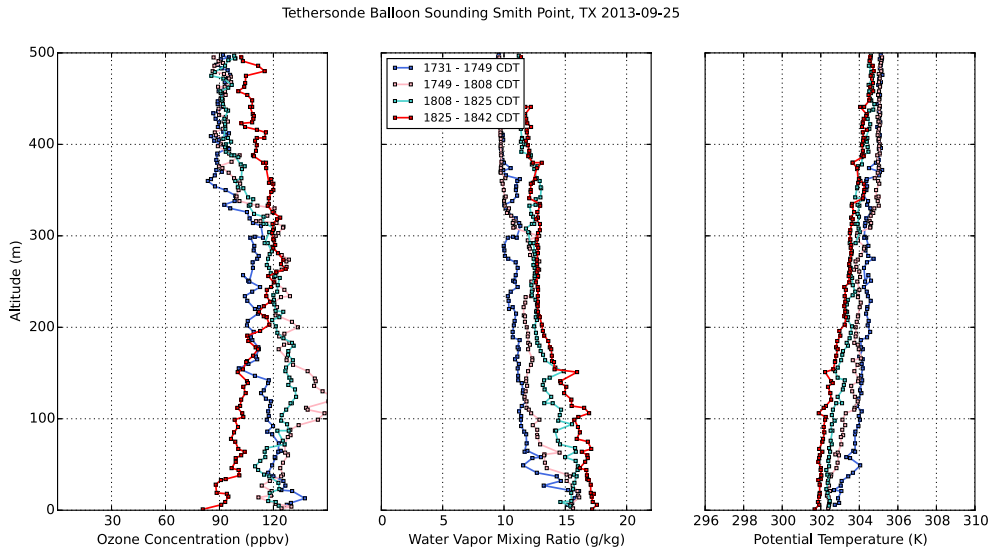


Figure 2.13 09/25/2013 Tethersonde soundings of O₃ concentration, water vapor mixing ratio, and potential temperature at Smith Point from (a) 14:31 – 15:42 CDT, (b) 16:00 – 17:11 CDT, (c) 17:31- 18:42 CDT from the surface to 500 m

By 17:30 CDT, the gulf and bay breezes made their way over Smith Point (Figure 2.14). At the surface, O₃ concentration rose from 80 to 175 ppbv during the bay breeze passage (Figure 2.7).

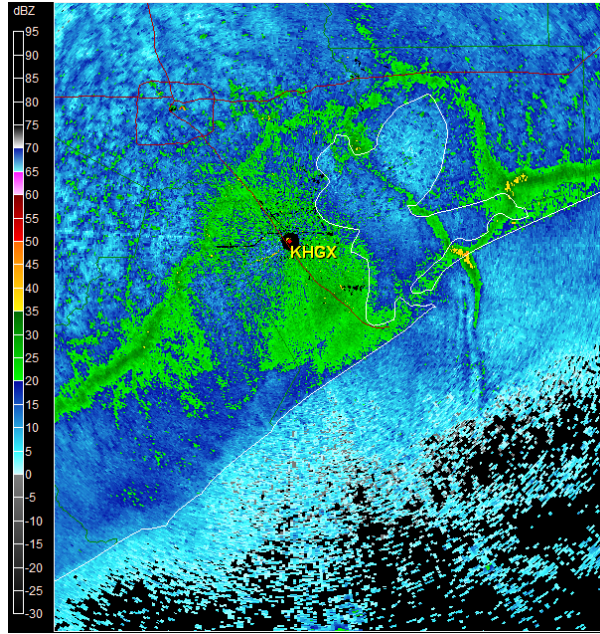


Figure 2.14 09/25/2013 Houston/Galveston, TX (KHXG) radar reflectivity in dBZ of the bay and gulf breezes at 22:30 UTC (17:30 CDT) passing over Smith Point.

Water vapor mixing ratio increased from 9 to 18 g/kg, temperature decreased from 36 to 32 degrees C, and wind direction shifted from E to SW during the passage of the bay breeze between 17:28 to 18:00 CDT (Figure 2.15). This stagnant, O₃-rich air at the edge of the gulf breeze and bay breeze front acted as a convergence zone for ascent of air. The associated O₃ concentrations were 120 ppbv from the surface to 100 m and up to 150 ppbv at 100 m – 320 m by 17:49, as observed by the tethered sonde soundings. By 18:25 CDT, O₃ concentrations of 120 ppbv were observed within the layer between 200 to 360 m while the surface concentration retreated to 90 ppbv (Figure 2.13c).

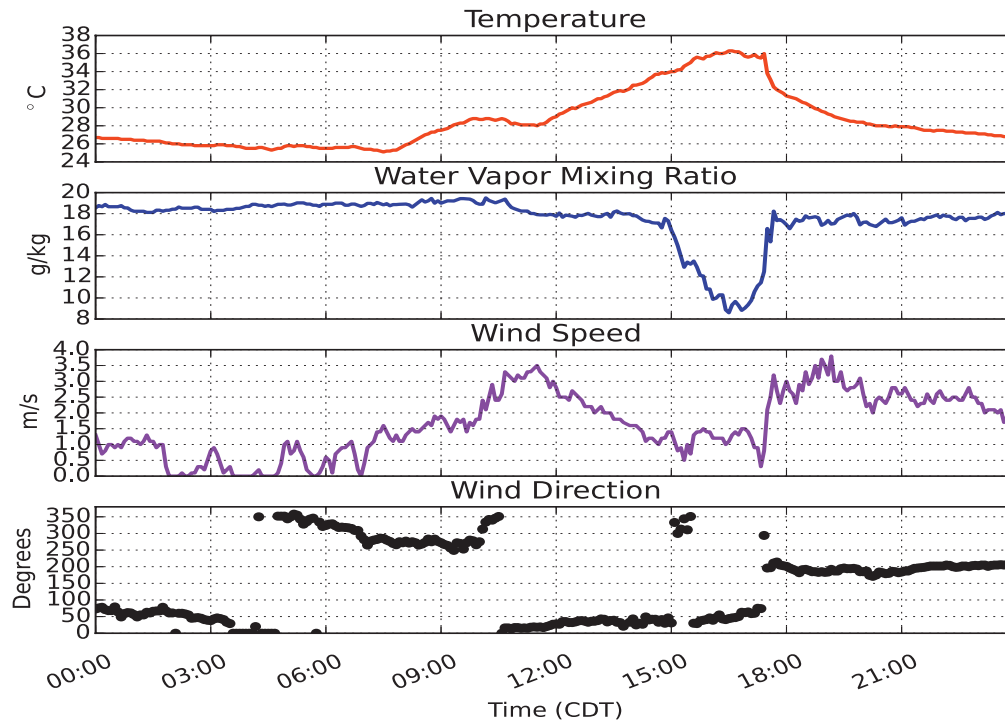


Figure 2.15 09/25/2013 surface WeatherPak observations of temperature, water vapor mixing ratio, wind speed, and wind direction from MARAF platform at Smith Point.

2.5 Discussion and Conclusions

2.5.1 Discussion

Microscale and mesoscale meteorological processes are essential to understanding and forecasting the dispersion of background and local pollution through growing boundary-layer/frontal mixing and bay/gulf breezes. Shown here are case studies where high O_3 events were directly influenced by boundary-layer dynamics and recirculation of air driven by thermally direct circulations. While the theme for coastal pollution recirculation is the same for each case – pollutants are transported out to the adjacent body of water where concentrations increase and are

transported back over the land when the bay or gulf breeze forms, specific and important differences remain between these two cases.

The case study in Edgewood, MD (29 July 2011) demonstrates both vertical mixing and bay breeze phenomena. Entrainment shortly after sunrise led to an increase in surface O_3 from around 25 to 75 ppbv within two hours. Back trajectories show that O_3 aloft originated over western and central Pennsylvania six hours earlier, and from near Baltimore one hour before. Later that day, the bay breeze reached the Edgewood site first as a shallow, short-lived (10 min) burst of O_3 above 100 ppbv, reformed several hours later as a smaller bay breeze, and then reformed once again as a larger-scale incursion lasting roughly two hours. O_3 concentration remained above 85 ppbv for 4 hours after due to the second and third bay breezes. In all bay breeze events, the air showed meteorological characteristics of having been over the Chesapeake Bay – lower temperatures and higher humidity. These air parcels also showed chemical signatures characteristic of reduced venting – higher concentrations of primary pollutants CO and NO_x as well as O_3 , where the latter could be the result of faster photochemistry over the cloud-free bay. These bay breezes were frequent, but not strong enough to penetrate inland to areas not directly influenced by the coast (e.g., the breeze that did not affect the Edgewood site ~3km inland but did affect the site located directly on the coast). Edgewood's coastal location, at a convergence zone with specific mesoscale dynamics, is a key factor for unique pollution episodes not seen at other MDE monitoring stations.

The case study at Smith Point, TX demonstrated a broad mid-to-late day event with O_3 in excess of 80 ppbv for 5 hours when NW winds aloft brought pollution

from the Port of Houston area, including petrochemical plants, that mixed to the surface at Smith Point. Around 17:30 CDT, the winds shifted dramatically to the south / southwest bringing air from over the gulf and the Galveston Bay to the MARAF and NATIVE site, with concentrations of O₃ that exceeded 125 ppbv at the surface for over an hour.

For this case, light to calm winds throughout most of the afternoon allowed the pollution to stagnate and build up over Houston, Galveston Bay and the gulf where active photochemistry occurred for an extended period of time. Concentrations of O₃ observed at Smith Point were mostly due to the transport of precursors from the chemical plants and the Houston Metro area. A major shift in wind as the bay and gulf breeze developed in the early evening resulted in a huge impact on pollution at the surface, over a broad horizontal extent.

In both cases, the marine boundary layer was shallow, resulting in the buildup of O₃ concentrations confined to a wedge close to the surface as it passed over land. Edgewood experienced an extremely shallow bay breeze < 100 m deep with O₃ surface concentrations between 113 ppbv and 75 ppbv around 100 m. Conditions measured at Smith Point were also representative of a shallow marine boundary layer, however, this was not part of the bay breeze passage that occurred later in the day. Smith Point, on a small peninsula in Galveston Bay, is susceptible to marine-like conditions without much forcing from specific bay breezes. The profiles that captured the conditions of the marine boundary layer over Smith Point measured a shallow layer < 200 m deep with O₃ surface concentrations between 132 and 70 ppbv around 200 m. These observations further demonstrate the buildup of O₃ concentration over

the bay due to slower deposition rates, higher photolysis rates, and trapping of emissions over the bay, as discussed by Goldberg et al. [2013].

Differences between Edgewood and Smith Point arise from the locations relative to large bodies of water, types of emissions from urban centers, and regional buildup of background concentrations over several days vs. a quick burst of local emissions. Detailed case studies as described here are important for determining meteorological conditions and relevant scales (i.e., synoptic, mesoscale, and microscale) of pollution episodes. This knowledge can lead to better air quality forecasts. Most regional atmospheric chemistry models, such as the Community Multiscale Air Quality model (CMAQ) in regulatory or forecasting operational mode, are run at 12-km resolution and have difficulty resolving some of the drivers of the largest pollution episodes such as vertical transport and horizontal gradients near coastal sites. Higher resolution (< 4 km) is required to resolve bay/gulf breezes (Loughner et al., 2011). However, CMAQ run at 1 km for both Edgewood and Smith Point was unable to capture the high O_3 transport due to the multiple bay breeze circulations from the Chesapeake Bay at Edgewood and the single, strong bay breeze from the Galveston Bay at Smith Point. Despite the inability to produce effects of the bay breeze at Smith Point in CMAQ largely due to the low emissions bias upwind of this location, the model was able to accurately represent the gulf breeze over the immediate Houston area during this day's event. This could be due to the much larger spatial extent along and across the gulf breeze frontal boundary. Thus, accurate representation of these phenomena can sometimes be difficult even at fine spatial

resolution (1 km) depending on frequency, duration, biases in upwind emissions, and horizontal/vertical extent of the bay breeze event.

2.5.2 Conclusions

The tethersonde is a powerful tool for studying composition and circulation in the lowest few hundred meters of the atmosphere, where air can be quickly mixed vertically, pollutants have the greatest impact on human health, and where aircraft measurements may be restricted.

We present two case studies that exemplify the importance of mesoscale and microscale meteorological processes on air quality. Large concentration gradients can exist both vertically and horizontally due to small-scale meteorological features that are difficult to accurately predict. In the absence of perfect emissions inventories, a detailed model characterization of the flow at high resolution may be the only way to successfully resolve high pollution events in locations subject to bay/gulf breezes. In each case, the driving mechanism for the observed pollution episode is the coupling of chemistry and small-scale meteorological features. These coupled processes include:

- Mixing down of polluted air from the residual layer air
- A shallow marine boundary layer trapping emissions
- Localized wind shifts
- Recirculation of pollution from the meso-high set up over the bay/gulf and meso-low set up over the adjacent land.

The effects on air quality by thermally direct circulations are important to consider when analyzing data from monitoring stations susceptible to marine influences. While monitoring stations close to the bay or gulf will help characterize the marine effects, they may not be representative of the air quality over an adjacent metropolitan area. Many of the world's large cities are located near major bodies of water. For other cities with coastline configurations similar to those near Baltimore/Washington and Houston Metro, the results presented here may be helpful in understanding the circulation and causes of severe pollution events.

Chapter 3: Overall Impacts of Bay Breeze and Thunderstorm Circulations on Surface O₃ at a Site along the Chesapeake Bay from 2011-2016 (Mazzuca et al., 2018 – in review)

3.1 Introduction

Boundary-layer O₃, a secondary pollutant formed by complex chemical reactions, has been known to have negative effects on public health and plants by increasing the risk of mortality from respiratory ailments (Burnett et al., 1994; Bell et al., 2004; Jerrett et al., 2009) and harming vegetation photosynthesis (Chameides et al., 1999; Fishman et al., 2010). In addition to precursor emissions, O₃ at or near the surface is dependent upon meteorological conditions (i.e., cloud cover, incoming solar radiation, large-scale circulation, boundary-layer height and associated turbulence, temperature, and humidity) (Seaman and Michelson, 2000; Hegarty et al., 2007, Bloomer et al., 2009). The concentration of O₃ at the surface is regulated by the United States EPA as a criteria pollutant with a current standard of 70 (75 2008 standard) ppbv and is calculated as the daily maximum of an 8-hr running mean.

While areas commonly associated with high O₃ concentrations are at or downwind of metropolitan centers, coastal cities and regions are also frequently susceptible to these high concentrations due to thermally-direct recirculation events (e.g., sea, lake, bay breezes), or hereafter for this analysis, referred to as bay breezes. The bay breeze is a reasonably small-scale circulation feature that forms from a pressure gradient differential due to the temperature contrast between the air over land and water, favored in weak synoptic flow (Sillman 1999; Simpson 1994; Miller

et al., 2003; Wentworth et al., 2015). The conditions necessary for bay breezes to form are the same conditions that favor photochemical production of O₃: warm surface and air temperatures, light winds, ample solar radiation, and large-scale subsidence. When bay breezes occur, they can advect high concentrations of O₃, originally transported out over the bay with the mean flow, back over land (Sillman et al., 1993; Banta et al., 2005; Evtyugina et al., 2006; Darby et al., 2007; Loughner et al., 2011; 2014, Mazzuca et al., 2017) with additional buildup of O₃ precursor accumulation over the bay and less venting over the water (Goldberg et al., 2014). A study by Wentworth et al. (2015) found that sites in the Greater Toronto Area affected by the lake breeze circulation recorded O₃ at least 30 ppbv higher than sites outside the circulation.

In the Houston area, the likelihood of O₃ episodes has been shown to depend not only on rapid photochemical production and background concentrations, but also on decreasing concentrations due to convective venting by both shallow and deep convection (Langford et al., 2010). Vertical transport from deep convection can vent pollution up and out of the boundary layer, ultimately decreasing surface O₃ concentration (Thompson et al., 1994). In the case of a bay breeze and deep convection near bodies of water, horizontal transport from the bay can increase concentration of O₃ at the surface over the adjacent land in a situation where the marine boundary layer exhibits higher O₃, while vertical transport can potentially offset this increase in O₃ if these two events occur simultaneously or in close succession. It is therefore unknown what the net effect on O₃ concentration at the

surface will be given the combination of both a bay breeze and a thunderstorm during daylight hours.

While both bay breezes and thunderstorms have been shown to have a considerable influence on surface O₃ concentrations, the local net effect of these two mesoscale forcings has not yet been sufficiently quantified. This results in the following research questions:

1. What is the net effect on surface O₃ concentration from these mesoscale features when they occur both separately and in combination?
2. How does surface O₃ concentration respond to the occurrence of these mesoscale circulations as emissions of O₃ precursors are reduced?

In section 3.2, the monitoring site observations, the analysis methodology, the bay breeze detection algorithm, and the thunderstorm detection scheme are described. In section 3.3, results of the influence of bay breezes and thunderstorms are discussed. Section 3.4 focuses on modeling limitations, future use of the technique, and information gained from this analysis.

3.2 Data and Methodology

3.2.1 Observations and Characterization of the Analysis Site – Edgewood, MD

The site chosen for the study, Edgewood, MD (39.41N, 76.297W), an MDE monitoring station, is known for its high O₃ episodes. This site has observed the highest design value, calculated as the 3-year average of the 4th annual highest daily maximum 8-hour concentration of O₃ (ppbv), out of all of the Maryland O₃ monitors

from 2005- 2013, and the 2nd and 3rd highest from 2013-2016 (Table 3.1). The location was also chosen due to its proximity to the Chesapeake Bay and its associated rivers and estuaries, thus providing information about the meteorological influence at the land-water interface (Figure 3.1).

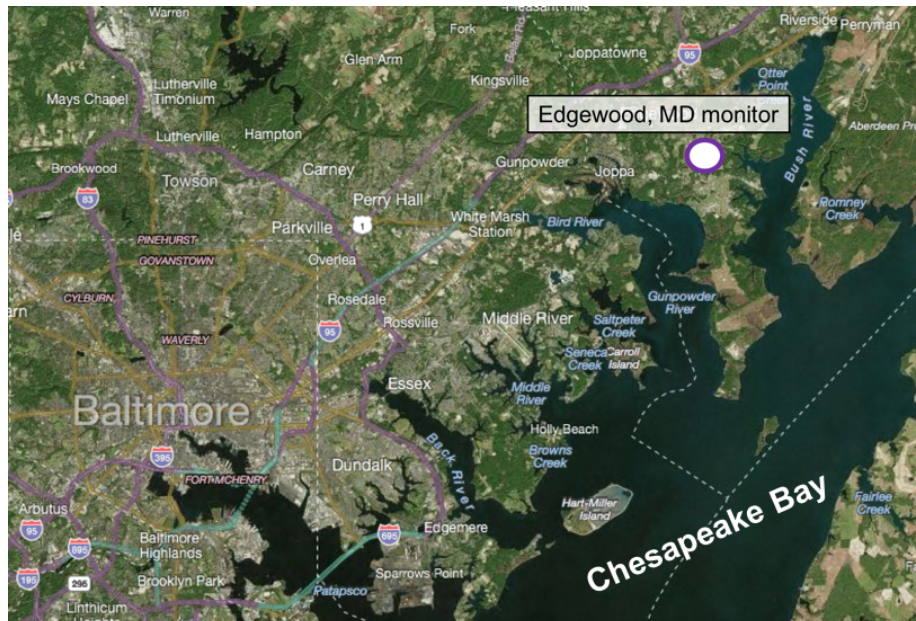


Figure 3.1 Location of the Edgewood, MD O₃ monitor and meteorological site (white circle) and its relative distance from the Chesapeake Bay, rivers, and a major urban area (Baltimore, MD).

Meteorological parameters (temperature, pressure, relative humidity, wind speed, wind direction) and the concentration of O₃ have been monitored for more than 20 years. This analysis incorporates 1-minute data provided by MDE between the hours of 11:00 – 19:00 Eastern Standard Time (EST; UTC-5) for June, July, and August from 2011 - 2016. This analysis also uses the annual list of the 8-hour O₃ concentrations exceeding the 2008 health-based National Ambient Air Quality Standard (75 ppbv) from MDE (2011-2016). (<http://mde.maryland.gov/programs/Air/AirQualityMonitoring/Pages/HistoricalData.aspx>)

A climatology (Figure 3.2) constructed for the Edgewood, MD site from 2011-2016 demonstrates the shift to stronger SSW winds during the warmest part of the day (~12 – 18 EST) in June and July from a light S/SE direction in the morning, likely by a combination of the synoptic SW winds and the bay breeze that is often also in the SW – SSW direction. The wind during the month of August shows more of a southerly component throughout the day. Figure 3.2 also shows the wind steadiness calculated as the ratio of scalar-averaged to vector-averaged wind speeds, where numbers closest to 1 represents steadier winds. The steadiness peak occurs during the warmest hours of the day in June, July, and August, likely associated with the bay breeze. There may also be a contribution to the wind steadiness peak in August from the synoptic setup, e.g., lee-troughing, as the bay-land temperature gradient is smaller due to a warm bay by late summer.

Table 3.1 EPA monitor-level design values calculated as the 3-year average of the annual 4th highest daily maximum 8-hour O₃ concentration (ppbv) at each O₃ monitor in Maryland (source: <https://www.epa.gov/air-trends/air-quality-design-values>). The colored boxes represent the highest design value (red), the second-highest design value (orange), and the third-highest design value (yellow) for each time bin. It should be noted that table does not account for the 2016 exceptional events in its design values.

	Design Values (ppbv)									
Local Site Name	2005-2007	2006-2008	2007-2009	2008-2010	2009-2011	2010-2012	2011-2013	2012-2014	2013-2015	2014-2016
Aldino	91	89	82	78	78	82	78	73	70	73

Beltsville							80	75	69	68
Blackwater NWR							75	70	66	66
Calvert	81	79	74	77	79	83	77	73	68	69
Davidsonville	90	87	80	79	81	87	81	74	69	
Edgewood	94	91	87	89	92	93	85	75	71	73
Essex	87	85	78	78	80	84	78	72	69	72
Fair Hill	93	90	84	80	81	86	82	77	73	76
Frederick Airport	83	82	76	75	76	79	74	70	67	67
Furley			67	67	74	75	72	64		69
Hagerstown	79	78	74	73	72	75	71	67	65	66
Horn Point								73	64	64
HU-Beltsville	85	83	78	78	79	82	76	70	68	69
Millington	83	83	78	75	74	82	80	74	69	70
Padonia	77	80	75	77	77	82	78	72	71	72
PG Equestrian Center	91	87	78	77	79	87	81	76	69	71
Piney Run	76	73	71	71	71	76	71	68	64	65
Rockville	86	84	78	74	76	77	74	68	68	68
South Carroll	86	83	78	76	76	79	74	69	67	68
Southern Maryland	85	82	75	75	77	83	78	73	68	70

Edgewood, MD Climatology 2011-2016

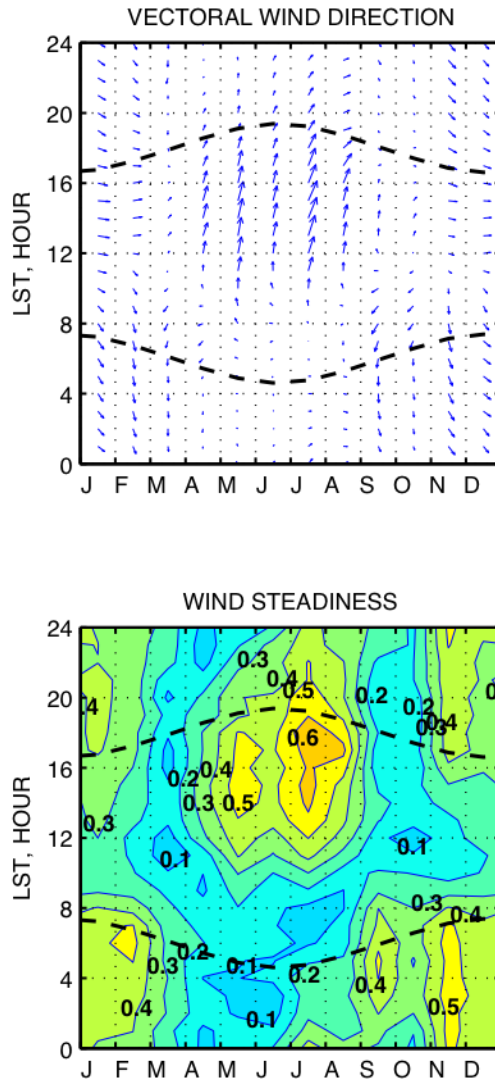


Figure 3.2 10-m wind climatology at Edgewood, MD from 2011-2016. Top: Vectorial wind direction with notable SSW-SW wind direction during peak heating times (09:00 – 17:00 EST) during June, July, and August. Bottom: Wind steadiness (the ratio of scalar-averaged to vector-averaged wind speeds, where numbers closest to 1 represents steadier winds) with peak values in July – August from ~13:00 – 17:00 EST, likely associated with bay breezes and other mesoscale circulations. The dashed horizontal lines in the top and bottom plots indicate the time of sunrise and sunset.

A positive correlation between O_3 and temperature has been well characterized (Jacob et al., 1993; Sillman and Samson, 1995; Bloomer et al., 2009; He et al., 2013) and is observed in the analysis shown this paper. Figure 3.3

demonstrates the relationship between O_3 concentration and temperature at Edgewood from 07:00 – 19:00 EST for 2011-2016 and then for 2013-2016 for the 5th, 25th, 50th, 75th, and 95th percentiles for the distribution of 1-hourly averaged O_3 concentrations. The slope for 2011-2016 is 2.78 ppbv/°C (Figure 3.3, left panel) whereas the slope for 2013-2016 is 1.76 ppbv/°C (Figure 3.3, right panel). The results agree with Bloomer et al., 2009, which analyzed the increase in O_3 per °C in two separate regimes (prior to 2002 and post 2002). The reported slopes from that paper in the Mid-Atlantic were 3.3 ppbv/°C (pre-2002) and 2.2°C (post 2002). In analysis presented here, the smaller slope for the years neglecting 2011 and 2012 can be expected since 2011 and 2012 were both anomalously warm and exhibited highest NO_x emissions of the 2011-2016 time period, thus yielding higher O_3 concentrations than the years following. The response of the highest concentrations of ozone to the highest temperatures seems to have changed from leveling off to accelerating, but the number of observations is small and requires further investigation.

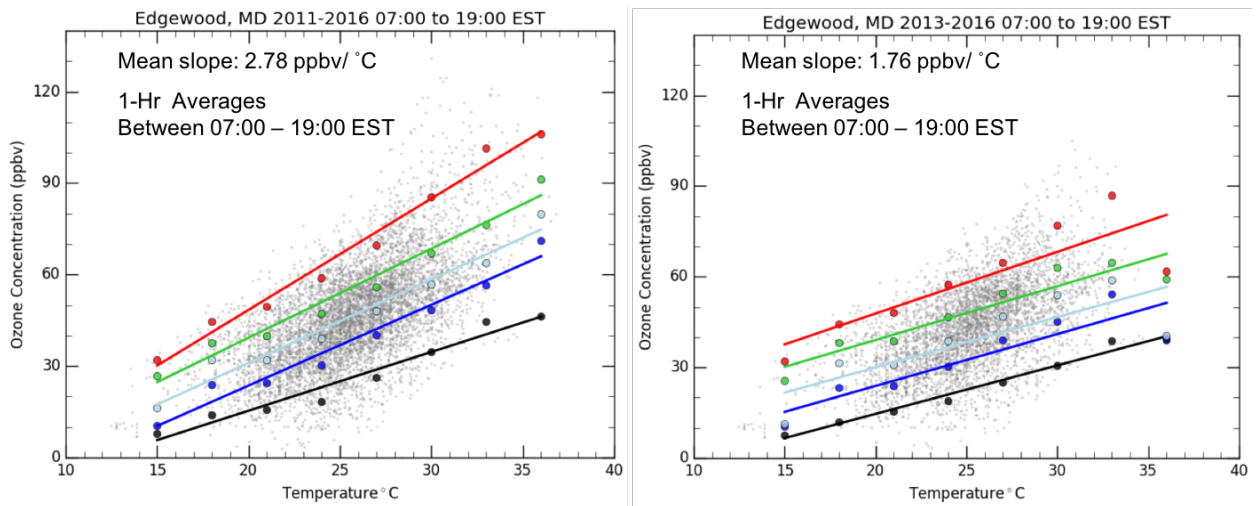
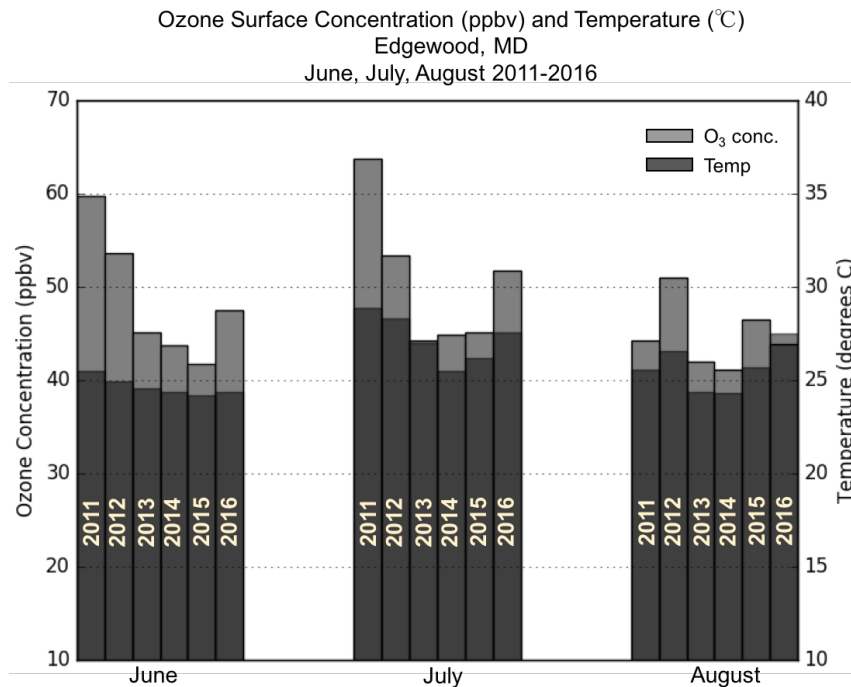


Figure 3.3 O_3 concentration (ppbv) vs. temperature (°C) in 3°C bins from 15 – 37°C with the colored lines representing the 5th, 25th, 50th, 75th, and 95th percentiles of the 1-hr averaged O_3 concentration (gray dots) between 07:00 – 19:00 EST at Edgewood,

MD. A higher slope is observed on the left pane (2011-2016) than the right (2013-2016) demonstrating the higher O₃ concentrations and temperatures observed in 2011 and 2012 compared to the other years of the analysis and the efficacy of abatement measures.

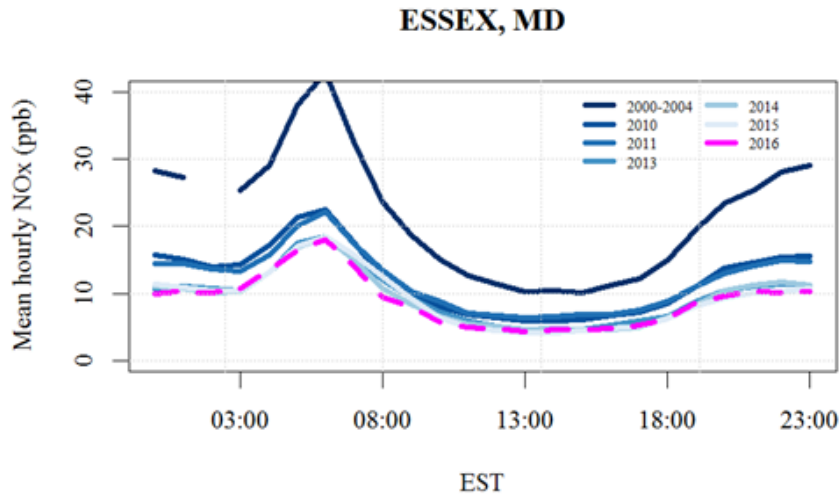
The relationship between O₃ concentration and temperature for each month and for each year during the analysis is further investigated in Figure S9, where 2011, 2012, and 2016 were highest for both temperature and O₃ concentration for June and July, but the highest temperature did not necessarily correspond with the highest O₃ concentration for August.



S9. Bar graphs of mean hourly O₃ concentration (light gray, left y-axis) and temperature (dark gray, right y-axis) for each year from 2011-2016 grouped by month for June, July, and August at Edgewood, MD. Notable from this graph are the higher O₃ concentrations and temperatures in June and July than August, especially in the years 2011, 2012, and 2016. August does not have the same yearly trend that June and July have for both O₃ concentration and temperature.

While 2016 was the warmest year for August, O₃ concentration was less than the previous year. It is important to note that there were significant reductions in the

mean NO_x concentration in the last 10 years in Maryland that are likely responsible for both the lower O₃ concentrations observed at Edgewood and the changing relationship between O₃ and meteorology. The reductions in NO_x concentrations are shown in Figure S10 at Essex, a MDE monitoring site near Edgewood, from 2010 – 2016. It noted in this figure that while NO_x concentrations have drastically decreased due to NO_x emissions controls since the 2000-2004 time period, 2011 observed relatively high NO_x concentrations compared to the concentrations observed between 2013-2016.



S10. Mean hourly NO_x concentrations at Essex, MD for years from 2000 – 2016 where 2000 – 2004 represents the pre-NO_x State Implementation Plan (SIP) to reduce NO_x concentrations.

3.2.2 The Bay-breeze Identification Algorithm (BIA)

Bay breezes were identified by a detection algorithm, the Bay-breeze Identification Algorithm (BIA), developed for this study. This algorithm applies a low-pass filter to 1-minute u and v components of wind data, which are then converted into wind direction and wind speed. The purpose of this filter is to exclude

noise, which may obscure the signal of the bay breeze. It is applied separately to the original data two times, for each. The spectral cut-off of the filters were adjusted such that two signals emerge, one encompassing a slowly varying signal (diurnal + synoptic) and the other a faster varying signal (mesoscale + diurnal + synoptic).

BIA uses the latitude and longitude of the location of interest to determine when the slower varying wind signal (diurnal + synoptic) and the faster varying wind signal (mesoscale + diurnal + synoptic) were in the direction of the water, by using the land-mask variable from WPS (the WRF Preprocessing System) output (Skamarock et al., 2008). By using the WPS land-mask variable, a user can easily obtain the coastal configuration at any latitude/longitude at a chosen resolution without having to run full WRF, making it computationally inexpensive, user-friendly, and easily accessible. The surface tiles have water flags to indicate whether surface water is present in the grid box. A search radius from 0 to n (where n is a user specified outer radius from the site location) determines whether a water flag exists at the surface tile in 1-degree azimuth bins from 0-360 degrees (Figure 3.4).

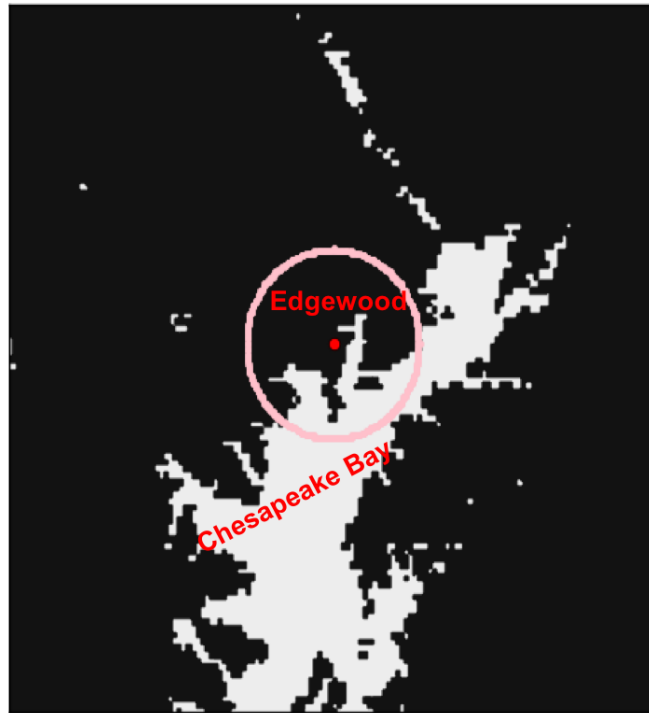


Figure 3.4 WRF WPS land-mask variable at 300 x 300 m resolution grid spacing where black is the land, white is the water (Chesapeake Bay and its associated estuaries), and the pink circle is the user specified search radius for land and water flags centered around Edgewood, MD.

The bay breeze flag is turned on when all of the following occur:

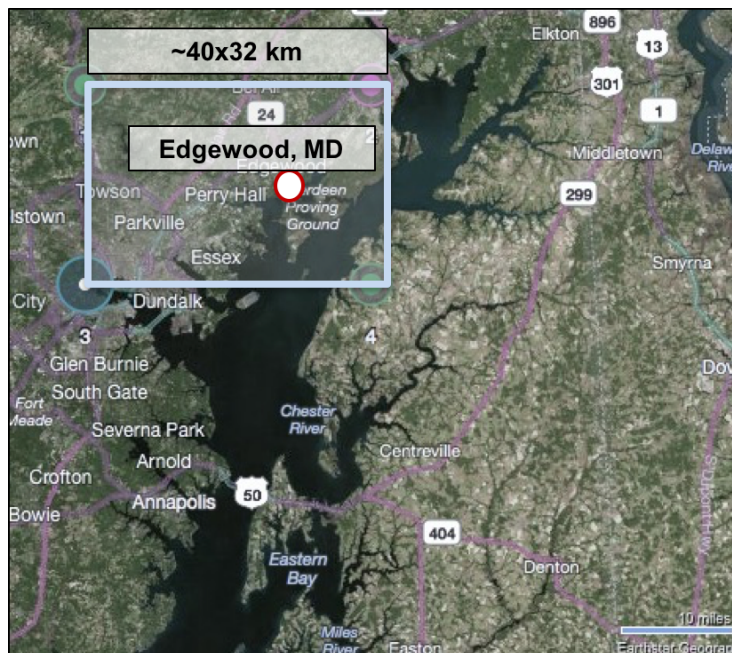
- Flag 1.** The direction of the faster varying signal is from the water (excluding the areas of extremely shallow inlets that are only a few meters or less in depth)
- Flag 2.** The direction of the faster varying signal deviates from the slower varying signal by a chosen threshold (in this case, 15°)
- Flag 3.** The slower varying signal is not out of the E to NNW directions for potential false-positives (350 - 90°)

Flag 2 serves to eliminate false-negatives in the case that the larger-scale (slower varying winds) are also coming from the water. Flag 3 helps to decrease the number of false-positives by excluding cases where the large-scale winds are from the NNW-

NNE, or, directions typically unconducive for bay breeze development (e.g., low-pressure circulation).

3.2.3 Thunderstorm Detection Criteria

Thunderstorm days were determined by using the Earth Networks Total Lightning Network (ENTLN) lightning data (provided by Earth Networks, Inc.) (Heckman, 2014) for the analysis time period within a user-specified latitude / longitude box, in this case, over Edgewood, MD (Figure S11).



S11. Latitude / longitude box for ENTLN lightning detection. Days are considered “thunderstorm days” at Edgewood, MD if lightning exists within the box of interest. The technique was successful when compared to one month of hand analysis radar reflectivity using a composite radar archive provided by the NWS.

The ENTLN data includes both intra-cloud (IC) and cloud-to-ground (CG) flashes within the latitude / longitude domain. Days where lightning was observed were further analyzed using the NOAA Weather Prediction Center (WPC) composite radar to verify the lightning technique accuracy. The WPC surface analysis was used to

determine whether the observed lightning was associated with frontal or pre-frontal convection vs. a pop-up air mass thunderstorm, which is a quasi-random event. For verification of the lightning detection technique, the thunderstorms identified by the lightning detection method were compared to and matched with areas of reflectivity from the radar composite for the month of July 2011.

3.3 Results

3.3.1 Bay Breeze Detection

3.3.1.1 BIA Validation

BIA was validated by identifying days that agreed with bay breezes detected in an analysis by Stauffer et al. (2015a) at the same site (Edgewood, MD) for each day in the month of July 2011 (Table 3.2). The bay breeze criteria in the Stauffer et al. analysis were as follows:

1. Wind shift from calm/off-shore to on-shore
2. Increase in dew point of at least 1°C within 1-hour after onset of wind shift
3. No fronts analyzed by the WPC analysis

The information in Table 3.2 demonstrates that BIA matched the Stauffer et al. analysis 87% of the days (27/31 days), while treating the latter as truth. The 4 days that differed consisted of 2 days with a potential false-positive and 2 days with a potential false-negative analyzed by the BIA. The automation of BIA allows for many years to be examined more easily than with a hand-analysis.

Table 3.2 Validation of the Bay-breeze Identification Algorithm (BIA) against bay breezes identified in Stauffer et al., 2015a. In the two columns labeled Stauffer et al. 2015a and BIA-data: **yellow shading**: Stauffer does not match BIA-data, **green shading**: Stauffer bay breeze matches BIA-data. In the column labeled BIA-RTMA: **yellow letter**: BIA-RTMA matches Stauffer analysis, but not BIA-data, **red letter**: BIA-RTMA does not match either of the other two other columns, **green letter**: BIA-RTMA bay breeze matches the BIA-data bay breeze. Plain black letter: techniques match each other on non-bay breeze days.

	Bay Breeze (Y/N)	Bay Breeze (Y/N)	Bay Breeze (Y/N)
Date	Stauffer et al. 2015a	BIA-data	BIA-RTMA
		(using 1-min data)	(using 1-hrly RTMA output)
7/1/11	N	N	N
7/2/11	Y	N	N
7/3/11	N	N	Y
7/4/11	N	N	N
7/5/11	Y	Y	Y
7/6/11	N	N	N
7/7/11	Y	Y	Y
7/8/11	N	N	N
7/9/11	N	N	N
7/10/11	N	N	N
7/11/11	N	N	N
7/12/11	N	N	N
7/13/11	N	N	N
7/14/11	N	Y*	Y
7/15/11	N	N	N
7/16/11	N	Y	N
7/17/11	N	N	N
7/18/11	N	N	N
7/19/11	Y	N	Y
7/20/11	N	Y	Y
7/21/11	N	N	N
7/22/11	Y	Y	N
7/23/11	Y	Y	N
7/24/11	N	N	N
7/25/11	N	N	N
7/26/11	Y	Y	Y
7/27/11	N	N	N
7/28/11	N	N	Y
7/29/11	Y	Y	Y
7/30/11	N	N	N
7/31/11	Y	Y	Y

3.3.1.2 BIA Detection of a Short-lived Event

Since bay breezes occur at varying spatial and temporal scales, identifying bay breezes that are short-lived, but have a significant impact on surface O₃ concentration can be difficult. In an analysis for 29 July 2011 at Edgewood, MD detailed in Mazzuca et al. (2017), two separate bay breezes were observed by changes in thermodynamic variables (temperature and water vapor mixing ratio) at the Edgewood MDE site, and three separate bay breezes were observed at a second Edgewood monitor closer to the bay, a measurement site set up for the DISCOVER-AQ project (MARAF location) At the MDE site, the first bay breeze had occurred from ~15:15 – 16:25 and the second bay breeze occurred from ~17:00 – 19:00 EST (Mazzuca et al., 2017). BIA detected two bay breezes, identical in both time and wind direction to the previously analyzed bay breezes (Figure 3.5). This demonstrates that BIA has the capability to detect short-lived and shallow bay breezes that can significantly increase surface O₃ concentration in a short amount of time.

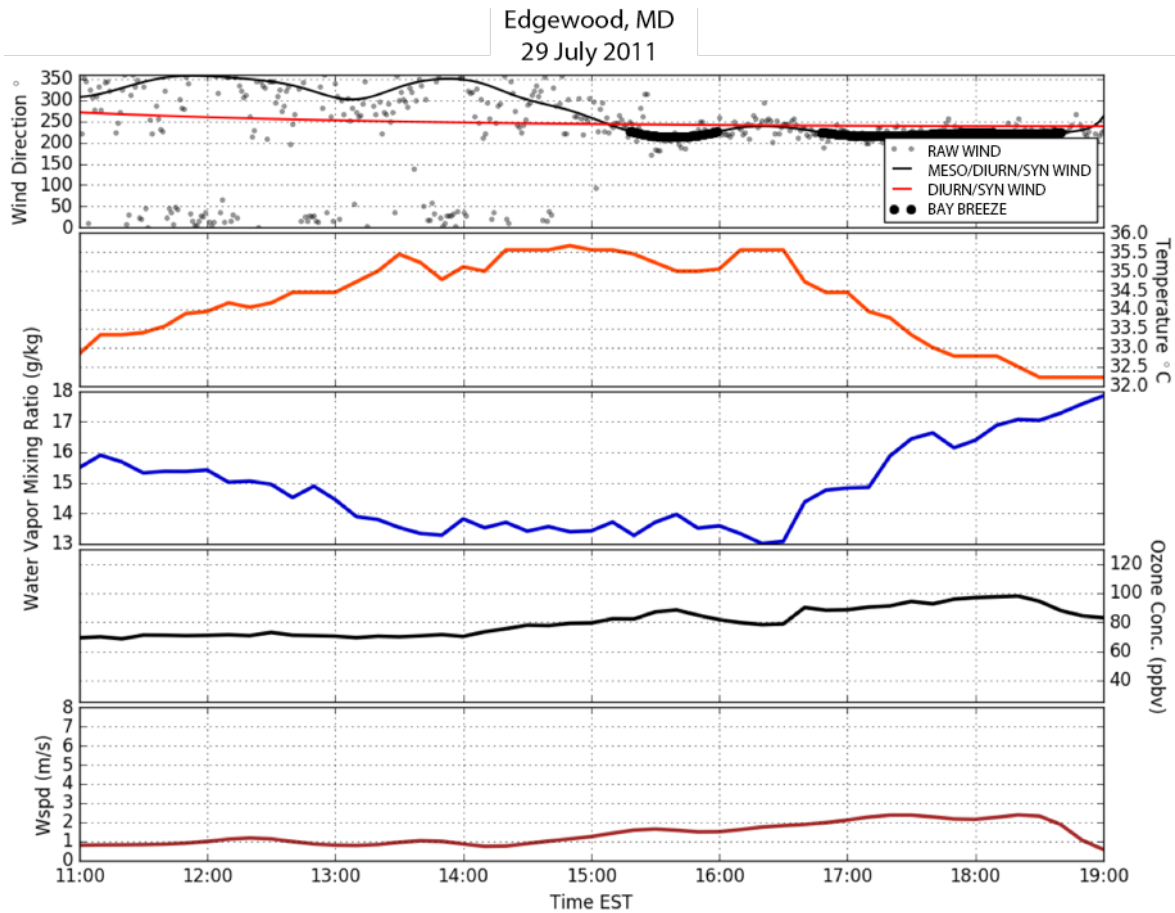


Figure 3.5 Meteorological and O₃ 1-minute observations at the MDE site at Edgewood, MD on 29 July 2011. Top panel: dots: raw wind data, thin black line: the faster varying wind signal, red line: the slower varying wind signal, thick black line: times when BIA detects a bay breeze. 2nd panel (orange): temperature (°C), 3rd panel (blue): water vapor mixing ratio (g/kg), 4th panel (black): O₃ concentration (ppbv), bottom panel (red): wind speed (m/s).

3.3.1.3 BIA using Real-time Mesoscale Analysis (RTMA) Model Output

With the goal of using BIA for forecasting purposes and/or to understand the bay breeze influence at coastal sites with limited to no observations, the NWS Real-Time Mesoscale Analysis (RTMA) was tested as input to the algorithm. The RTMA is a gridded, high resolution (archived 2.5 km and 1-hourly output) analysis/assimilation product of near-surface weather

(<http://www.nco.ncep.noaa.gov/pmb/products/rtma/>). The RTMA was used to determine if BIA can detect whether a bay breeze occurred for each day in July 2011 during the analysis time period, and if it can detect short-lived bay breezes during a case study day on 29 July 2011 when the input is at a coarser resolution than 1-minute (1-hourly RTMA output).

BIA-RTMA Month of July 2011 Performance

To determine the performance of the Bay-breeze Identification Algorithm with RTMA output (BIA-RTMA), the analysis was run for the month of July 2011 during the time period of 11:00 – 19:00 EST, modifying the algorithm for hourly resolution ingestion, and compared to bay breeze days determined from both the Stauffer et al. (2015a) analysis and BIA with 1-minute data (BIA-data; Table 3.2). The summary of this comparison is shown in Table 3.3. The totals from this comparison are:

- Total days where BIA-RTMA matches other analysis: 27
- Total days where BIA-RTMA does not match other analysis: 4

This comparison demonstrates that BIA-RTMA captures small-scale bay breezes with a success rate of 87% compared to the other two analyses (Stauffer et al. and BIA-data) for one month, providing that the combined success of the Stauffer et al. and the BIA-data are valid. The BIA-RTMA can be a useful method for determining bay breeze days for research by using the RTMA as reanalysis, as well as for forecasting by using the RTMA's operational output.

Table 3.3 Validation of BIA-RTMA by comparison with the Stauffer et al. analysis and BIA with 1-minute data (BIA-data) for the month of July, 2011 over the analysis time period (11:00-19:00 EST)

BIA-RTMA Comparisons:	# of days
BIA-RTMA bay breeze matches Stauffer et al. analysis <i>only</i> :	3
BIA-RTMA bay breeze matches BIA-data <i>only</i>	2
BIA-RTMA bay breeze matches <i>both</i> Stauffer et al. and BIA-data	5
BIA-RTMA no bay breeze matches <i>both</i>	17
BIA-RTMA bay breeze <i>does not match</i>	4
Total days BIA-RTMA matches other analysis:	27
Total days BIA-RTMA does not match other analysis:	4

BIA-RTMA Case Study – 29 July 2011

To understand if BIA-RTMA can be used to identify if the event occurred and the approximate timing of a short-lived bay breeze, this analysis looked at the case study of 29 July 2011 discussed in section 3.3.1.2. BIA-RTMA correctly identified the bay breeze and its timing. While the BIA-RTMA bay breeze detection identifies the correct time (~15:00 – 19:00 EST), it is unable to capture the existence of two separate events in the manner that these events are identified by BIA. This demonstrates the limitations that models have in their ability to correctly identify the structure of short-lived mesoscale events (Figure 3.6).

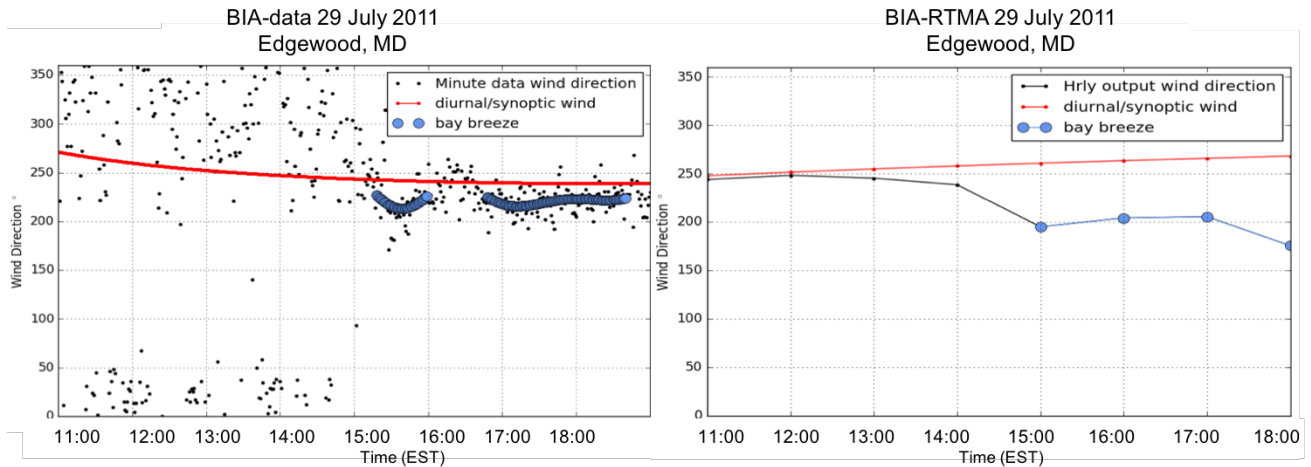


Figure 3.6 Bay breeze day on 29 July 2011 at Edgewood, MD Left: BIA-data (bay breeze identification using 1-minute data) where the black dots are the raw minute data, the red line is the diurnal + synoptic signal, and the blue dots are where BIA-data detect a bay breeze. Right: BIA-RTMA where the black line is the 1-hrly model output, the red line is the diurnal + synoptic signal, and the blue dots are where BIA-RTMA detects a bay breeze.

3.3.2 The Role of Bay Breezes and Thunderstorms on Surface O₃

Concentrations

Out of 552 days within the analysis time period, 330 days (60%) had neither a bay breeze or thunderstorm, 102 days (18%) had a bay breeze only, 71 days (13%) had a thunderstorm only, and 49 days (9%) had both a bay breeze and a thunderstorm (Figure 3.7).

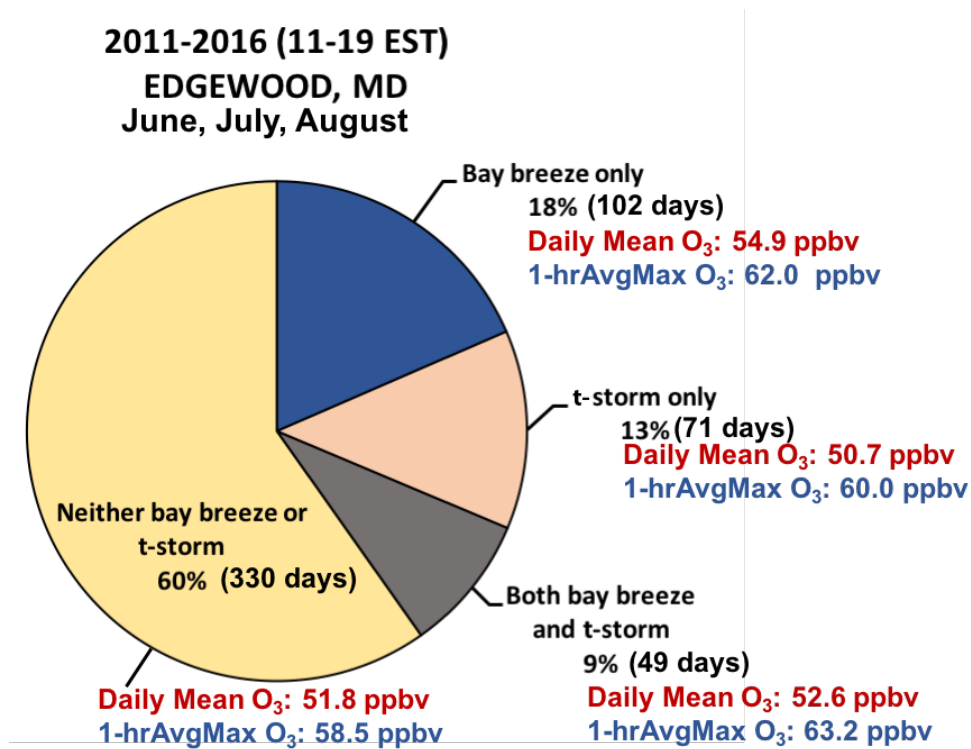


Figure 3.7 Pie chart of the percent of days and number of days that exhibit the four different meteorological categories (yellow: neither bay breeze nor thunderstorm, blue: bay breeze only, tan: thunderstorm only, gray: both a bay breeze and a thunderstorm) during the analysis time period. In red: the average of the daily mean O₃ concentrations for each meteorological category, and in blue: the average of the daily 1-hr avg. max O₃ concentrations for each meteorological category in ppbv.

3.3.2.1 Bay Breeze vs. Non-Bay Breeze Days

During the analysis time period, days were identified as “bay breeze” or “non-bay breeze” from BIA processed data. Overall, O₃ concentration was highest on bay breeze days (Figure 3.8). The largest difference, 6 ppbv, in mean surface O₃ concentrations between bay breeze days and non-bay breeze days was observed in 2011. The change in the average of the daily 1-hour averaged maximum O₃ was also the largest in 2011 with a difference of 8 ppbv between bay breeze days vs. non-bay breeze days. The mean O₃ concentration had the smallest difference between bay

breeze and non-bay breeze days in both 2015 & 2016 (0.7 ppbv), and the average of the daily 1-hour avg. max O₃ had the smallest difference between bay breeze and non-bay breeze days in 2016 (0.9 ppbv difference). This suggests that as the air became cleaner due to emission reductions, bay breezes may have had less of an effect on surface O₃ concentration. A test to understand the significance of mean O₃ concentrations between bay breeze and non-bay breeze days is performed over the analysis time period, where the null hypothesis is that the mean O₃ concentration is the same between bay breeze and no bay breeze days. From a t-test, the null hypothesis was rejected (t-value: 1.96; p-value: 0.05), suggesting that the difference in mean O₃ concentration between bay breeze and no bay breeze days is significant and not random. It should be noted however, that there are limitations in the ability to perform a significance test with the right-skewed data.

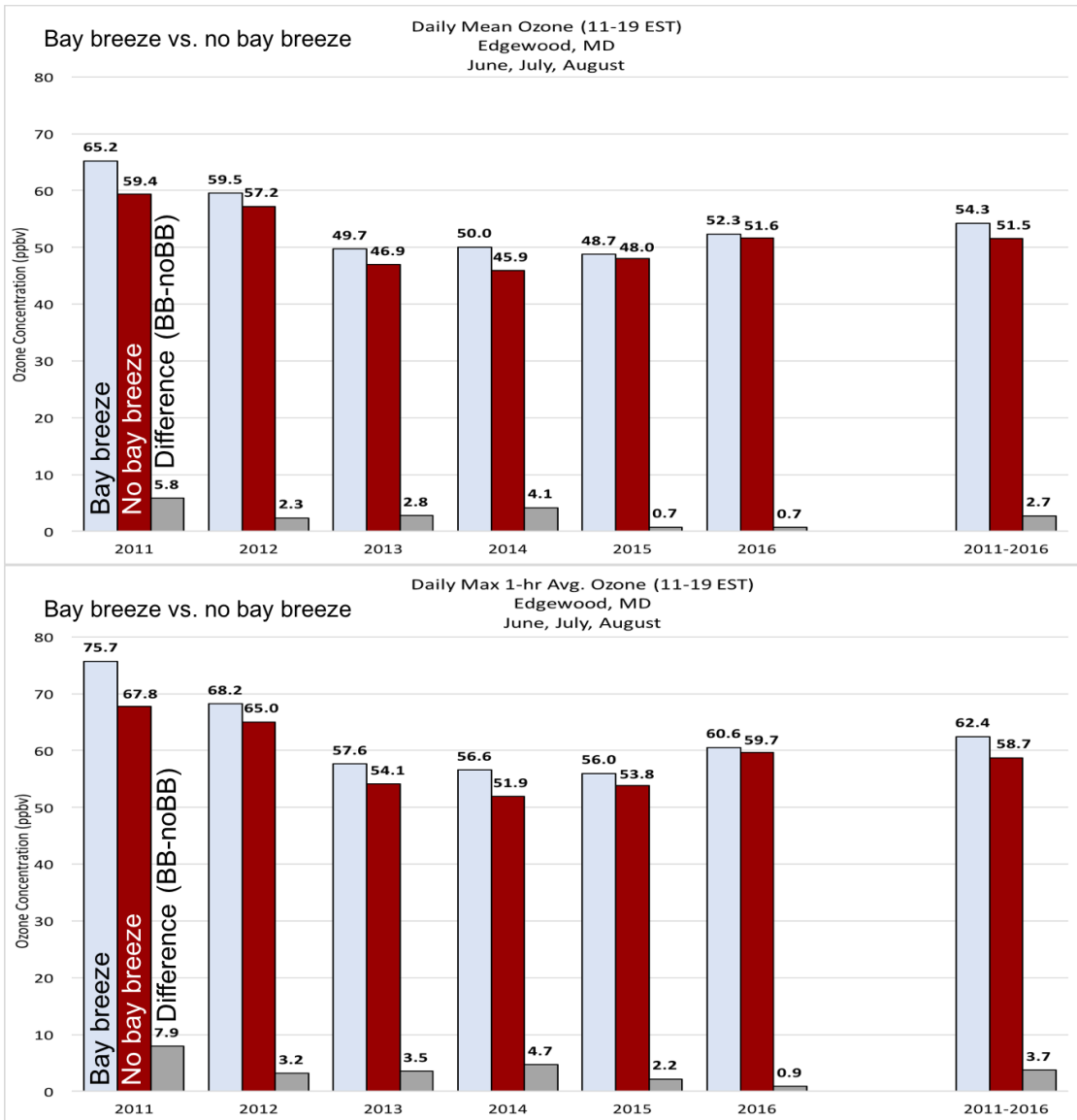


Figure 3.8 Bar chart of the average of daily mean O₃ concentrations for bay breeze days (light blue), days without a bay breeze (brown), and the difference in O₃ concentration between bay breeze and no bay breeze (gray) during the analysis time period for each year and all years. Top: average of the daily mean O₃ concentration (11-19 EST) for each year (June, July, August) for bay breeze days, no bay breeze days, and the difference. Bottom: Average of the daily 1-hr average max O₃ concentrations for bay breeze days, no bay breeze days, and the difference.

3.3.2.2 Thunderstorm vs. Non-Thunderstorm Days

Thunderstorms identified by the detection of lightning during the analysis time period (11-19 EST) were used to determine “thunderstorm days” and “no

thunderstorm days”. Overall, the daily mean O₃ concentration during the analysis time period was lower on thunderstorm days than days without a thunderstorm. However, the 1-hr avg. max O₃ concentration was higher on thunderstorm days than days without a thunderstorm (Figure 3.9). A test was performed during the analysis time period to understand whether the difference between thunderstorm and non-thunderstorm days were significant, with a null hypothesis of the same mean O₃ concentrations on thunderstorm days vs. non-thunderstorm days. From a t-test, the null hypothesis was unable to be rejected (t-value: -0.70; p-value: 0.48), therefore indicating that the difference in mean O₃ concentration between thunderstorm and non-thunderstorm days is not significant and the relationship may have happened at random. There is some uncertainty in the ability to perform a significance test with the type of data being evaluated (skewed and uneven sample groups). This analysis also does not account for fair weather cumulus clouds, which can also be effective in venting the boundary layer, and would be contained in the “no thunderstorm day” category. A further investigation should be conducted to fully understand the effects of polluted boundary-layer venting by moist convection.

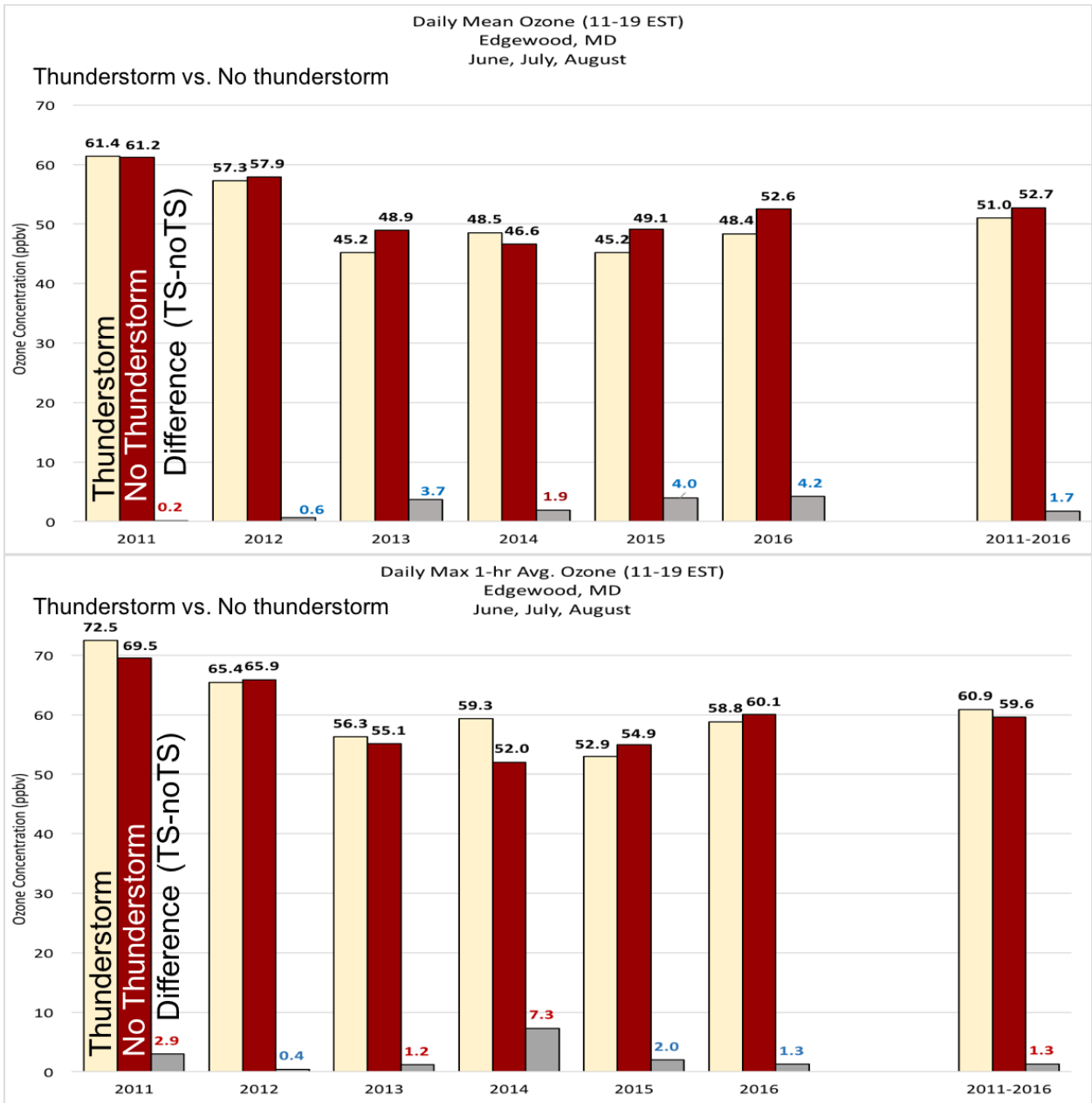


Figure 3.9 Bar chart of the average daily mean O₃ concentrations for thunderstorm days (yellow), days without a thunderstorm (brown), and the difference in O₃ concentration between thunderstorm days and no thunderstorm days (gray) during the analysis time period for each year and all years. Top: average of the daily mean O₃ concentration (11-19 EST) for each year (June, July, August) for thunderstorm days, no thunderstorm days, and the difference. Bottom: Average of the daily 1-hr average max O₃ concentrations for thunderstorm days, no thunderstorm days, and the difference. The numbers on the gray bars (difference) are colored by red (positive difference between TS-noTS) and blue (negative difference between TS-noTS).

3.3.2.3 Late morning/Early afternoon and Late afternoon Thunderstorms and O₃ Concentrations

Thunderstorms were identified within the analysis time period (11 – 19 EST) and then further parsed into late morning/early afternoon (early; 11-14 EST), late afternoon (late; 14-19 EST), and both early and late afternoon (both; 11-19 EST) storms by the timing of flashes from the lightning data. The mean O₃ concentration for the time periods (early afternoon, late afternoon, and entire afternoon) were calculated for each of the categories (Figure 3.10).

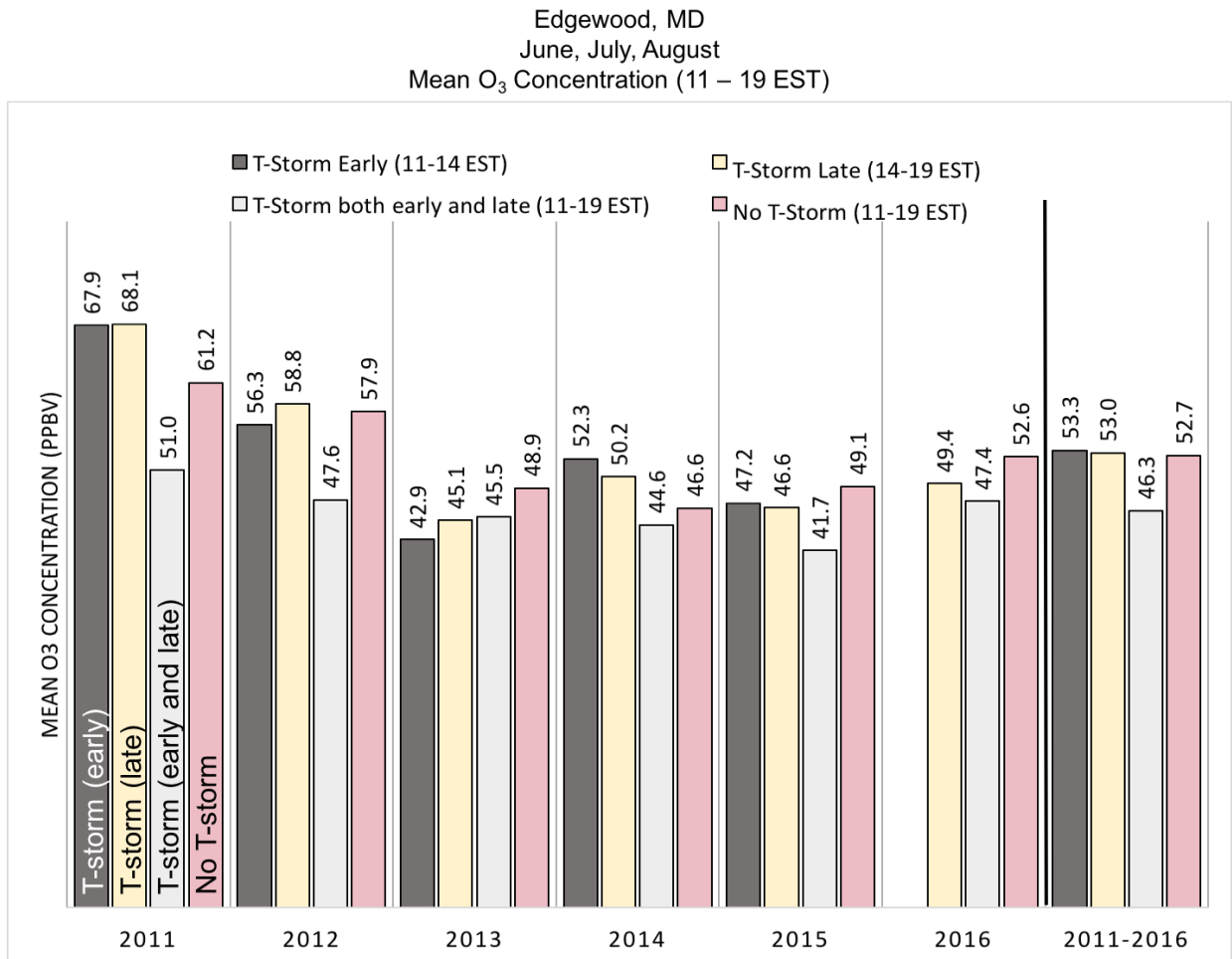


Figure 3.10 Bar chart of the average daily mean O₃ concentrations for thunderstorm days (dark gray, yellow, light gray) and no thunderstorm days (pink), where the thunderstorm days are separated by when the thunderstorm had occurred (early: 11-14 EST; late: 14-19 EST; both: storms either spanned through both time periods or there was more than one storm that occurred in both time periods). Overall, the difference in O₃ concentration on thunderstorm days with either a thunderstorm in early afternoon or a thunderstorm in late afternoon is not significantly different from days with no thunderstorm.

Overall, the mean O₃ on thunderstorm days was lowest on days where there were storms both early and late, with no discernable concentration difference between days with storms *only* early, *only* late, or *without* a thunderstorm. Since conditions favorable for high O₃ events are many times also the conditions favorable for pop-up single-cellular convection, if a small thunderstorm occurs either early or late in the day and moves out of the area, there is the possibility of there being high O₃ before the storm, as well as the potential for precursors and high O₃ to be transported back to the site from areas that were not affected by thunderstorms. However, on days with a thunderstorm in both the early and late afternoon, the O₃ was low compared to the other three categories (early storm only, late storm only, or none).

3.3.2.4 Frontal vs. Non-frontal Thunderstorms and O₃

Thunderstorms were further classified into two categories, frontal vs. non-frontal, for the analysis time period (11:00 – 19:00 EST, June – August, 2011-2016). This classification allows us to examine any differences in O₃ concentrations between these two fundamentally different types of meteorological phenomena. Days where the thunderstorm detection algorithm (section 2.3) identified a thunderstorm were further investigated by examination of WPC surface analysis maps (<http://www.wpc.ncep.noaa.gov/html/sfc2.shtml>) to determine whether the observed

convection during the analysis time period was associated with frontal/pre-frontal convection (a synoptic-scale feature) or an air-mass thunderstorm with a smaller-scale forcing. While thunderstorm days were mostly made up of frontal convection, the average of the daily mean O₃ concentration on days with frontal/pre-frontal convection was lower than days with non-frontal/pop-up storms (50.7 vs. 53.6 ppbv) (Figure 3.11), likely due to larger vertical transport rates, more cloud cover, and a larger spatial/temporal extent with the frontal convection. Next, thunderstorm types were further broken up into combinations with bay breezes. The highest mean O₃ concentration on a thunderstorm day was observed on days with both a bay breeze and a non-frontal storm (BB & non-frontal storm); however, this was the least likely combination, with the lowest number of days (Figure 3.11). The remainder of the combinations (BB & frontal storm, NoBB & frontal storm, and NoBB & non-frontal storm) did not significantly differ from one another in terms of mean O₃ concentration (Figure 3.11).

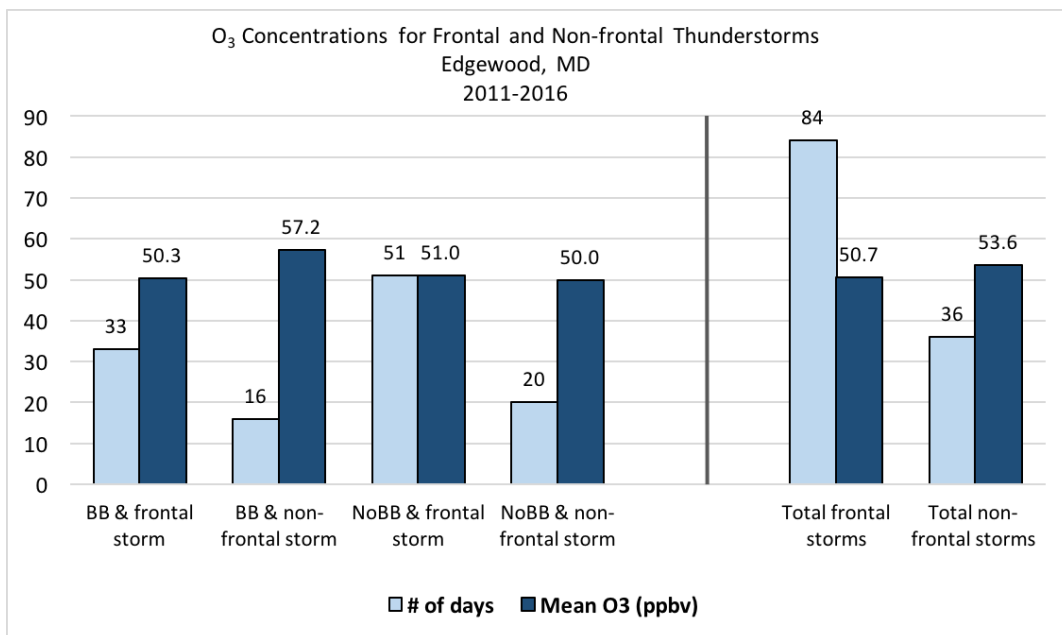


Figure 3.11 Bar chart of O₃ concentration on days with frontal thunderstorms in comparison to days with non-frontal, or, thunderstorms not associated with forcing by a synoptic-scale front (e.g., pop-up thunderstorm by bay breeze convergence) during the analysis time period (11:00 – 19:00 EST, June-August, 2011-2016) at Edgewood, MD. Light blue: # of days for each meteorological category (BB: bay breeze days, NoBB: no bay breeze days); Dark blue: Daily mean O₃ concentration (ppbv) for the days that exhibit each meteorological category. Days with frontal thunderstorms were more than double the number of days with non-frontal thunderstorms during this analysis time period. Non-frontal thunderstorms were generally associated with higher daily average O₃ concentrations.

Next, days are broken up into the following meteorological categories:

- Bay breeze only
- T-storm only
- Both a bay breeze and t-storm
- Neither a bay breeze or t-storm

3.3.3 The Relationship between Days with Extreme O₃ (O₃ Exceedances / High O₃ Events) and Days with a Mesoscale Circulation (Bay Breezes, Thunderstorms, or Both)

To investigate if mesoscale meteorological events such as bay breezes and thunderstorms can be used to statistically predict coastal air quality events, conditional probabilities are calculated for each of the following meteorological categories: thunderstorm only (TS), a bay breeze only (BB), or both (TS&BB). These probabilities are calculated for both an O₃ exceedance (denoted OE; 2008 EPA-defined O₃ exceedance event of 8-hour max O₃ higher than 75 ppbv) and a high O₃ event (H-O₃; defined as days when mean O₃ between 11-19 EST exceeds the seasonal mean (for June, July, and August) O₃ + 1 stdev between those hours) given the

previously defined meteorological categories. Understanding the probabilities of O₃ exceedance events and high-O₃ events are important for defining extremes. It is important to also consider how many extreme O₃ days also experienced a BB, TS, both, or neither to better understand the relationship that exists between atmospheric chemistry and dynamics.

3.3.3.1 Percentage of OE and H-O₃ Days with a Bay Breeze, Thunderstorm, Both, or Neither

Out of the 552 days analyzed between June, July, and August 2011-2016, 33 were OE days and 73 were H-O₃ days. The percentage of days that also had a BB, TS, both, or neither is shown in Figure 3.12. Of the OE days, 39% had a BB, 24% had a TS, 15% had a BB & TS, and 52% had neither. Out of the days with H-O₃, 32% had a BB, 18% had a TS, 10% had a BB and TS, and 60% had neither (Figure 3.12). For the days that exhibit extreme O₃ by both definitions, mesoscale events (i.e., BB and TS) make up 40 – 50% of the days, with BB days making up the largest number of days of extreme O₃ that also had a mesoscale event.

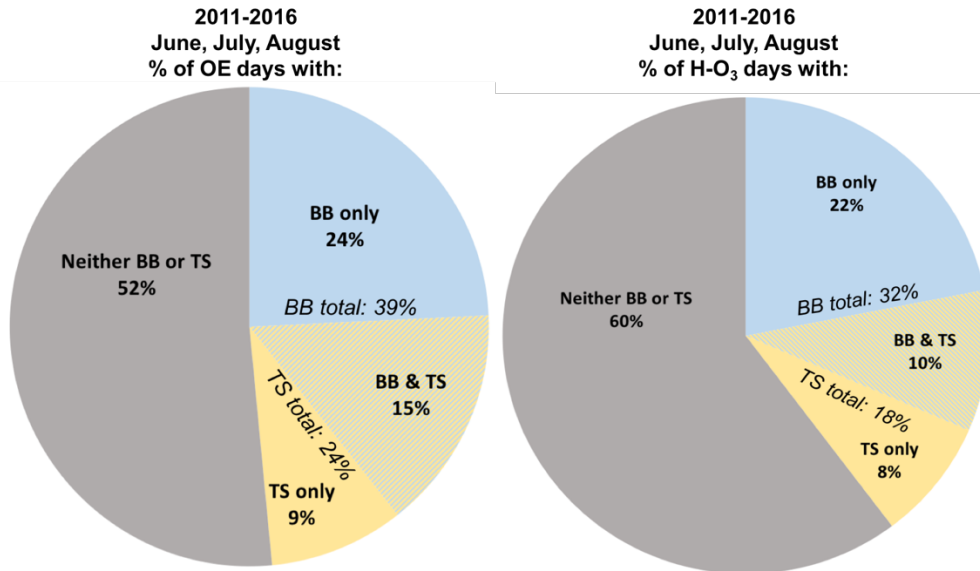


Figure 3.12 Pie charts of the % of days with an O₃ exceedance (OE; left) and % of days with a H-O₃ event (H-O₃; right) that had also exhibited at bay breeze (BB; light blue), thunderstorm (TS; yellow), both (BB & TS; hatched yellow and blue), and neither (neither BB or TS; gray) for June, July, and August 2011-2016 between 11-19 EST at Edgewood, MD.

3.3.3.2 Conditional Probabilities of an O₃ Exceedance Event using the EPA Definition and the H-O₃ definition given a Mesoscale Event

For the O₃ exceedance definition (OE), the estimated conditional probabilities of an OE given either a bay breeze or a bay breeze in combination with a thunderstorm (10% for BB & TS, 8% for BB only; Table 3.4: top) are both higher than the unconditional probability of an OE (6%). The year 2011 had the highest probability of an OE given a BB only, TS only, and both a BB & TS (Table 3.5; left). For the high-O₃ definition of O₃ (H-O₃), the estimated conditional probabilities of an H-O₃ event given either a bay breeze or a bay breeze in combination with a thunderstorm (14% for BB & TS, 16% for BB only; Table 3.4: bottom) are also both higher than the unconditional probability of an H-O₃ (13%).

Table 3.4 Conditional probabilities of an OE or H-O₃ given the occurrence of a bay breeze, thunderstorm, or both for June, July, and August 2011-2016. Top: percentage of days with a 2008 EPA-defined O₃ exceedance event (OE; 8-hr max O₃ higher than 75 ppbv) given the occurrence of thunderstorm only (TS), a bay breeze only (BB), or both (TS&BB); Bottom: Percentage of days with daily mean O₃ exceeding the yearly mean O₃ + 1 stdev (H-O₃) given the occurrence of a thunderstorm only (TS), a bay breeze only (BB), or both (TS&BB)

2011-2016	P(OE)	P(OE TS)	P(OE BB)	P(OE TS&BB)
	6%	4%	8%	10%
2011-2016	P(H-O₃)	P(H-O₃ TS)	P(H-O₃ BB)	P(H-O₃ TS&BB)
	13%	8%	16%	14%

The years with the highest proportion of an H-O₃ event given each meteorological category were a mix of different years, unlike the 8-hour max definition (OE) which was dominated by 2011 (Table 3.5; right). How one defines high O₃ concentration affects both the unconditional probability of an O₃ event occurring as well as the conditional probability of a mesoscale meteorological event influencing the O₃ event, as shown by the differences in percentages between OE and H-O₃ events.

Table 3.5 Left: Years with the highest proportion of an O₃ exceedance (8-hr max > 75 ppbv) given the occurrence of a bay breeze, thunderstorm or both; Right: the years with the highest proportion of daily mean O₃ exceeding the yearly mean + 1 stdev given these mesoscale events.

Years with highest proportion of an OE	Years with highest proportion of H-O₃
P(OE) 2011 17%	P(H-O ₃) 2013 16%
P(OE TS) 2011 9%	P(H-O ₃ TS) 2011 & 2016 9%
P(OE BB) 2011 24%	P(H-O ₃ BB) 2015 25%
P(OE TS & BB) 2011 33%	P(H-O ₃ TS & BB) 2011 33%

Examining the distribution of daily mean O₃ concentration (11-19 EST for June, July, August 2011-2016) for each meteorological category, much of the distribution is made up of days without a bay breeze or thunderstorm, as one would expect, since bay breeze and thunderstorm events are episodic in nature. However, while the days with mesoscale circulations are not as frequent, they have significant implications for the right-tail of the distribution (Figure 3.13). As expected from Table 3.4, bay breeze days (Figure 3.13; blue colors) make up an important part of the right-tail of the hourly-averaged O₃ distribution. However, while it may be interpreted from Table 3.4 that days with thunderstorms would not have much of a contribution to high O₃, it is evident that days with thunderstorms also contribute to the right-tail of the distribution and therefore cannot be discounted (Figure 3.13; maroon color). Overall, in terms of mean and max concentrations, the highest average of the daily mean O₃ and the highest max daily 1-hr average O₃ occur on days with a bay breeze only. The lowest average of the daily mean O₃ and the lowest average of the daily 1-hour max O₃ occurs on days with thunderstorms only and days with neither a bay breeze or a thunderstorm (as shown previously in Figure 3.7).

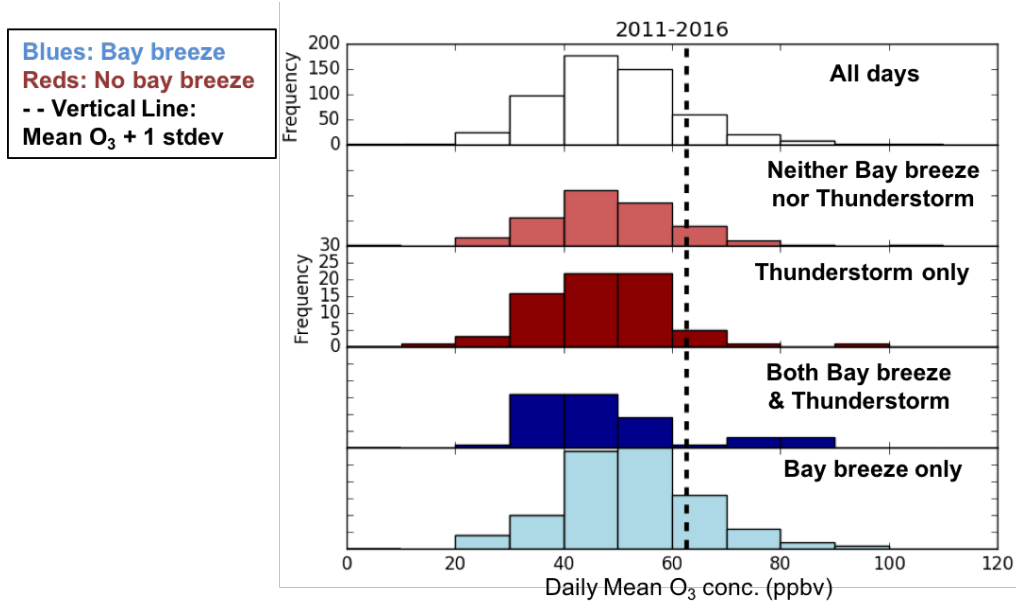


Figure 3.13 Distribution of daily mean O₃ concentration (ppbv) at Edgewood, MD from 2011-2016 during the analysis time period (11:00 – 19:00 EST) for all days (top row), days without a bay breeze or thunderstorm (2nd row), days with a thunderstorm only (3rd row), days with both a bay breeze and a thunderstorm (4th row), and days with a bay breeze only (last row). From the 3rd row down (days with a mesoscale circulation), the y-axis (frequency) is changes to clarify the relative contribution of each mesoscale event on the less-frequent tail-end of the O₃ distributions.

3.4 Discussion

The O₃ concentration during the analysis time period from 2011-2016 at Edgewood demonstrates a turning point of the site’s long-time notoriety as the primary out of attainment monitor in Maryland and having among the highest O₃ concentrations along the eastern seaboard. By understanding the role of mesoscale events on O₃ at Edgewood during this time period, the information learned from this site can be generalized for other coastal sites that are at a different point in their progress toward O₃ attainment. Similar to the relationship between bay breezes and O₃ concentrations at Edgewood prior to 2012, bay (sound) breezes in the New York and Connecticut (e.g., Long Island Sound breezes) area are currently likely to have

much more influence on the modulation of O₃, and may be a better predictor of O₃ exceedances as well as high O₃ events.

Something of consideration not analyzed here is O₃ production sensitivity (NO_x or VOC limited scenarios) during the land-water breeze recirculation at coastal sites. In Mazzuca et al., 2016, it is shown that in the Houston Metro area, an area subject to Gulf and Galveston Bay breezes, the sensitivity of O₃ production changes by time of day and proximity from the urban center. The relationship between mesoscale events and O₃ production sensitivity near coastal sites may be overlooked in analysis and modeling studies.

Bay breezes can be a good predictor of high O₃ as shown in 2011 and 2012, but not as good for the 8-hour max definition of an exceedance. When the definition of an EPA O₃ exceedance is used (OE) vs. the definition of high O₃ (H-O₃) in the conditional probabilities, the results vary. For example, the percentage of days that had an OE vs. H-O₃ given a bay breeze for the analysis time period are different by 8% (OE: 8%; H-O₃: 16%). The years with the highest proportions for each O₃ event definition also changes, such that all of the highest proportions were observed in 2011 for the OE definition, but for the H-O₃ definition, there was a mix of years with the highest proportion. This demonstrates the importance of how one defines thresholds that indicate extremes - especially as they relate to formulating policy.

This chapter discusses the impacts of mesoscale meteorology on surface O₃ at a coastal monitor over a six-year period. During this time period, the site had experienced significant changes in mean O₃ concentration (a general decreasing trend) and the number of exceedance episodes. To understand the physical

mechanism responsible for these meteorological or chemical phenomena in greater detail, beyond the scope of this paper, a high-resolution meteorological and chemical modeling study would be useful to quantify some of the uncertainties in boundary-layer mixing, bay breeze development and mixing, thunderstorm vertical mixing, and effects from negatively buoyant mid-tropospheric downdraft air on the surface. This modeling study would be useful in further investigating the parts of the right-tail of the right-skewed daily O₃ distribution, where on bay breeze and thunderstorm days, there is an observed bimodal O₃ distribution. A bay breeze forecast would be a valuable part of air quality forecasting in locations that have a higher probability of an O₃ exceedance given a bay breeze.

In the context of regulatory modeling, it is unlikely that these types of events can be resolved at 12-km horizontal resolution, or even 4-km resolution, due to the horizontal and vertical scale of these features. Even if the RTMA forecast is used with BIA (BIA-RTMA) in real-time to detect bay breezes for better air quality forecasting, accurate O₃ concentrations over the water from the regulatory model would be needed to understand the impact of O₃ advection from the bay to the land. However, it is known that the regulatory models, for example the Community Multiscale Air Quality (CMAQ) model, can over-predict O₃ concentrations over the water as well as the land (Loughner et al., 2014). While BIA-RTMA was able to identify bay breeze days, it struggled to capture the correct timing and duration of events over the whole month of July, likely due to the RTMA.

3.5 Conclusions

An automated algorithm using a low-pass filter on u & v components of the wind, a land-mask, and user-specified flags was developed and proven to be a successful technique to identify bay breezes at Edgewood, MD, along the Chesapeake Bay. Compared to another bay breeze identification technique (Stauffer et al.) for the same site, BIA run with 1-minute observational data (BIA-data) matched 87% of the days with bay breezes. When compared to a case study day, BIA-data captured the same timing for a previously published hand-analysis bay breeze study at the same site indicating that BIA-data can effectively determine even small-scale and short-lived bay breezes. BIA run with RTMA model output at 1-hourly resolution (BIA-RTMA) matched the other two analyses (BIA-data and Stauffer et al.) 87% of the days for one month, indicating that BIA-RTMA can be used to determine bay breezes for research and potentially for air quality forecasting applications.

Prior to this analysis and part of the motivation for this study was the hypothesis that as O₃ precursor concentrations are reduced by regulations, O₃ exceedances would be less frequent without the assistance of pollutant recirculation by bay breezes. However, contrary to that hypothesis, this analysis suggests that as the air becomes cleaner near coastal areas due to air pollutant regulations, there reaches a point where even bay breezes cannot push the coastal site over the air quality standard since the air is too clean. Therefore, the relationship between bay breezes and O₃ exceedances diminishes as the air becomes cleaner, thus making bay breezes less of an O₃ exceedance predictor.

During the analysis time period, the highest daily mean O₃ for all years (11-19 EST; 2011-2016) was observed on bay breeze days and the lowest on days with a thunderstorm but no bay breeze. Also, it was shown that days where both a thunderstorm and a bay breeze occur do not necessarily have low O₃ concentrations, as 15% of OE days and 10% of H-O₃ days were made up of thunderstorm and bay breeze combinations. Furthermore, days with a bay breeze/thunderstorm combination were associated with the highest average daily 1-hr max out of all of the meteorological categories, indicating that thunderstorm days may be associated with very high O₃ concentrations, either before and/or after the storm, should a bay breeze occur.

For the timing of such thunderstorm activity, it is shown that there is little to no difference between O₃ concentration between days that experienced a thunderstorm in the early afternoon only vs. the late afternoon only. The only notable decrease in O₃ concentration is observed in situations where there are thunderstorms observed in both the early and the late afternoon, which may be caused by very efficient cleaning of pollutants by extensive rain and updrafts.

The estimated conditional mean daily 1-hr avg. max O₃ given the occurrence of a thunderstorm only was slightly higher than days without a thunderstorm or bay breeze, and the average of the daily 1-hr avg. max O₃ was overall highest on days with a thunderstorm/bay breeze combination. This indicates that thunderstorms may not necessarily help to clean out the O₃ pollution if high concentrations exist before the thunderstorm occurs, or, if high O₃ and precursors are transported back to the area after the storm occurs. Thunderstorms of varying sizes and strengths have differing

abilities to clean out the O₃ and entrain cleaner mid-tropospheric air into the boundary layer. In some cases, only a temporary O₃ decrease is observed, with no termination of the pollution episode. Since conditions that are favorable for thunderstorms are also conducive to O₃ production and bay breezes, in some cases, thunderstorm days may have higher O₃ concentrations than days without a thunderstorm.

With estimates of the conditional probability of an OE and H-O₃ given a bay breeze over a time period with emissions reductions, BIA can be applied to forecast model output to statistically predict the occurrence of coastal air quality events, particularly in regions of non-attainment such as New York and Connecticut, as precursor concentrations change in future emissions scenarios.

Chapter 4: Observations and Modeling of Thermally-direct Circulations and Implications for Trace Gases (Maryland and Colorado)

4.1 Introduction

The severity of air pollution is strongly dependent upon meteorology. As a weather pattern develops or event occurs, changes in meteorology are reflected, sometimes rapidly, in the concentrations of trace gases. It was shown in Chapter 3 that some weather events, such as bay breezes and thunderstorms, have a complicated relationship with surface O_3 . For example, when considering 8-hr average O_3 , some thunderstorms can clean and terminate an air pollution event. On other days that experience thunderstorms, especially when combined with a bay breeze, O_3 concentrations are slightly higher. Investigated in this section are case studies and a WRF simulation to better understand the dynamical mechanisms that lead to the varying responses that the concentration of O_3 has from bay breezes and thunderstorms. The case studies are conducted for two urban locations with very different geographic/topographic, but similarly urban locations, Maryland and Colorado, to demonstrate the similarities and differences in the resulting O_3 during and after land-water/topographic breezes and thunderstorms.

4.2 Methods

4.2.1 Observational Network

The DISCOVER-AQ field campaign was an aircraft and ground based observation field mission comprised of four deployments (MD-2011, CA-2013, TX-2013, and CO-2014) to better characterize air pollution, including the relationship between column and near-surface pollution. During this study, NASA's P-3B aircraft spiraled over ground sites several times a day to capture the horizontal, vertical, and temporal variability of trace gases and meteorology. Each deployment also had an array of ground sites with in-situ and remote sensing meteorological and trace gas instruments. A tethered balloon (tethersonde) operated by students from Millersville University was deployed at one site during each campaign, instrumented with a suite of chemical and meteorological analyzers to capture the variability between the lowest P-3B spiral altitude (~300m AGL) and the surface. This chapter focuses on the Maryland deployment (summer 2011) and the Colorado deployment (summer 2014).

4.2.2 The Weather Research and Forecasting (WRF) Model Simulation

Cloud-resolved simulations of the observed storms in Maryland were conducted using the Weather Research and Forecasting (WRF) model, version WRFV3.7.1 (Skamarock and Klemp, 2008), at 1 km and 333 m horizontal resolutions (Figure 4.1) using the 12Z 3 km High-Resolution Rapid Refresh (HRRR) analysis for initial conditions and boundary conditions on 22 July 2011. The simulation was run from 12Z on 22 July 2011 to 00Z on 23 July 2011. The following physics options were selected: the WRF Single-Moment 6-class scheme (WSM6) (Hong and Lim,

2006) for microphysics, the Rapid Radiative Transfer Model for General Circulation Models (RRTMG) (Iacono et al., 2008) for radiation (SW & LW), Noah (Koren et al., 1999; Tewari et al., 2004) for the land surface, and Yonsei University (YSU) (Hong et al., 2006) for the planetary boundary layer (PBL). Large-eddy simulation mode (LES) was also tested in the inner-most domain, but the resulting simulation was more representative when the PBL was parametrized in both domains.

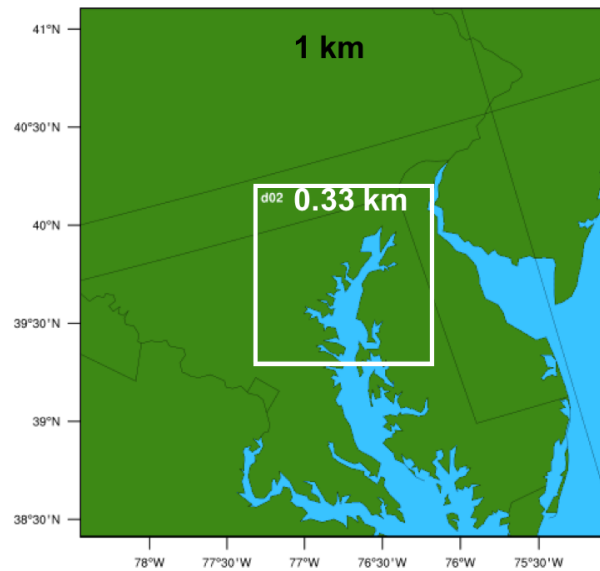


Figure 4.1 WRF model domain set up: 1km grid spacing for d01 (outer domain; black square) and 333m grid spacing for d02 (inner domain; white square).

Table 4.1 Model Parametrization Options for WRF run

Model Options for WRF V3.7.1	
Radiation	LW/SW: RRTMG
Surface Layer	Revised MM5

Land Surface Model	Noah
Boundary Layer	YSU
Cumulus	None
Microphysics	WSM-6
Nudging	Water vapor based on lightning flash observations
Damping	Water vapor

A lightning nudging technique using Earth Networks gridded lightning data (ENTLN), for both intra-cloud and cloud to ground lightning, was implemented to improve the timing and location of the simulated storms relative to the observed radar reflectivity (discussed further in the next section). The simulation has 90 vertical levels and output every hour until convection initiation, every 5 minutes during the storm, and every 15 minutes after the storm.

4.2.2.1 Lightning Data Assimilation (LDA)

As detailed in Fierro et al. (2012, 2014, 2015) and based on Li et al. (2017), flashes were assimilated into the WSM6 microphysics scheme by adding water vapor at constant temperature to the mixed-phase region (~ the layer between the -20 and 0°C isotherms) where and when a flash occurs in a model grid column (Eq. 4-1)

$$q_v = Aq_{sat} + Bq_{sat} \tanh(CX) [1 - \tanh(Dq_g^\alpha)] \quad (4-1)$$

In (4-1), X is the gridded number of flashes from the ENTLN data in a given grid column, A and B are coefficients of % RH to define the minimum and asymptotic value of the function, C and D define the slope of the function, q_{sat} is the water vapor saturation mixing ratio (g/kg), q_g is the graupel mixing ratio (g/kg), and q_v is the water vapor mixing ratio (g/kg). The following LDA coefficients were used in the simulation: $A = 0.93$, $B = 0.19$, $C = 0.01$, $D = 0.25$, and $\alpha = 2.2$. Similar to Fierro et al. (2015) and Li et al. (2017), the LDA coefficient A was adjusted to a higher relative humidity threshold (0.81 to 0.93), such that the increase of q_v is only applied in the grid cells that contain lightning that also have a simulated relative humidity $\leq 93\%$. In addition, the most representative simulation contained a change in the location of the layer in which the water vapor nudging is applied relative to the technique used in the Fierro et al. studies. As discussed in Marchand and Fuelberg (2014) and applied in Li et al., (2017), by nudging water vapor in a layer below or around 700 hPa instead of applying the nudging to the mixed-phase region, the convective updrafts can be initiated from the boundary layer and better represent weakly forced deep convection (Fierro et al., 2015). In this simulation, nudging was applied to the layer between 261 K and 285 K, which corresponds roughly to the 700 hPa level. In addition, to avoid spurious convection by any large water vapor mixing ratios contained in the initialization, water vapor damping was applied to grid cells in the previously defined layer, prior to the onset of deep convection, for relative humidity above 75%. By applying the LDA technique and increasing the water vapor (q_v) within the specified layer, an increase in the local virtual potential temperature

perturbation drives the buoyancy accelerations needed for an updraft. Without the use of this computationally fast nudging, the storms are not represented in the model.

4.3 Results

4.3.1 Observations: 22 July 2011 Bay Breeze and Thunderstorm Case Study in Maryland

After local noon (12 EDT; UTC-4) on 22 July 2011 during the Baltimore/Washington deployment of the DISCOVER-AQ field campaign, convection was initiated near two of the surface sites, Edgewood and Essex, MD, from surface convergence and upward vertical motion forced by the Chesapeake Bay Breeze (Figure 4.2). The synoptic set-up on this day was a relatively large area of high-pressure, with mesoscale lows due to the high temperatures observed on this day, and a weak cold front to the northwest that was no longer indicated on the surface analysis by evening. During the bay breeze (Figure 4.1), there was a notable increase in observed surface specific humidity and surface trace gases as well as a wind shift from WSW to SSW at the Edgewood, MD site (Figure 4.2). Shortly after the bay breeze, thunderstorms close to the site were responsible for a drop in specific humidity (5 g/kg decrease) and trace gas concentrations (40 ppb ozone decrease) as the drier, cleaner mid-tropospheric air from the downdraft had reached the site and subsequent boundary-layer venting had occurred upwind of the site.

Specific humidity (g/kg; top)
 SODAR wind direction (background colors) and surface trace gas concentration (lines) Edgewood, MD 07-22-2011 (bottom)

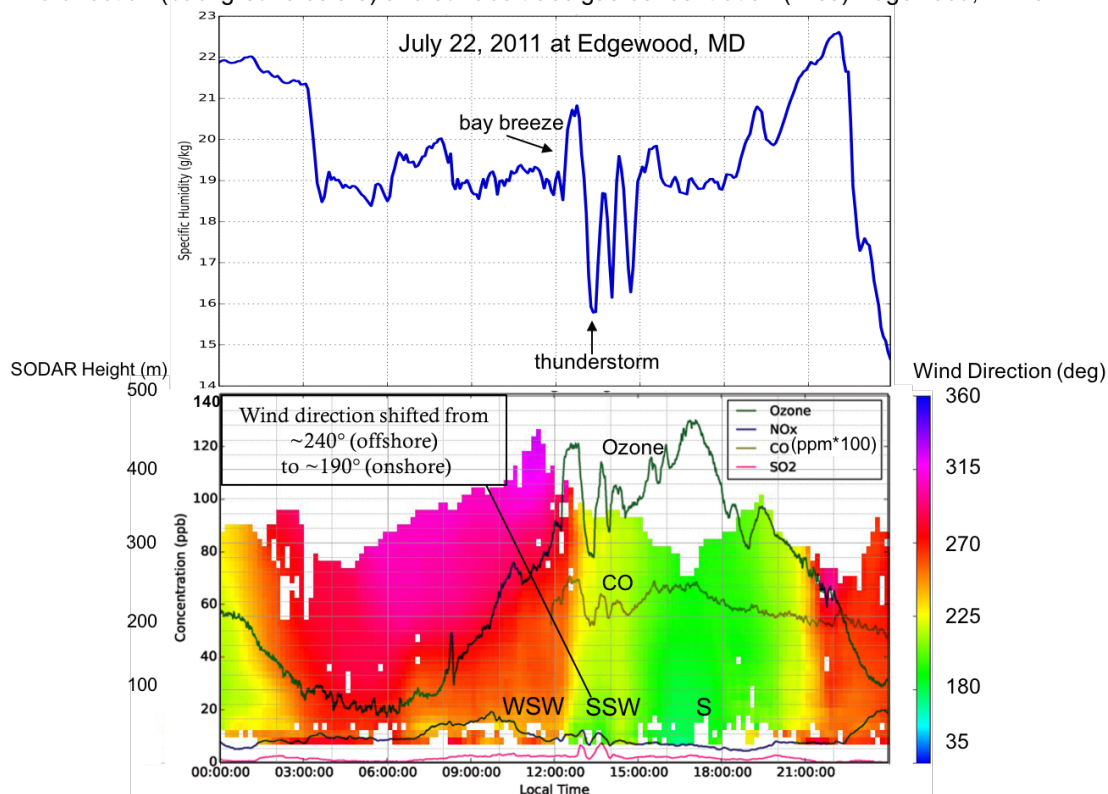


Figure 4.2 07/22/2011 Edgewood, MD site. Top: 2-m specific humidity (g/kg). Bottom: wind direction with height derived from SODAR wind profiler (colors) and labeled surface trace gases: ozone (dark green), NO_x (blue), SO₂ (pink), and CO (olive green). Steep decrease in trace gas concentrations after local noon as a result of pop-up thunderstorms.

The storms were short-lived single-cell thunderstorms with a duration of ~1 hr each, resulting in ~2 hrs of boundary-layer venting. While the storms were small in their horizontal spatial extent, they were very tall, overshooting events (Figure 4.3). However, while these storms likely aided in transporting surface pollution out of the boundary layer, which led to a temporary decrease in surface concentrations, the storms had little to no effect on the maximum 8-hr average O₃ concentration at Edgewood and Essex, MD. In fact, both Edgewood and Essex, MD violated the 8-hr O₃ standard, where Edgewood was the site of the state-wide maximum O₃ exceedance

with an 8-hr maximum value of 97 ppbv on that day, even in the presence of the thunderstorms.

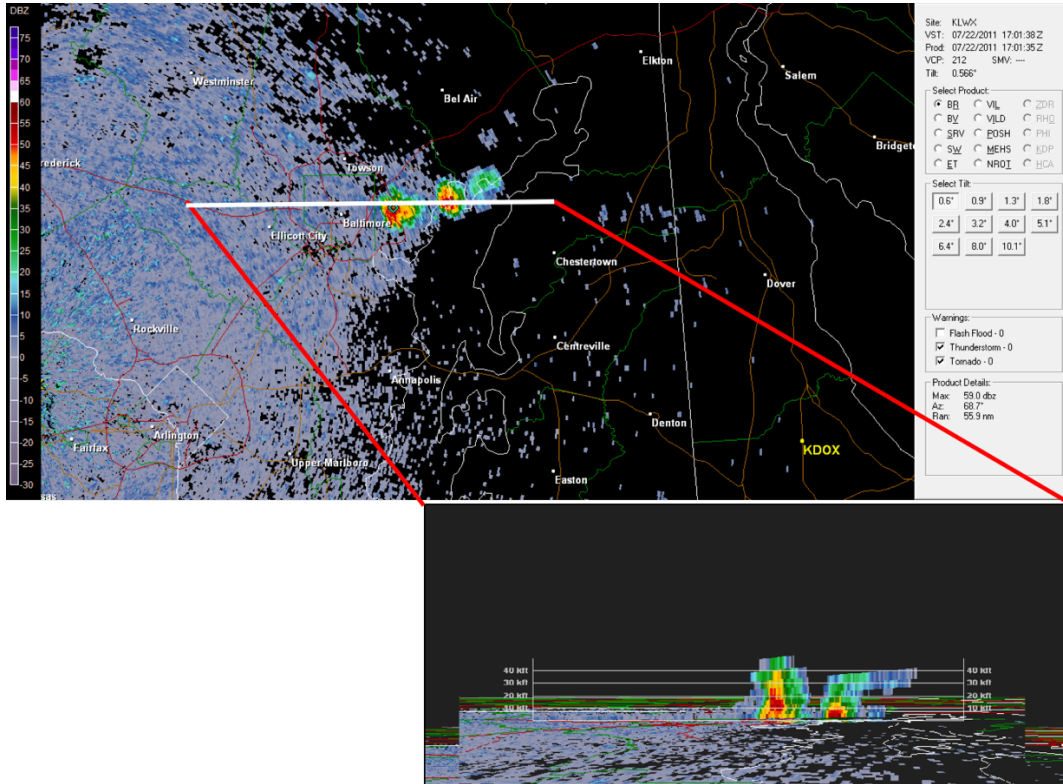


Figure 4.3 Radar reflectivity (dBZ) at 17:01 UTC (13:01 EDT) of the storms of interest. White line: line of the vertical cross-section slice as shown in the lower panel. The vertical cross-section shows the altitude of the storms reaching around 50 kft (15.2 km) during the time of this cross-section, likely near or overshooting the tropopause. The storm reached a maximum altitude of ~60 kft (18.3 km) during its peak.

In the first combined vertical profile with the P-3B and the tether sonde after the storm (around 13:30 EDT), there is an elevated layer of O₃ between 100 and 800m AGL (Figure 4.4). In the second combined profile after the storm (around 15:50 EDT), turbulent processes created a well-mixed layer between the surface and the boundary

layer top (~1600m) with high O₃ concentrations over 100 ppbv extending down to the surface (Figure 4.4).

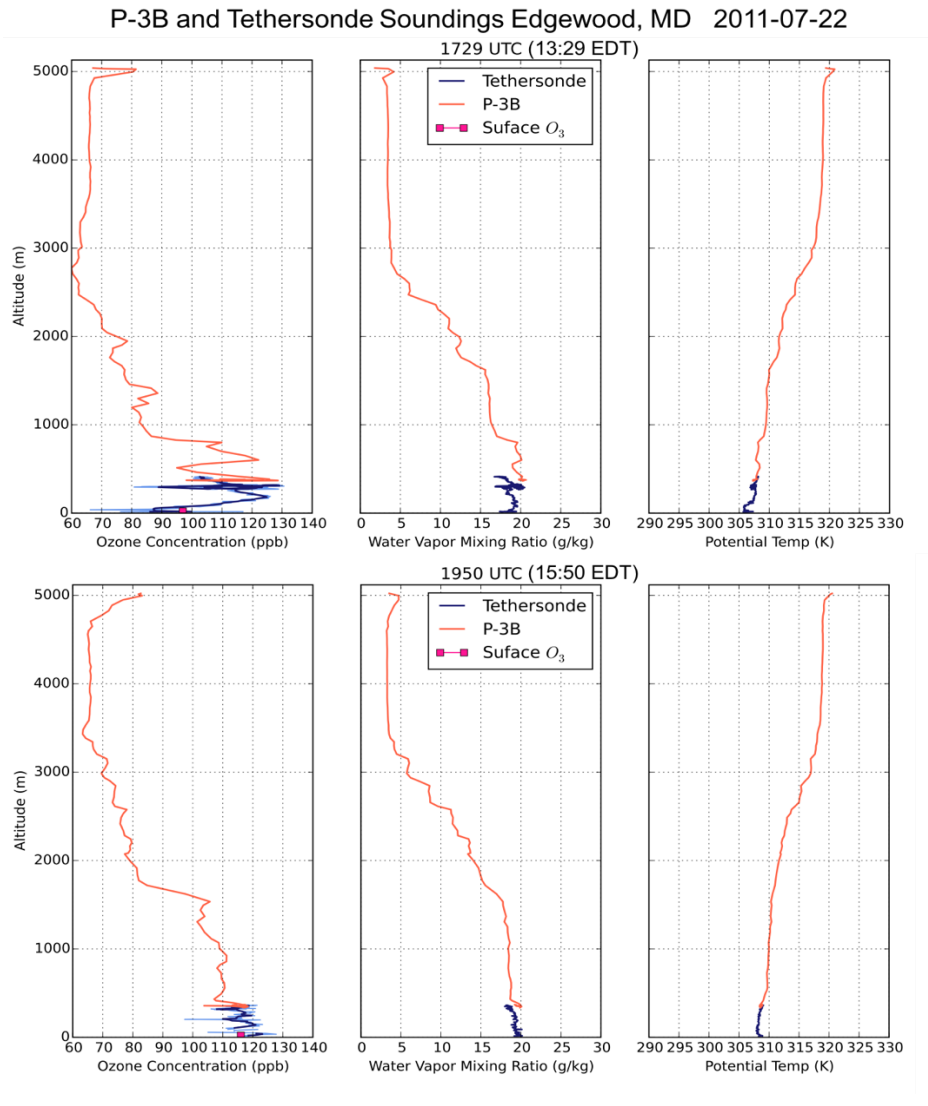


Figure 4.4 P-3B profiles (orange), tethered balloon profiles (blue), and surface O₃ (pink square) for the second spiral of the day (first spiral after the storm; top) and the third spiral of the day (bottom). First panel: O₃ concentration (ppb) with height in AGL; Second panel: water vapor mixing ratio (g/kg) with height, and potential temperature (K) with height.

Since the storms were relatively small in their horizontal spatial (a few km) and temporal extent (~1hr), they only decreased O₃ concentrations locally, not regionally, as otherwise observed from storms forced by large-scale dynamics. Because the air

transported to the site after the thunderstorm came from the Baltimore area as indicated in a NOAA Air Resources Laboratory (ARL) HYbrid Single- Particle Lagrangian Integrated Trajectory (HYSPLIT) model back trajectory (Figure 4.5), the concentration of O₃ and its precursors increased substantially after the thunderstorm to levels that were higher than previously observed before the thunderstorm (Figure 4.2).

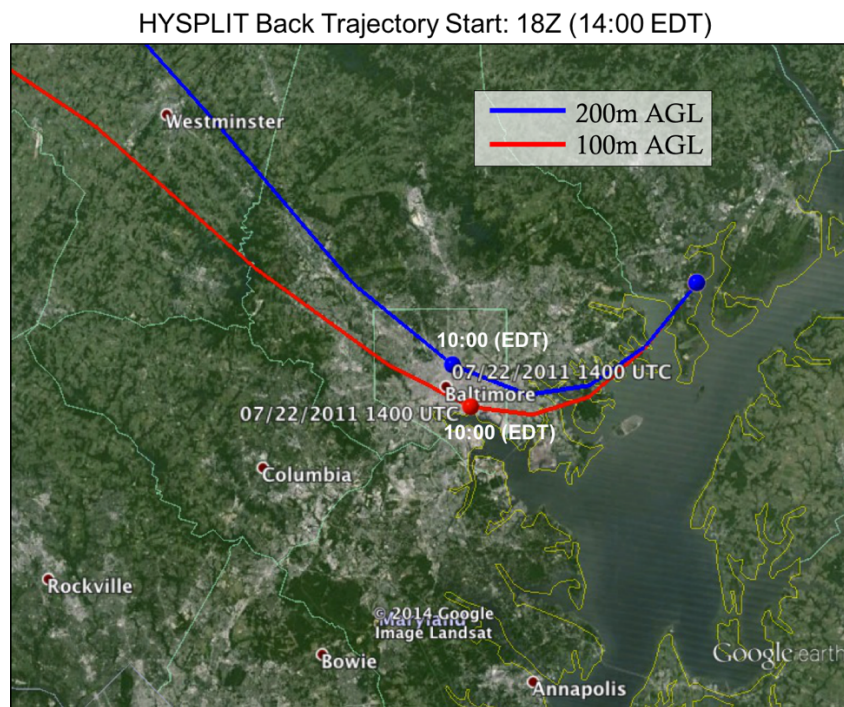


Figure 4.5 HYSPLIT back trajectory initialized by the North American Mesoscale (NAM) model at 18Z (14:00 EDT) at Edgewood, MD. Blue line: trajectory at 200m; red line: trajectory at 100m. Dots on the trajectories represent the location at the given time (10:00 EDT). These trajectories indicate that the air transported to Edgewood, MD after the thunderstorms had passed through the Baltimore metropolitan area at the end of rush hour and is likely the source of the high O₃ and precursor concentrations observed at the Edgewood site in the afternoon after a temporary reduction in concentrations.

Some sites that were not affected by the storms of interest within the DISCOVER-AQ domain, for example Aldino and Fairhill, observed a relatively steady increase in O₃ concentration and a notable increase during peak daytime heating between 14-16 EDT. The sites that were affected by the thunderstorms, Edgewood and Essex, experienced notable decreases in O₃ concentration during and temporarily after the storm, but returned to high O₃ concentrations after the passage (Figure 4.6). During this day, the thunderstorms had little to no effect on the sites exceeding the 8-hr O₃ standard.

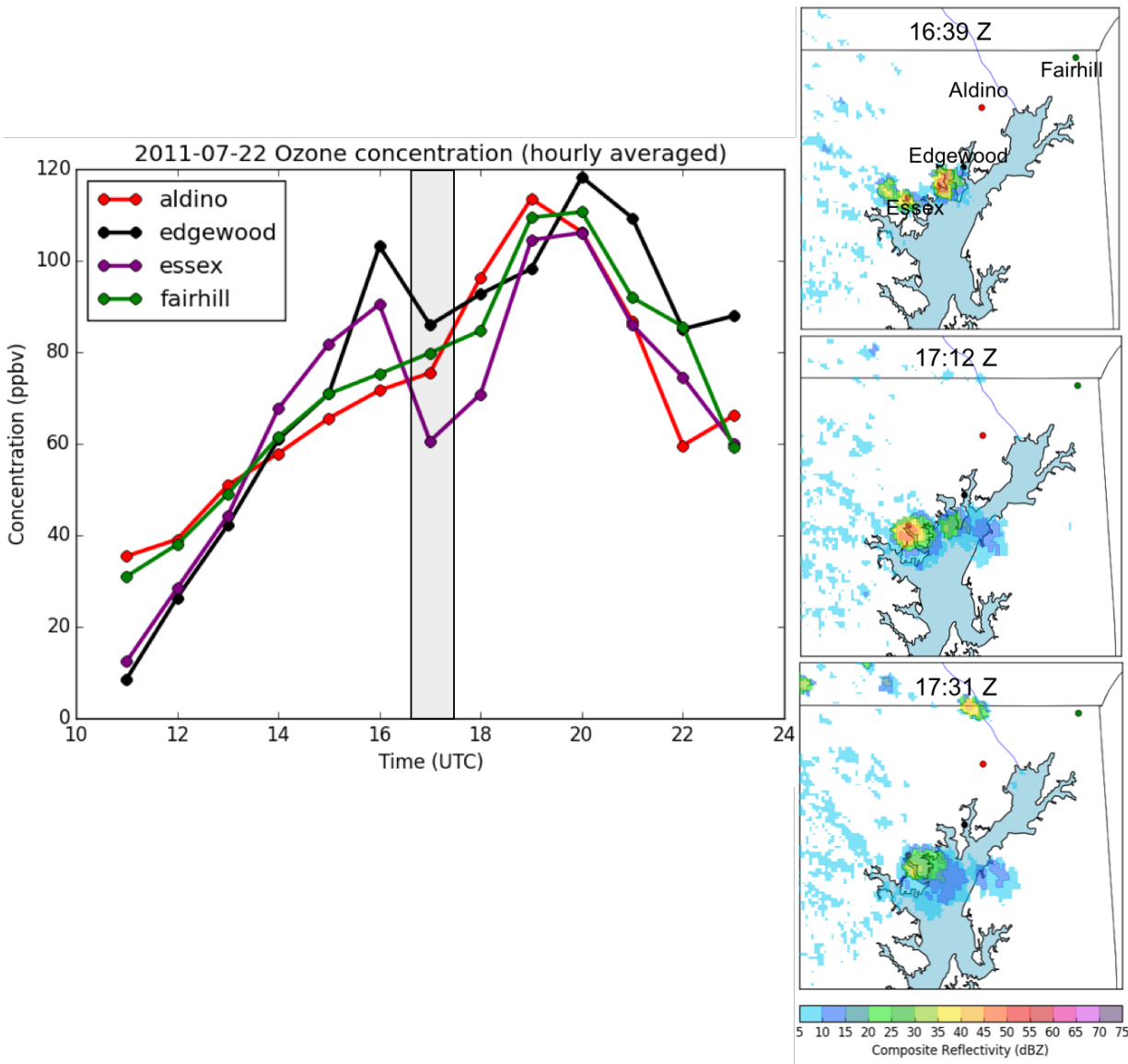


Figure 4.6 Left: Surface O₃ concentration (ppbv) at Aldino, Edgewood, Essex, and Fairhill, MD. Right: Site locations and composite radar reflectivity (dBZ) from Sterling, VA (KLWX) demonstrating the relative thunderstorm extent and sites directly affected (Edgewood and Essex) for three different stages of the thunderstorms. The shaded box on the left indicates the time during the time series of O₃ concentration that corresponds to the radar reflectivity on the right. Note that the eastern cell dies out first.

4.3.2 WRF Modeling: 22 July 2011 Combined Bay Breeze and Thunderstorm Case Study in Maryland

To understand the variety of complex mesoscale processes that occurred in the DISCOVER-AQ project domain on this day, the WRF model was run at fine resolution (333 m horizontal and 90 vertical levels) with the goal of capturing the bay breeze and the thunderstorms and to understand mixing and pollutant distribution. However, it should be noted that even at fine resolution, it is difficult for numerical weather prediction models to properly identify and simulate the timing, location, and intensity of quasi-random convection in the absence of large-scale dynamical triggers or data assimilation techniques.

At the two Edgewood monitors used during DISCOVER-AQ, the Millersville University (MU) site and the Maryland Department of the Environment (MDE) site, which were ~2.7 km apart (Figure 4.7), observations of water vapor mixing ratio were compared to each other and to the WRF model output. To correct for the erroneous storms and to obtain a simulation of the observed storms in the correct place and time, the lightning data assimilation technique (LDA) explained in Section 4.2 was performed using ENTLN lightning data and water vapor damping. The water vapor concentrations after damping are similar to those concentrations observed at the ground sites (Figure 4.8). The simulations shown here are with LDA and damping.

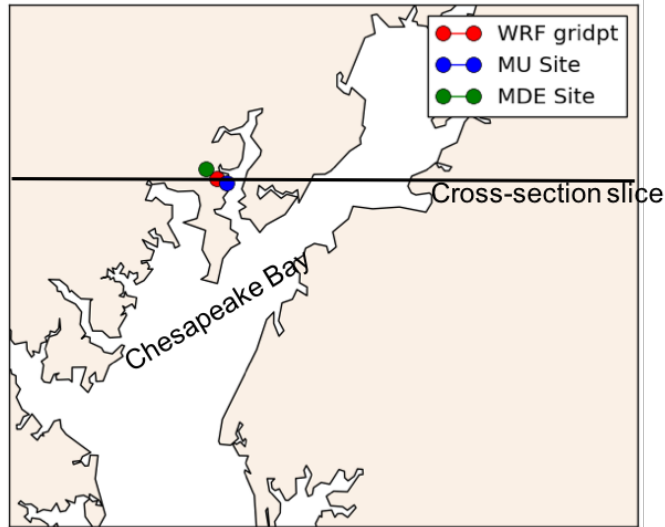


Figure 4.7 Locations of the Millersville University site (MU; blue), the Maryland Department of the Environment site (MDE; green), and the middle grid point from the WRF simulation between the two sites (WRF; red). Line: cross-section slice used in Figure 4.10.

While there is significant over-prediction of water vapor mixing ratio in the model output before damping begins at 16:00 UTC (12:00 EDT) due to over-prediction in the initial conditions by an erroneous water vapor observation appearing to be assimilated into the HRRR output, WRF correctly identifies the timing of the bay breeze (Figure 4.8). The bay breeze is correctly identified in WRF with respect to timing and relative change in water vapor.

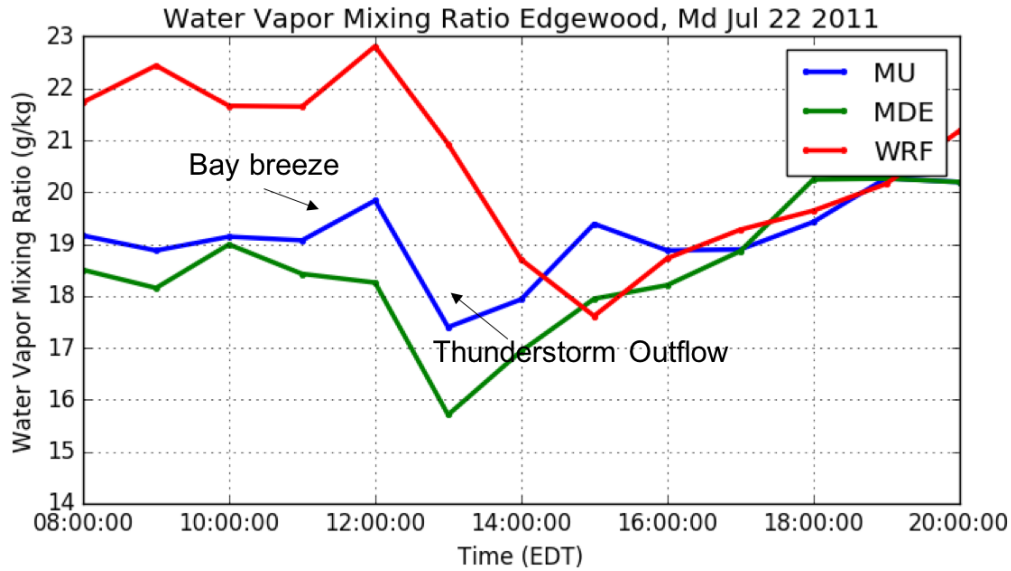


Figure 4.8 Surface water vapor mixing ratio (g/kg) observations at the MU site (blue) and the MDE site (green), and 2m WRF output (red). The observations are hourly averaged. The MU and MDE sites were ~2.7 km away from each other with the MU site closer to the bay with more influence from the bay breeze and the thermal internal boundary layer.

Disregarding the artificial high bias (dark blue) during initialization, the general distribution of 2-m water vapor in the model agrees well with the observations (colored circles; Figure 4.9) at the MDE (EPA monitoring site) surface sites as the bay breeze began to form, showing that there is a realistic representation of the bay breeze without too far inland penetration (Figure 4.9).

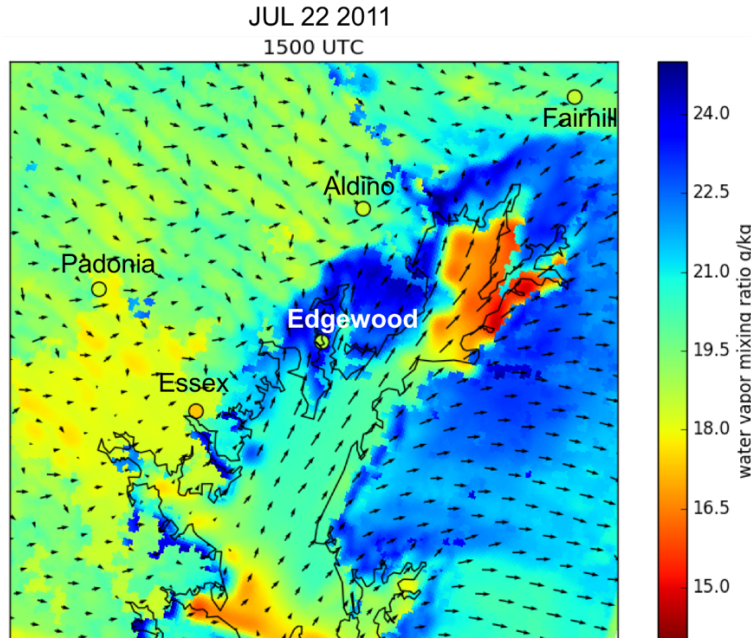


Figure 4.9 2-m WRF water vapor mixing ratio (g/kg) and the observations at MDE monitors in the domain (colored circles). MDE observations are the 15 minute average from 14:45 – 15:00 UTC.

The water vapor mixing ratio in the combined P-3B spiral and tethered balloon profile immediately after the bay breeze passage and before the thunderstorm initiation around 12:00 EDT matches the water vapor mixing ratio from WRF, and is able to capture the high water vapor concentrations observed throughout the boundary layer near the bay breeze front, despite the unrealistically high water vapor from the initialization (Figure 4.10). By the next combined profile around 13:40 EDT, the P-3B observations between ~300-800 m show larger amounts of water vapor than the model, however the tethered sonde which profiled ~30 minutes later, agrees well with the drier water vapor concentrations in the lower boundary layer in the model (Figure 4.10). This demonstrates the rapid changes that meteorological variables can exhibit in a short amount of time, which can be difficult to model accurately.

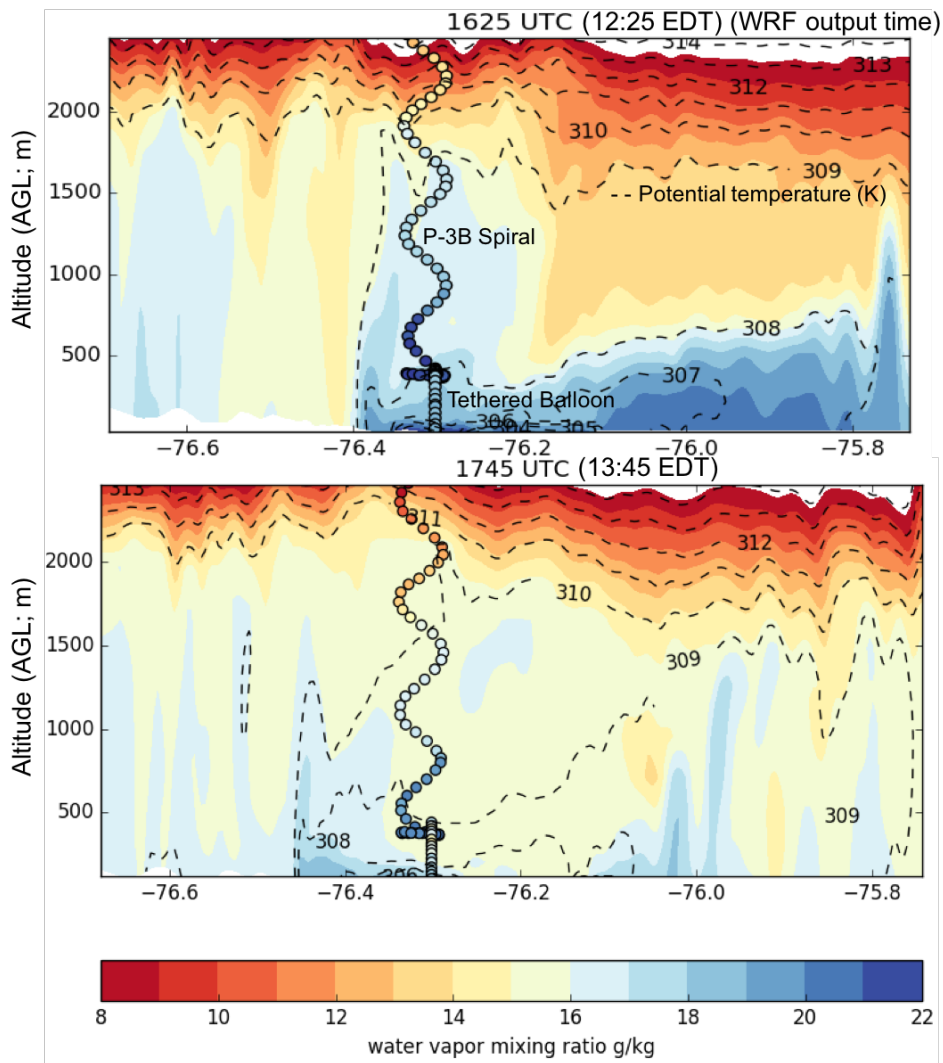


Figure 4.10 Vertical cross-section of WRF water vapor mixing ratio with height across the slice denoted in Figure 4.7 at the times that matched the observations best within a 30 minute window. The timing for the P-3B spiral was between 15:30-15:49 UTC (11:30 – 11:49 EDT) and the tethered balloon profile was taken between 15:30 – 16:04 UTC (11:30 – 12:04 EDT) for the first combined profile (top panel) and the P-3B spiral was between 17:35 – 17:54 UTC (13:35 – 13:54 EDT) and the tethered balloon profile was taken between 18:20 – 18:40 UTC (14:20 – 14:40 EDT) for the second combined profile (bottom panel). Dashed lines are modeled potential temperature (K).

With use of the LDA technique, radar reflectivity from the observed deep convection was appropriately simulated in the model (Figure 4.11). In the simulation,

the thunderstorms were slightly more intense in reflectivity than observed, however the model captured similar timing, location, and dissipation of the isolated storms. Additionally, with the use of LDA, the simulation represents the upward vertical transport of boundary-layer air associated with the updraft (Figure 4.12). The storms were only able to temporarily (during and after the storm) alter the composition of the air in the boundary layer. Even storms with rapid vertical transport, overshooting tops, and drier and cleaner downdrafts seem to be no match against the horizontal transport of moist, polluted air after the storm dissipates. While these storms were tall, their horizontal extent was small and did not have wide-spread influence on surface meteorological and chemical composition. However, with a meteorological simulation that adequately simulates the mesoscale dynamics observed on this complex weather day, a further inspection of the mixing, upward vertical transport, and origins of downdrafts should be addressed with the use of chemical tracers in WRF.

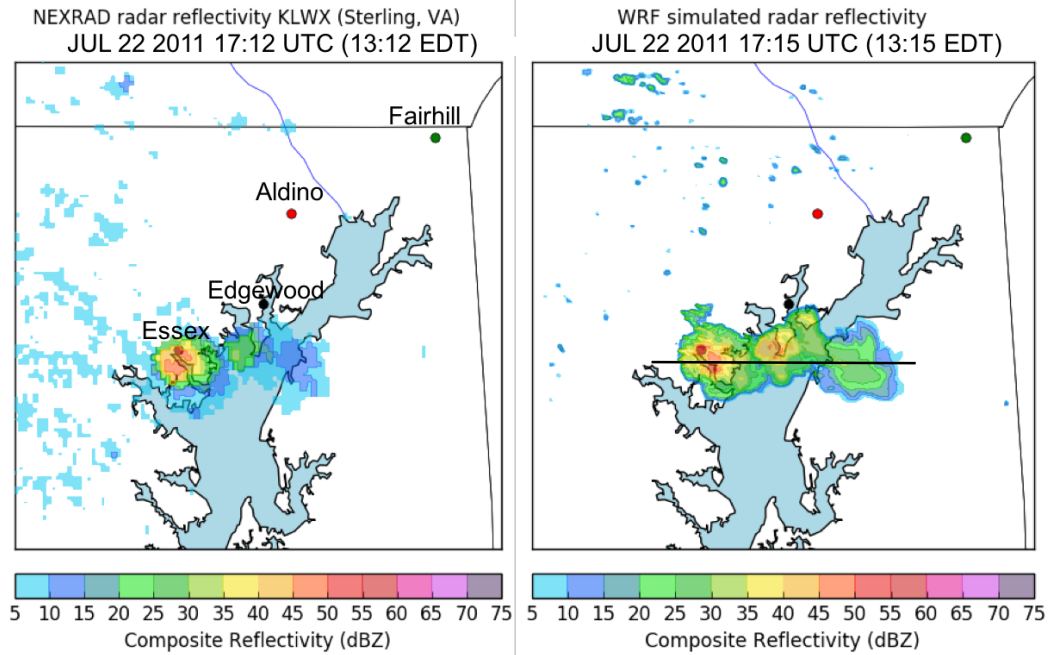


Figure 4.11 Left: Observed composite radar reflectivity from NEXRAD KLWX (Sterling, VA) in dBZ and right: modeled composite radar reflectivity from the WRF simulation using the LDA technique during the dissipation stage of cell near Edgewood and the peak intensity of the cell over Essex.

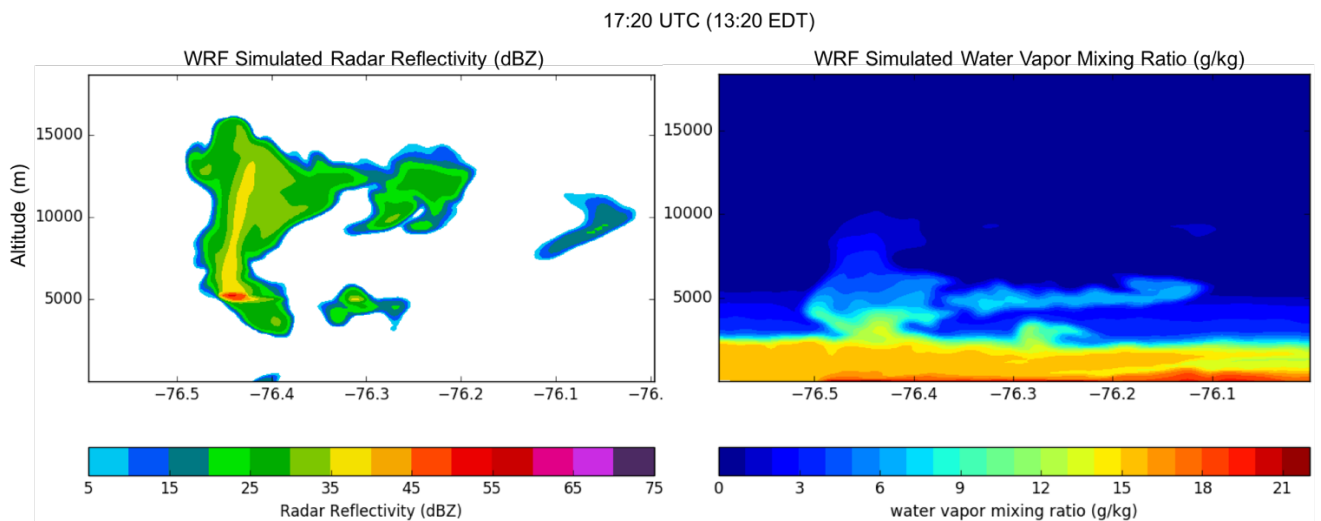


Figure 4.12 Vertical cross-section of radar reflectivity (left) in dBZ and water vapor mixing ratio (right) in g/kg from the slice denoted by the black line in Figure 4.11 (right). This is around the time of maximum reflectivity for the western-most cell while the eastern-most cell is in its dissipation stage. In the water vapor cross-section, there is notable water vapor present in upper-altitudes and above the boundary layer demonstrating vertical transport, however, it is also notable that the boundary layer is not affected by the drier mid-tropospheric downdraft air.

4.3.3 Observations: 29 July 2014 Mountain Breeze and Thunderstorm Case Study in Colorado

The final deployment of DISCOVER-AQ took place in the Denver, CO metro area in July-August 2014 in association with the Front Range Air Pollution and Photochemistry Experiment (FRAPPE). The location chosen for this case study Golden-NREL on a small plateau at the foothills of the mountains, which was also the site of the tethersonde, P-3B aircraft spirals, and an array of surface instrumentation (Figure 4.13).

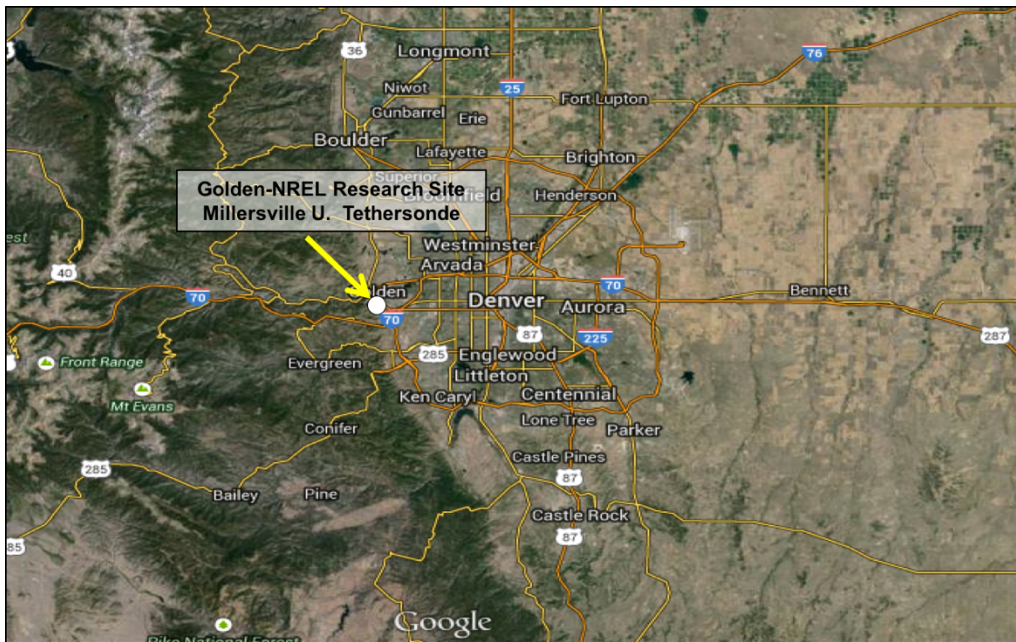


Figure 4.13 Terrain map of the area referred to as the Front Range of Colorado, as well as Golden-NREL, CO, one of the surface and spiral sites during the DISCOVER-AQ deployment in July-August 2014 and the site chosen for the case study described in this section.

This deployment of DISCOVER-AQ experienced complex meteorology as a result of pop-up thunderstorms due to daytime heating over the mountains and mesoscale circulations associated with the Denver Cyclone (Vu et al., 2016), all interacting with the moisture feed from the North American (NA) Monsoon. However, while the NA monsoon was responsible for supplying water vapor over a large scale, and thus changing the stability over the area affected, the storms that occurred during this deployment have individual characteristics and sources of initiation due to local topography and interactions with synoptic forcing. During this campaign, 8 out of 24 flight days were associated with thunderstorms according to an inspection of radar reflectivity from KFTG (Denver International Airport) that had affected the Golden, CO site. In July, the Front Range was wetter than average, as the 5th wettest July on record (Sullivan et al., 2016). In addition, there were only seven O₃ exceedances at Colorado monitors in July 2014 in comparison to 44 the year before (2013) and 61 two years prior (2012) (Sullivan et al., 2016). Since there was convection quite frequently during the deployment, an investigation of Convective Available Potential Energy (CAPE) and its probability distribution at Golden, CO was conducted to understand whether deep convection in this year was anomalous. The CAPE values were derived from the North American Regional Reanalysis (NARR; Mesinger et al., 2006). According to the probability distribution of the reanalysis, CAPE values for 2014 at Golden were slightly larger than those of the average between 2005-2016 at 18 UTC (local noon) for CAPE > 500 J/kg, particularly in July with two separate populations >1000 J/kg (Figure 4.14). This indicates that July had the potential to be

more convectively active in 2014 than previous years during local noon, thus likely having a role in the relatively low O₃ concentrations observed during the campaign.

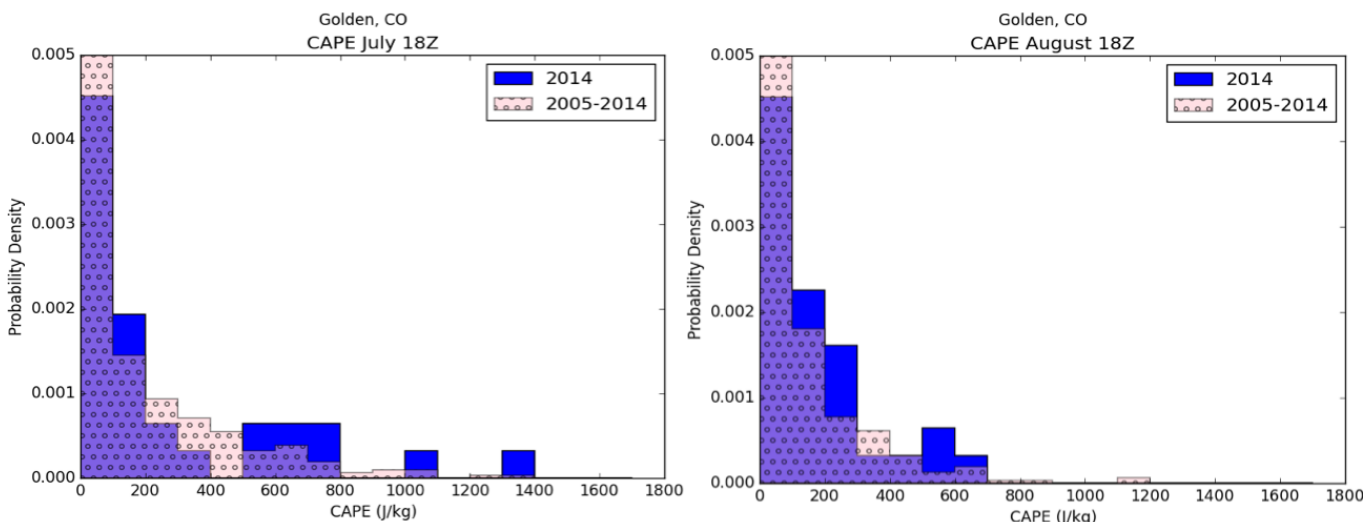


Figure 4.14 Normalized probability distribution of Convective Available Potential Energy (CAPE) in J/kg for July and August, 2014 at Golden-NREL, CO at 18Z (12 MDT). Blue blocks are for 2014 only, pink blocks with circles are for 2005-2014, and the overlap is in purple. The probability distribution of CAPE for values > 500 J/kg is higher in July and August for 2014 than for 2005-2014.

Of particular interest, thunderstorms observed during the campaign in the Front Range often acted to terminate the pollution episode, where in the case study from Maryland, the thunderstorm had little to no effect on surface O₃ concentration after the storm, or on average on thunderstorm days. At Golden, many of the days with a thunderstorm resulted in lower hourly O₃ concentrations compared to days without thunderstorms, particularly during August 2014 (Figure 4.15). One of the days, 29 July 2014, was chosen for a case study, as the pollution episode was terminated by thunderstorms in the area.

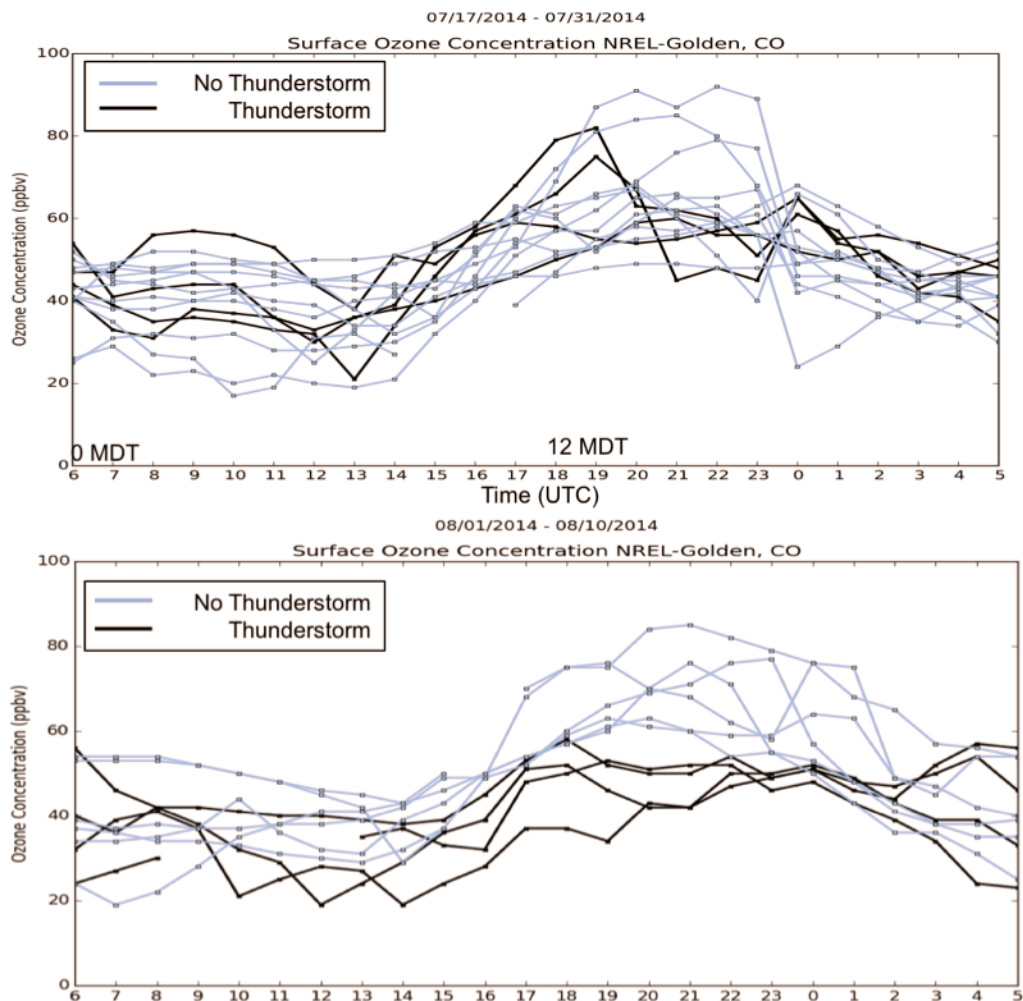


Figure 4.15 Hourly averaged O_3 concentration vs. time (UTC; where MDT is UTC-6) during the DISCOVER-AQ CO deployment (07/17/14 – 08/10/2014). Top: O_3 vs. time of day for July and Bottom: O_3 vs. time for August. Blue lines are days that did not exhibit a thunderstorm and thunderstorm and black lines are days that had a thunderstorm, based on the examination of radar reflectivity.

July 29, 2014 featured relatively high pressure over the CO area with some clouds, but generally conducive for photochemical smog production. O_3 rose from an average of 40 ppbv in the morning to an hourly average above 80 ppbv by local noon (18 UTC) at Golden. As the surface heated throughout the morning, the winds were mostly from the east, as upslope mountain flow (Figure 4.16).

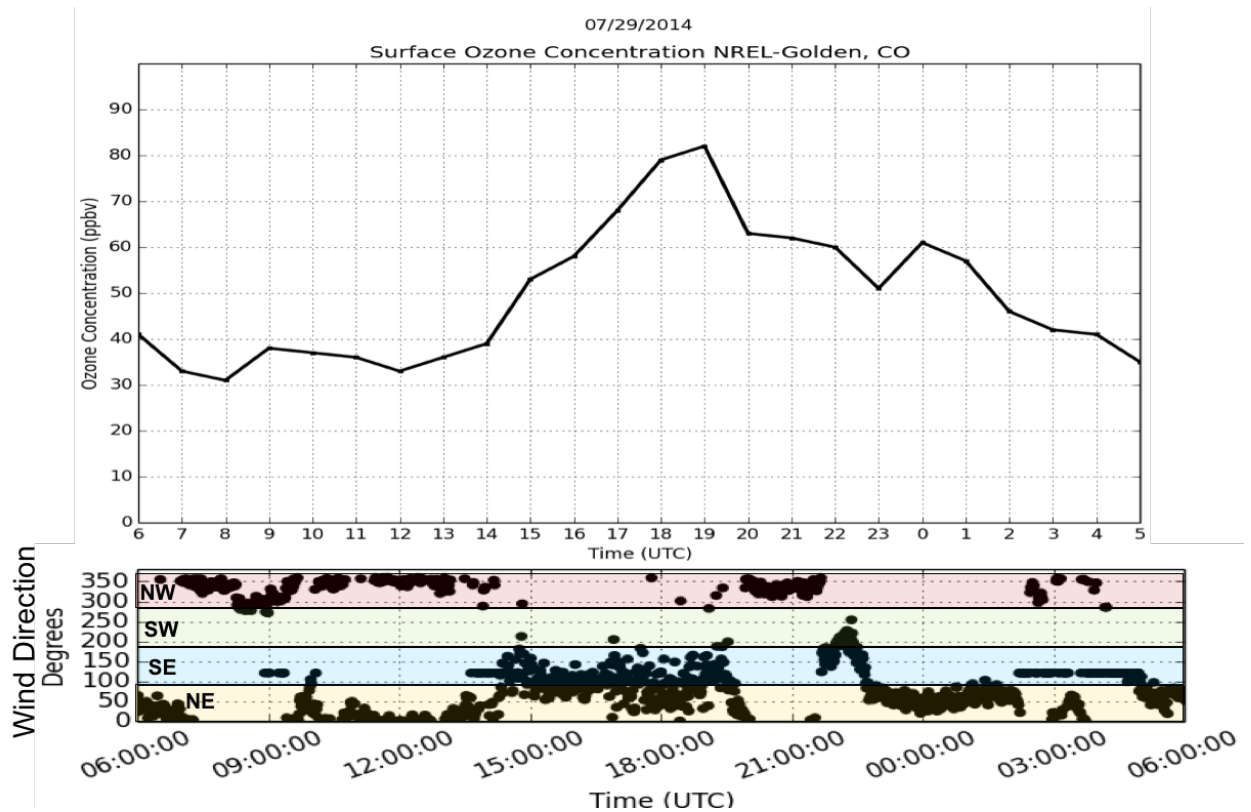


Figure 4.16 Top: Hourly averaged O₃ concentration on 29 July 2014 in UTC (where MDT is UTC-6). Bottom: 1-minute avg. wind direction (0-360°), color coded by the direction from which the winds are blowing (yellow: NE, blue: SE, green: SW, red: NW) from bottom to top.

However, shortly after 13:00 MDT, similar to the Maryland case study and typical for Colorado, an afternoon thunderstorm had popped up over the mountains that moved over the site, along with outflow from a larger mesoscale complex to the east, potentially forced by the DCVZ (Figure 4.17).

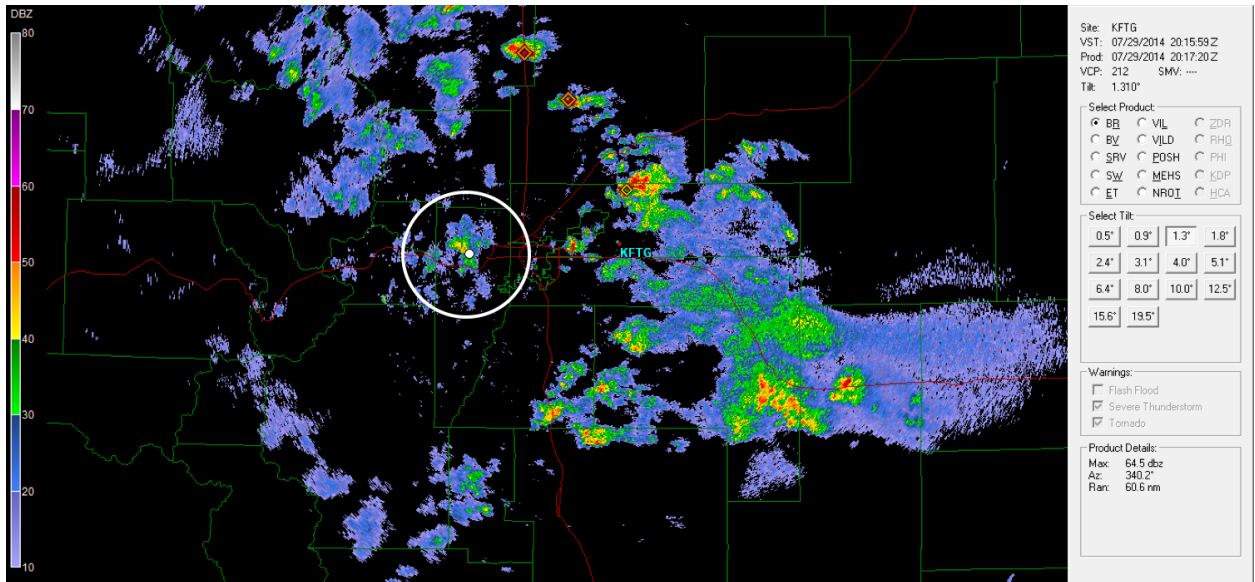


Figure 4.17 Radar reflectivity at 1.3° tilt from the Denver International Airport (KFTG) on JUL 29 2014 at 14:15 MDT (20:15 UTC). The white dot is the location of the site (Golden, CO) and the circled storm is the one that directly influenced the site. Outflow was also observed at the site from the larger system to the east.

As the storms began to impact the site, the winds shifted from E to NW, and then eventually back to easterly later in the afternoon. While there were still several hours of sunlight after the storm had passed, with outflow from a nearby storm transporting air from Denver to the site, O₃ levels never returned to previous levels remained below levels experienced prior to the storm. This differs from the Maryland storm case, where the O₃ concentration had risen to higher levels post-storm than before the storm.

4.4 Discussion

The WRF simulation for the Maryland storm was run at fine resolution to capture the mesoscale events that were short-lived and had a relatively small spatial extent. It should be noted that even running the simulation at fine resolution does not

necessarily mean that the model will capture quasi-random events correctly, without the use of additional nudging or assimilation techniques. However, in models used for regulatory chemical modeling, the resolution (both vertical and horizontal) is much coarser than the simulation shown here. Given how difficult it is to simulate the correct small-scale but impactful meteorology, regulatory models run at coarse resolution are missing some of these important mesoscale features (bay breezes, mountain breezes, and thunderstorms). In the absence of accurate meteorological simulations, the chemical models miss the modulation of surface O₃ by mesoscale events at sites near bodies of water or complex terrain. An effort should be made in making improvements to the resolution of meteorology in the regulatory chemical modeling framework, such that these mesoscale features are captured in the model and the resulting changes in O₃ are well represented.

An in-depth comparison of storms in two different areas, Maryland and Colorado, that are forced by topographic flow (bay breezes and mountain circulations), should be further investigated to determine if the responses in O₃ concentrations at the surface are due to storm dynamics or subsequent photochemistry and transport post-storm. In the Maryland analysis, the thunderstorm had little to no effect on the exceedance of the O₃ standard on the case study day, and it was also found in Chapter 3 that the O₃ average was higher on days with thunderstorms and bay breezes than days without, since the conditions favorable for O₃ are also favorable for mesoscale breezes and deep convection. It should also be noted that the different types of convective systems that arise from Colorado mountain dynamics may have very different effects on surface O₃. For example, storms forced by day-

time heating over the mountains vs. larger-scale convective complexes forced by the DCVZ may alter O₃ in different manners, and therefore can further complicate the impacts that thunderstorms have on surface O₃ along the Front Range.

4.5 Summary and Future Work

A day with two small-scale, but significant, mesoscale events (bay breeze and thunderstorms) occurred at one of the DISCOVER-AQ sites along the Chesapeake Bay during the 2011 deployment. The events on this day led to a variety of effects on surface O₃: a significant rise in O₃ concentrations during the bay breeze, a drastic decrease during the time of the thunderstorms, and another notable rise in O₃ concentrations after the thunderstorms had dissipated. A WRF simulation was performed to simulate the complex meteorology on that day. The WRF model was able to produce a relatively accurate bay breeze (in timing and location), considering its initialization error, and also a thunderstorm that compares well to the observed radar reflectivity, after using a LDA method. I will conduct a further investigation of vertical mass flux from boundary-layer venting and the sources and strength of the downdraft to better understand the vertical transport and interactions that had occurred within this storm that failed to terminate a pollution episode. While vertical transport in thunderstorms acts as a quick and powerful way of ejecting polluted boundary-layer air out of, and entraining cleaner mid-tropospheric air into the boundary layer, it has been shown here that in some cases, the large vertical transport velocities associated with deep convection are less influential than the subsequent horizontal transport of polluted air to the area of interest, during and after a thunderstorm. The small horizontal extent of the storms in this analysis did not clean

out pollutants upwind of the deep convective cells, therefore only temporarily reducing O₃ concentrations at sites that were directly affected by storm downdraft and outflow.

In a DISCOVER-AQ Colorado deployment case study, it was shown the site was subject to upslope mountain flow due to differential day-time heating and thunderstorm activity. On this day, O₃ concentrations at the site: increased during the time of upslope flow and surface heating, decreased from the thunderstorm, and in this case, did not recover after the storm. The topographically-induced mesoscale dynamics in the Colorado area are very complex, and thus can result in a variety of influences on surface O₃. A climatology at a Colorado site should be performed, similar to the Chapter 3 Edgewood, MD analysis, where a climatology of thunderstorms (with separation of thunderstorm types, e.g., pop-up, frontal, DCVZ), mountain breezes, and O₃ events are analyzed. This analysis would be useful in determining sources of predictability of an O₃ event or termination by mesoscale circulations. A WRF simulation with tracers may also be useful to understand vertical transport of the two different types of storm initiation (pop-up vs. DCVZ), downdraft origins, and subsequent horizontal transport, and to compare it to the Maryland WRF simulation case.

Chapter 5: Ozone Production and Its Sensitivity to NO_x and VOCs: Results from the DISCOVER-AQ Field Experiment, Houston 2013 (published as Mazzuca et al., 2016)

5.1 Introduction

Understanding the non-linear relationship between O₃ production and its precursors is critical for the development of an effective O₃ control strategy. Despite great efforts undertaken in the past decades to address the problem of high O₃ concentrations, our understanding of the key precursors that control tropospheric O₃ production remains incomplete and uncertain (Molina and Molina, 2004; Xue et al., 2013). Atmospheric O₃ levels are determined by emissions of O₃ precursors, atmospheric photochemistry, and transport (Jacob, 1999; Xue et al., 2013). A major challenge in regulating O₃ pollution lies in comprehending its complex and non-linear chemistry with respect to O₃ precursors, i.e., nitrogen oxides (NO_x) and volatile organic compounds (VOCs) that varies with time and location (Figure 5.1). Understanding the non-linear relationship between O₃ production and its precursors is critical for the development of an effective O₃ control strategy.

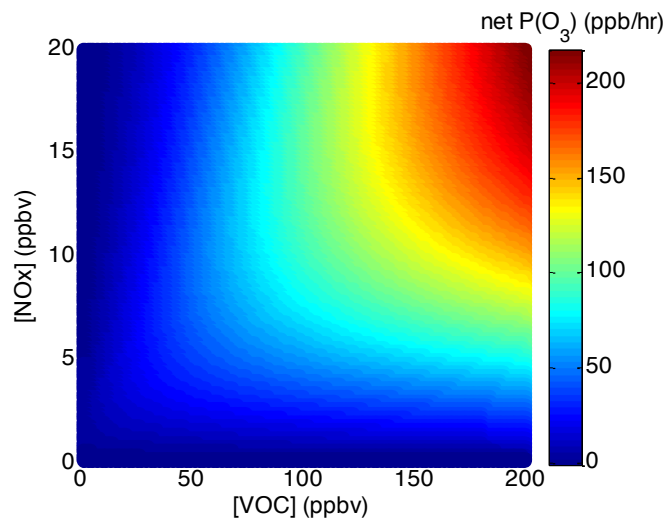


Figure 5.1 O₃ production empirical kinetic modeling approach (EKMA) diagram using box model results with NO_x levels varying from 0-20 ppbv and VOC levels from 0-200 ppbv while the mean concentrations of other species and the speciation of NO_x and VOCs observed during DISCOVER-AQ in Houston in 2013 were used to constrain the box model. This diagram clearly shows the sensitivity of O₃ production to NO_x and VOCs in Houston.

Sensitivity of O₃ production to NO_x and VOCs represents a major uncertainty for oxidant photochemistry in urban areas (Sillman et al., 1995; 2003). In urban environments, O₃ is formed through photochemical processes when its precursors, NO_x and VOCs, are emitted into the atmosphere from many sources. Depending on physical and chemical conditions, the production of O₃ can be either NO_x-sensitive or VOC-sensitive due to the complexity of these photochemical processes. Therefore, effective O₃ control strategies rely heavily on the accurate understanding of how O₃ responds to reduction of NO_x and VOC emissions, usually simulated by photochemical air quality models (e.g., Sillman et al., 2003; Lei et al., 2004; Mallet and Sportisse, 2005; Li et al, 2007; Chen et al., 2010; Tang et al., 2010; Xue et al., 2013; Goldberg et al., 2016). However, those model-based studies have inputs or

parameters subject to large uncertainties that can affect not only the simulated levels of O₃, but also the O₃ dependence on its precursors.

There are some observation-based studies of O₃ production and its relationships with NO_x and VOCs (e.g., Thielmann et al., 2002; Zaveri et al., 2003; Ryerson et al., 2003; Griffin et al., 2003; Kleinman et al., 2005a; Neuman et al., 2009; Mao et al., 2010; Ren et al., 2013). Kleinman et al. (2005a) studied five U.S. cities using in-situ aircraft observations and found that O₃ production rates vary from nearly zero to 155 ppb hr⁻¹ with the differences dependent on the concentration of O₃ precursors NO_x and VOCs. This study also found that in Houston, NO_x and light olefins are co-emitted from petrochemical facilities which led to the highest O₃ production rate of the five cities (Kleinman et al., 2005a). Using the data collected at a single surface location during the Study of Houston Atmospheric Radical Precursors (SHARP) field mission in the spring of 2009, the temporal variation of O₃ production was observed. It was VOC-sensitive in the early morning and NO_x-sensitive for most of the afternoon (Ren et al., 2013). This sensitivity is similar to the behavior observed in two previous summertime studies in Houston: the Texas Air Quality Study in 2000 (TexAQS 2000) and the TexAQS II Radical and Aerosol Measurement Project in 2006 (TRAMP 2006) (Mao et al., 2010; Chen et al., 2010). In a more recent study using measurements in four cities in China, O₃ production was found to be in the VOC-sensitive regime in both Shanghai and Guangzhou, but in a mixed regime in Lanzhou (Xue et al., 2013). In the work presented here, we provide results that demonstrate the spatial and temporal variations of O₃ production and its sensitivity to NO_x and VOCs. This information provides a scientific basis for the

development of a non-uniform emission reduction strategy for O₃ pollution control in urban and suburban areas, such as the greater Houston metropolitan area.

This work utilized observations made during the DISCOVER-AQ campaign in Houston in September 2013. This field campaign is unique due to the comprehensive air sampling performed over a large spatial (urban and suburban areas in and around Houston) and temporal (entire month of September 2013) range. Measurements were collected from various platforms, including the NASA P-3B and B-200 aircraft, ground surface sites, and mobile laboratories. Eight surface monitoring stations (Smith Point, Galveston, Manvel Croix, Deer Park, Channelview, Conroe, West Houston, and Moody Tower) were selected where the P-3B conducted vertical spirals (Figure 5.2) (https://www.nasa.gov/mission_pages/discover-aq/index.html).

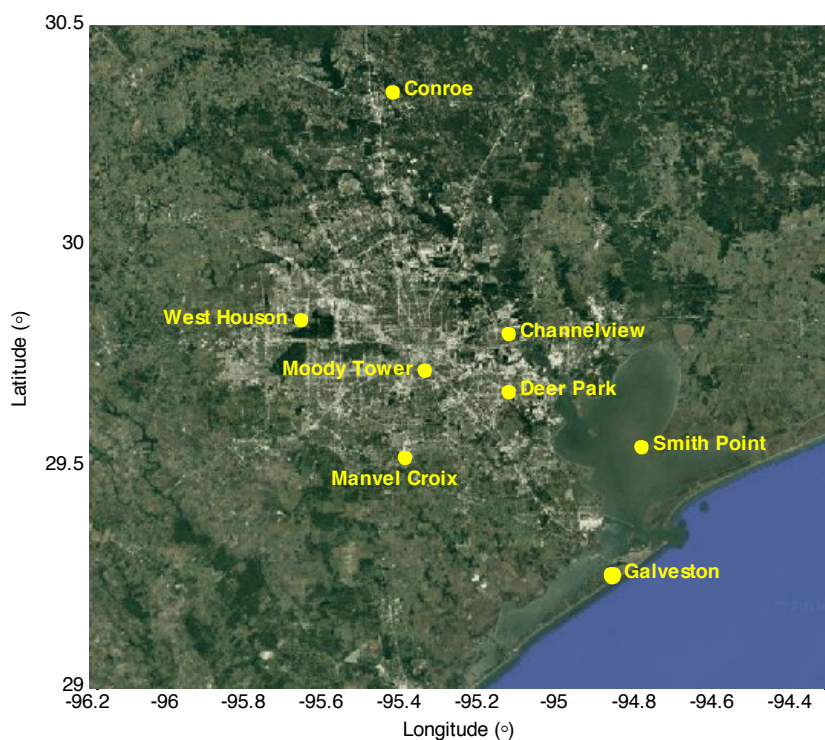


Figure 5.2 DISCOVER-AQ ground and spiral sites (yellow dots) during the September 2013 Houston campaign.

5.2 Methods

5.2.1 O₃ Production and Sensitivity

During the day, the photochemical production rate of O₃ is essentially the production rate of NO₂ molecules from HO₂ + NO and RO₂ + NO reactions (Finlayson-Pitts and Pitts, 2000). The net instantaneous photochemical O₃ production rate, P(O₃), can be written approximately as the following equation:

$$\begin{aligned}
 P(O_3) = & k_{HO_2+NO}[HO_2][NO] + \sum k_{RO_2i+NO}[RO_{2i}][NO] - k_{OH+NO_2+M}[OH][NO_2][M] - P(RONO_2) \\
 & - k_{HO_2+O_3}[HO_2][O_3] - k_{OH+O_3}[OH][O_3] - k_{O(^1D)+H_2O}[O(^1D)][H_2O] - L(O_3 + \textit{alkenes})
 \end{aligned} \quad (1)$$

where, *k terms* are the reaction rate coefficients; RO_{2i} is the individual organic peroxy radicals. The negative terms in Eq. (1) correspond to the reaction of OH and NO₂ to form nitric acid, the formation of organic nitrates, P(RONO₂), the reactions of OH and HO₂ with O₃, the photolysis of O₃ followed by the reaction of O(¹D) with H₂O, and O₃ reactions with alkenes. O₃ is additionally destroyed by dry deposition.

The dependence of O₃ production on NO_x and VOCs can be categorized into two typical scenarios: NO_x sensitive and VOC sensitive. The method to evaluate the O₃ production sensitivity as shown in Kleinman (2005b) uses the ratio of L_N/Q, where L_N is the radical loss via the reactions with NO_x and Q is the total primary radical production. Because the radical production rate is approximately equal to the radical loss rate, this L_N/Q ratio represents the fraction of radical loss due to NO_x. It was found that when L_N/Q is significantly less than 0.5, the atmosphere is in a NO_x-sensitive regime, and when L_N/Q is significantly greater than 0.5, the atmosphere is in a more VOC-sensitive regime (Kleinman et al., 2001; Kleinman, 2005b). It is noted however, that the contribution of organic nitrates impacts the cut-off value for L_N/Q to determine the O₃ production sensitivity to NO_x or VOCs, and this value may vary slightly around 0.5 in different environments (Kleinman, 2005b).

5.2.2 Box Model Simulations

An observation-constrained box model (Ren et al., 2013) with the Carbon Bond Mechanism Version 2005 (CB05) was used to simulate the oxidation processes in Houston during DISCOVER-AQ. P-3B measurements were used as input to constrain the box model. From the box model results, the O₃ production rate and its

sensitivity to NO_x and VOCs were calculated, also providing information to calculate O₃ production efficiency at different locations and at different times of day.

CB05 is a well-known chemical mechanism that has been actively used in research and regulatory applications (Yarwood et al., 2005). Organic species are lumped according to the carbon bond approach, that is, bond type, e.g., carbon single bond and double bond. Reactions are aggregated based on the similarity of carbon bond structure so that fewer surrogate species are needed in the model. Some organics (e.g., organic nitrates and aromatics) are lumped together. It was shown that the lifetime of alkyl nitrates is too long in CB05 and has been corrected in CB6r2 (Canty et al., 2015), but this should have minimal impact on our findings because the model is constrained to observations as indicated below.

The box model was run using measurements of long-lived inorganic and organic compounds and meteorological parameters (temperature, pressure, humidity, and photolysis frequencies), from the NASA P-3B. One-minute archived data were used as model input (available at <http://www-air.larc.nasa.gov/missions/discover-aq/discover-aq.html>). The model ran for 24 hours for each data point to allow most calculated reactive intermediates to reach steady state, but short enough to prevent the buildup of secondary products. An additional lifetime of two days was assumed for some calculated long-lived species such as organic acids and alcohols to avoid unexpected accumulation of these species in the model. At the end of 24 hours, the model generated time series of OH, HO₂, RO₂, and other reactive intermediates. The box model simulations covered the entire P-3B flight track during DISCOVER-AQ, including the eight surface sites where the P-3B conducted spirals. Note that unlike a

three-dimensional chemical transport model, the zero-dimensional box model simulations did not include advection or emissions. Although advection and emissions are certainly important factors for the air pollution formation, they can be omitted in the box model since all of the long-lived radical and O₃ precursors were measured and used to constrain the box model calculations. The box model analysis is necessary for O₃ production and its sensitivity to NO_x and VOCs because the box model was constrained to measured species (e.g., NO, NO₂, CO, HCHO, etc.) and meteorological parameters (e.g., photolysis frequencies) that are essential to calculate O₃ production rates. Even though there is good agreement in general between the box model and the 3D model, there are still some differences between the measurements and the output from the CMAQ model that are shown below (e.g., NO_x, CO, HCHO and photolysis frequencies).

5.2.3 WRF-CMAQ Model Simulations

The WRF model was run from 18 August 2013 to 1 October 2013 with nested domains with horizontal resolutions of 36, 12, 4, and 1 km and 45 vertical levels. This work utilized results from the 4 km domain. The modeling domains are shown in Figure 5.3 WRF was run straight through (i.e., was not re-initialized at all) using an iterative technique developed at the EPA and described in Appel et al. (2014). Observational and analysis nudging were performed on all domains. Model output was saved hourly for the 36 and 12 km domains, every 20 minutes for the 4 km domain, and every 5 minutes for the 1 km domain. WRF and CMAQ configuration options and inputs are shown in Table 5.1.

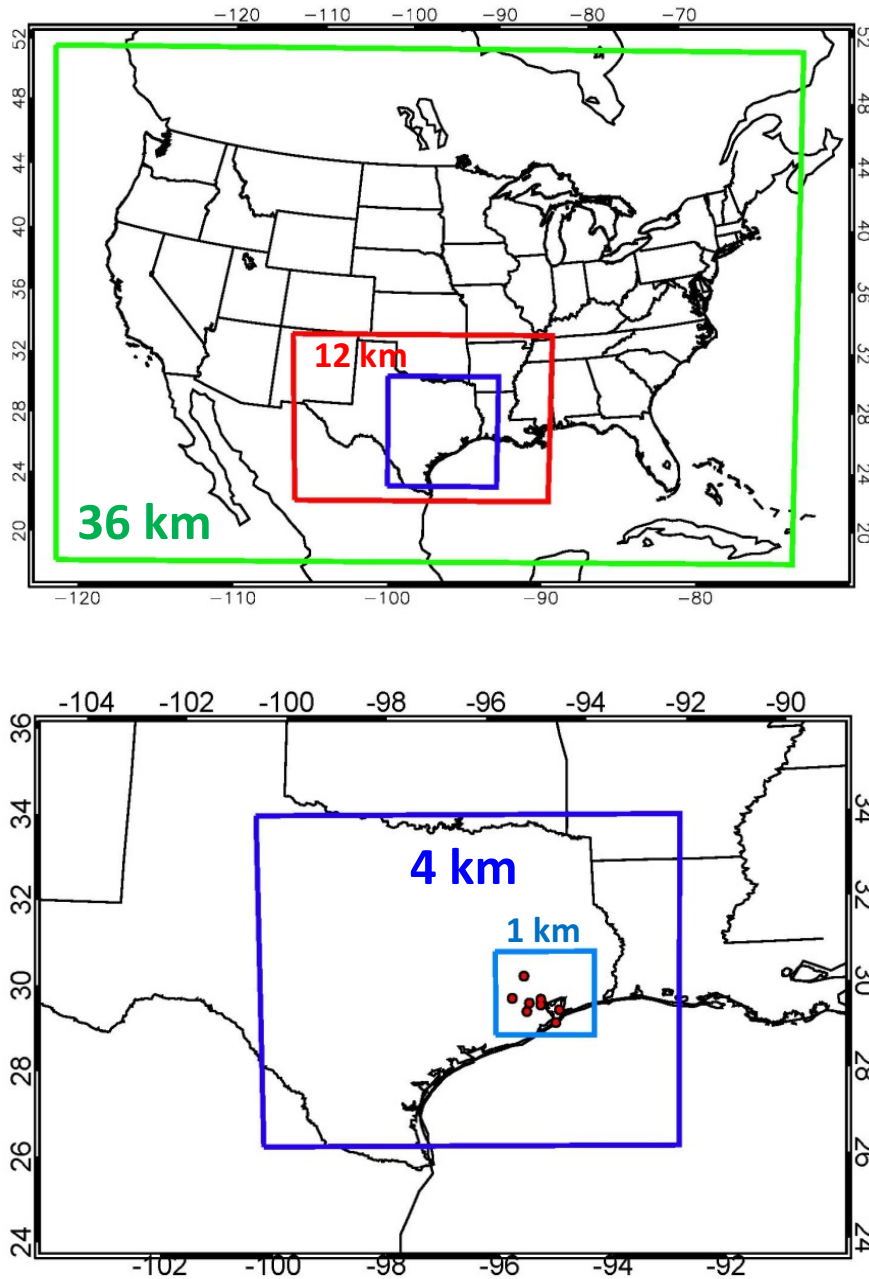


Figure 5.3 36, 12, and 4 km CMAQ modeling domains (top); 4 and 1 km CMAQ modeling domains. The red dots show the NASA P-3B aircraft spiral locations (bottom).

Table 5.1 WRF and CMAQ model options that were used in both the original and improved modeling scenarios.

Weather Research and Forecasting (WRF) Version 3.6.1 Model Options

Radiation	Long Wave: Rapid Radiative Transfer Model (RRTM) Short Wave: Goddard
Surface Layer	Pleim-Xiu
Land Surface Model	Pleim-Xiu
Boundary Layer	Asymmetric Convective Model (ACM2)
Cumulus	Kain-Fritsch
Microphysics	WRF Single-Moment 6 (WSM-6)
Nudging	Observational and analysis nudging
Damping	Vertical velocity and gravity waves damped at top of modeling domain
SSTs	Multi-scale Ultra-high Resolution (MUR) SST analysis (~1 km resolution)
Meteorological Initial and Boundary Conditions and Analysis Nudging Inputs	NAM 12 km
Observational Nudging Inputs	NCEP ADP Global Surface and Upper Air Observational Weather Data
CMAQ Version 5.0.2 Model Options	
Chemical Mechanism	Carbon Bond (CB05)
Aerosol Module	Aerosols with aqueous extensions version 5 (AE5)
Dry deposition	M3DRY
Vertical diffusion	Asymmetric Convective Model 2 (ACM2)

Emissions	2012 TCEQ anthropogenic emissions Biogenic Emission Inventory System (BEIS Version 3.14) calculated within CMAQ
Chemical Initial and Boundary Conditions	Model for OZone and Related chemical Tracers (MOZART) Chemical Transport Model (CTM)

WRF meteorological output was used to drive the CMAQ model offline. The 2012 baseline anthropogenic emissions from the Texas Commission on Environmental Quality (TCEQ) were used as input to CMAQ. These emissions contain the most-up-to-date Texas anthropogenic emissions inventory and a compilation of emissions estimates from Regional Planning Offices throughout the US. Biogenic emissions were calculated online within CMAQ with Biogenic Emission Inventory System (BEIS). Lightning emissions were also calculated online within CMAQ. CMAQ was run with the process analysis tool to output O₃ production rate (P(O₃)), O₃ loss rate (L(O₃)), and net O₃ production rate (net P(O₃)) as well as O₃ production efficiency (OPE).

5.3 Results

5.3.1 Photochemical O₃ Production Rate, Sensitivity, and Diurnal Variations

Figure 5.4 shows the net O₃ production rate (net P(O₃)) calculated using the box model along the P-3B flight track for all flight days during the Houston

deployment. There are several $P(O_3)$ hotspots over the Houston Ship Channel located to the east/southeast of downtown Houston as well as downwind, over Galveston Bay. This is expected because of large emissions of NO_x and VOCs from the Houston Ship Channel, where the highest $P(O_3)$ was observed – up to ~ 140 ppbv hr^{-1} . $P(O_3)$ values up to $\sim 80-90$ ppbv hr^{-1} were observed over Galveston Bay, mainly on September 25, 2013, consistent with high levels of O_3 observed across the Houston area on that day. Similar instantaneous O_3 production rates have been observed in two previous studies in Houston in 2000 and 2006 (Kleinman et al., 2002a; Mao et al., 2010).

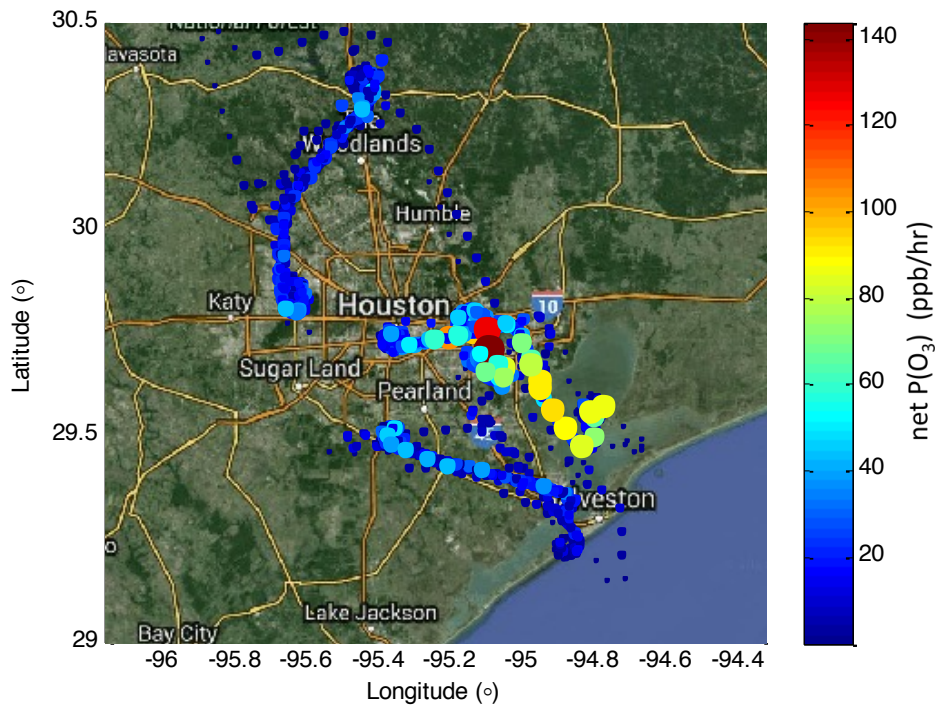


Figure 5.4 Net O_3 production rate ($net P(O_3)$) calculated from the box model results along the P-3B flight track during DISCOVER-AQ in Houston in 2013. The size of dots is proportional to $P(O_3)$.

Figure 5.5 shows the indicator L_N/Q of O_3 production sensitivity along the P-3B flight track for all flight days during the Houston deployment. $P(O_3)$ was mainly VOC-sensitive over the Houston Ship Channel and its surrounding urban areas due to large NO_x emissions. Over areas away from the center of the city with relatively low NO_x emissions, $P(O_3)$ was usually NO_x -sensitive.

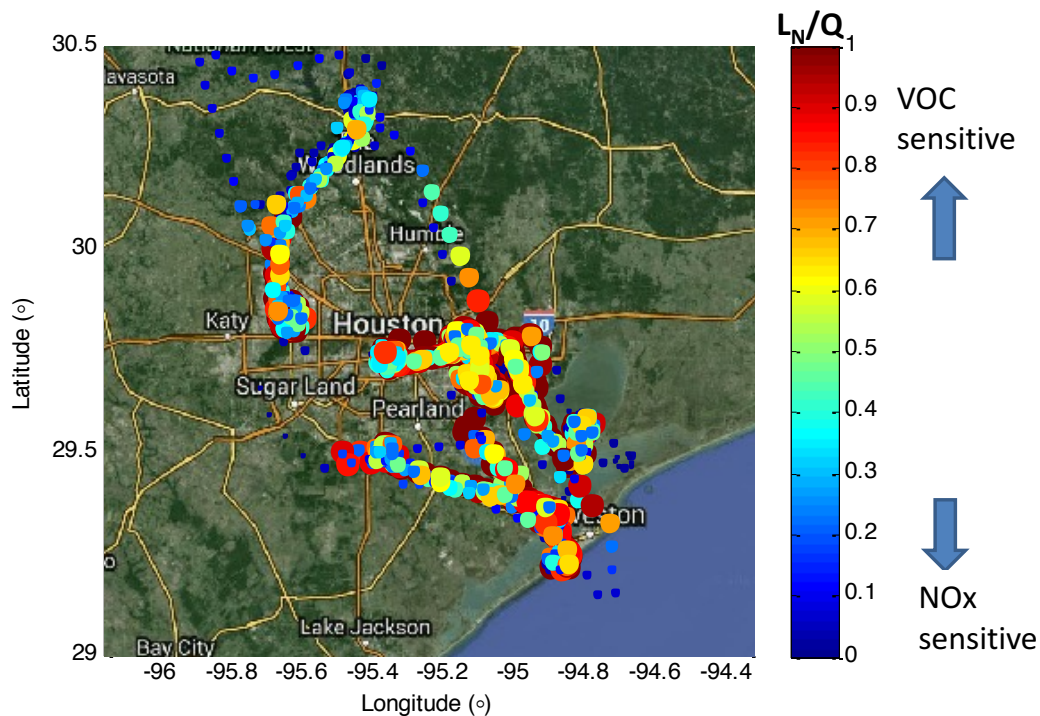


Figure 5.5 O_3 production sensitivity indicator, L_N/Q , along the P-3B flight track during DISCOVER-AQ in Houston in 2013. $P(O_3)$ is VOC-sensitive when $L_N/Q > 0.5$, and NO_x -sensitive when $L_N/Q < 0.5$.

Vertical profiles of $P(O_3)$, $L(O_3)$, and net O_3 production calculated using the box model results (Figure 5.6) show that:

- $RO_2 + NO$ makes about the same amount of O_3 as $HO_2 + NO$ in the model
- O_3 photolysis followed by $O(^1D) + H_2O$ is a dominant process for the photochemical loss of O_3

- the maximum net $P(O_3)$ appeared near the surface, below 1 km altitude

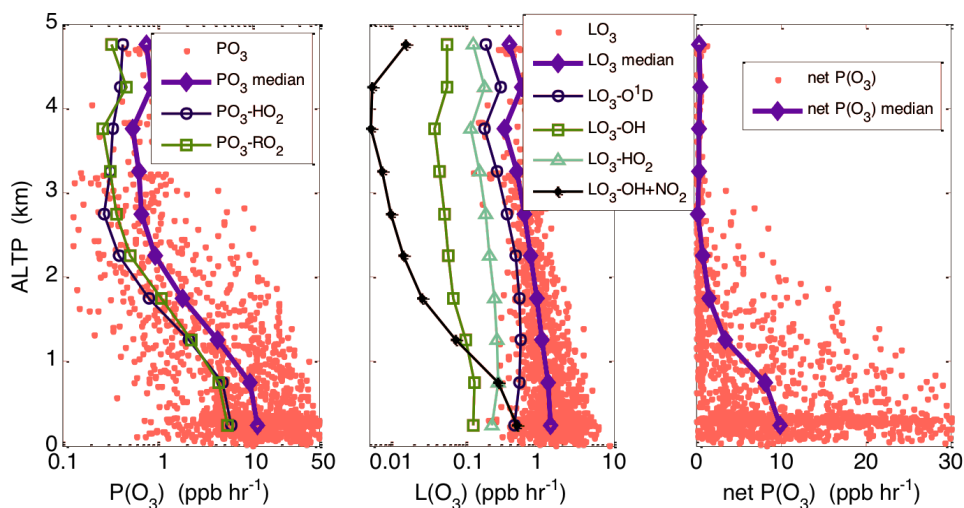


Figure 5.6 Vertical profiles of O_3 production rate (left), O_3 loss rate (middle), and net O_3 production rate (right) during DISCOVER-AQ in Houston in 2013.

In the diurnal variations of $P(O_3)$, it was shown that a broad peak existed in the morning with significant $P(O_3)$ in the afternoon the flight days during DISCOVER-AQ in Houston (Figure 5.7). The high $P(O_3)$ mainly occurred with $L_N/Q > 0.5$ (i.e., in the VOC sensitive regime).

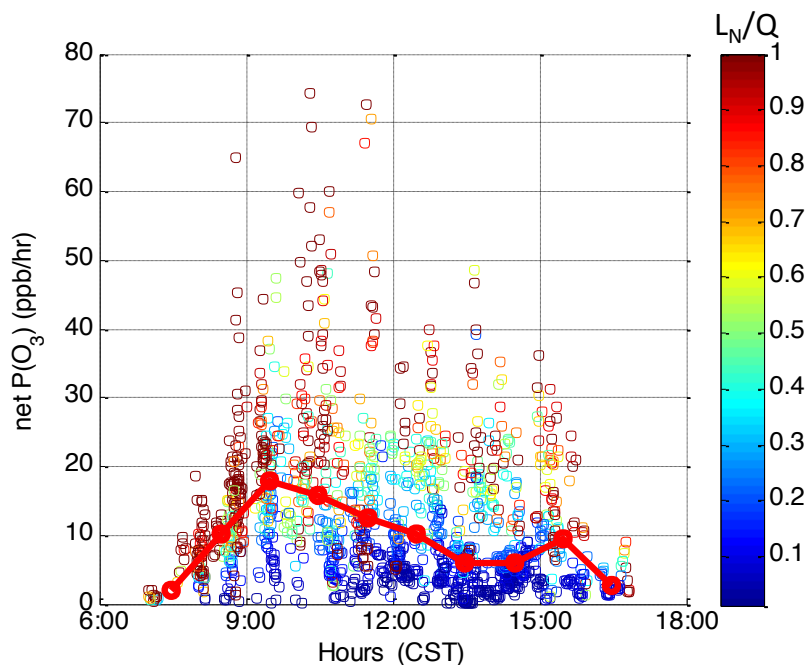


Figure 5.7 Diurnal variation of O_3 production rate colored with the indicator L_N/Q on ten flight days during DISCOVER-AQ in Houston in 2013. The solid red circles represent the median values in hourly bins of $P(O_3)$. Data are limited with the pressure altitude less than 1000 m to represent the boundary layer.

The diurnal variation of L_N/Q indicates that $P(O_3)$ was mainly VOC sensitive in the early morning and then transitioned towards the NO_x sensitive regime later in the day (Figure 5.8). High $P(O_3)$ in the morning was mainly associated with VOC sensitivity due to high NO_x levels in the morning (points in the red circle in Figure 5.8). Although $P(O_3)$ was mainly NO_x sensitive in the afternoon between 12:00 and 17:00 Central Standard Time, CST (UTC-6 hours), there were also periods and locations when $P(O_3)$ was VOC sensitive, e.g., the points with $L_N/Q > 0.5$ between 12:00 and 17:00 (CST) in Figure 5.8.

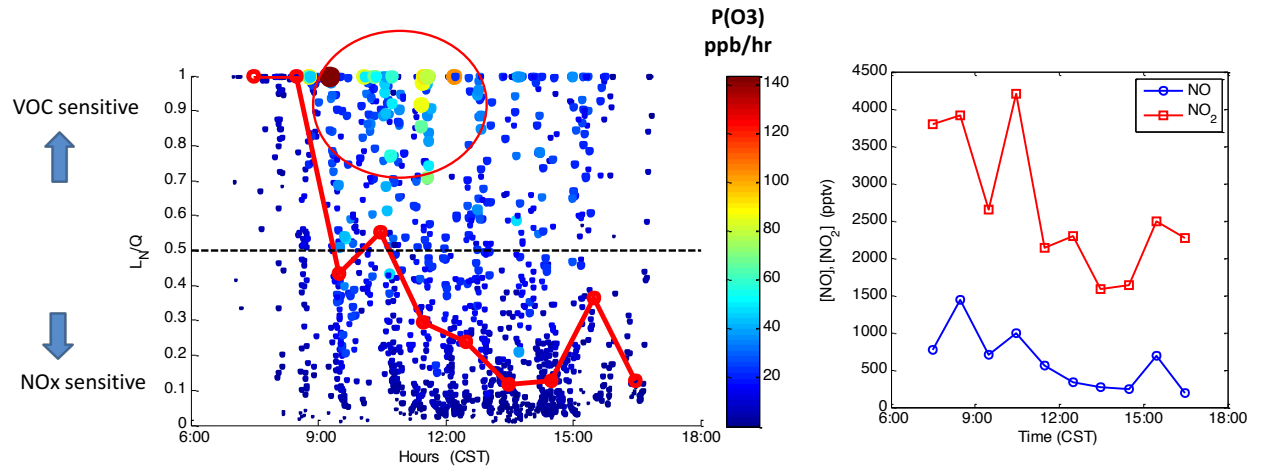


Figure 5.8 Diurnal variations of the indicator L_N/Q of O_3 production rate sensitivity colored with O_3 production rate and median hourly bins of L_N/Q shown in solid red circles (left) and median hourly NO and NO_2 concentrations (pptv) (right) below 1000 m during DISCOVER-AQ in Houston in 2013.

Diurnal variations of the O_3 production rate at eight individual locations where the P-3B conducted vertical spirals show that the O_3 production is greater than 10 ppb hr^{-1} on average at locations with high NO_x and VOC emissions, such as Deer Park, Moody Tower and Channelview, while at locations away from the urban center with lower emissions, such as Galveston, Smith Point, and Conroe, the O_3 production usually averaged less than 10 ppb hr^{-1} (Figure 5.9).

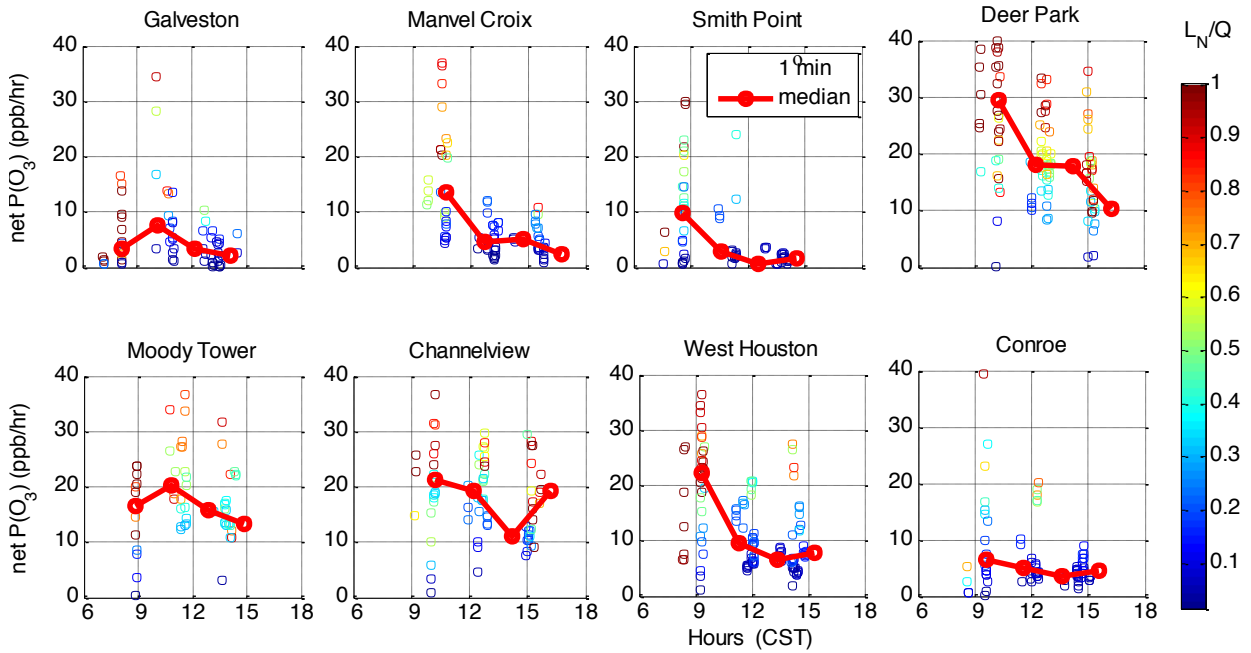


Figure 5.9 Diurnal variations of O_3 production rate at eight individual spiral locations. Individual points are 1-min data colored with L_N/Q and the linked red circles represent the median values in hourly bins of $P(O_3)$. Data are limited with the pressure altitude less than 1000 m to represent the boundary layer.

The dependence of $P(O_3)$ on the NO mixing ratio ($[NO]$) shows that when $[NO]$ is less than ~ 1 ppbv, O_3 production increases as the $[NO]$ increases, i.e., $P(O_3)$ is in NO_x sensitive regime. When the NO mixing ratio is greater than ~ 1 ppbv, O_3 production levels off, i.e., $P(O_3)$ is in a NO_x saturated regime (Figure 5.10).

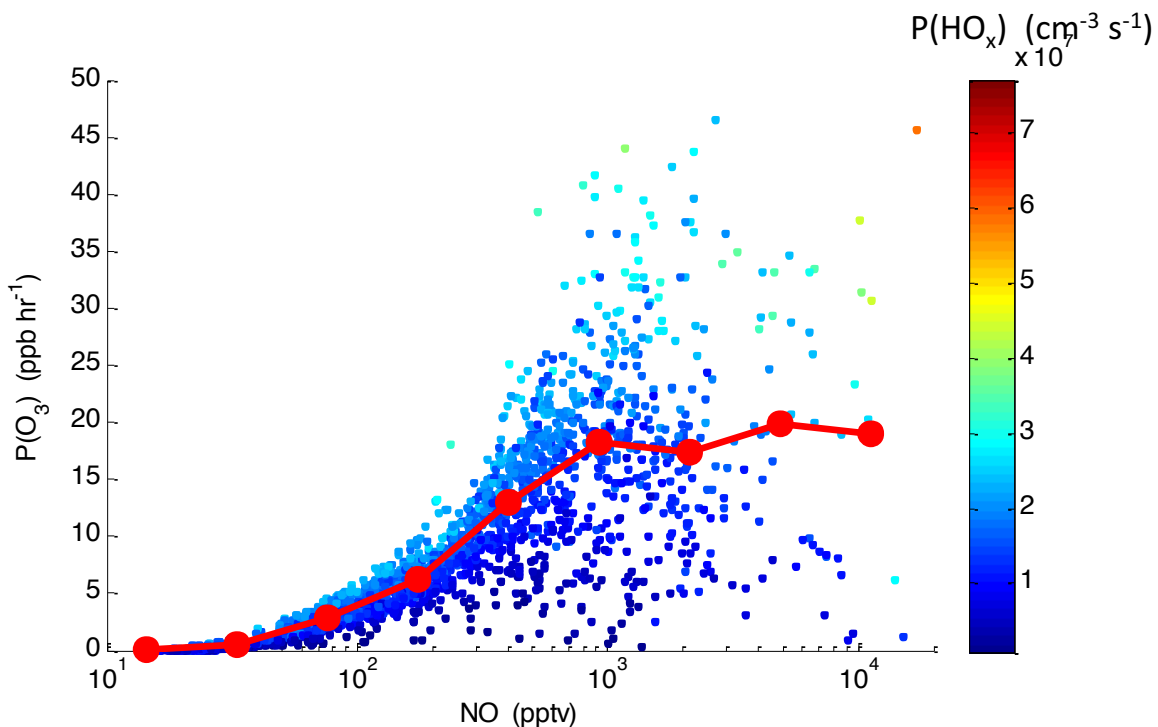


Figure 5.10 O₃ production as a function of NO mixing ratio. Individual data points are the 1-minute averages and are colored with the production rate of HO_x (= OH + HO₂) during DISCOVER-AQ in Houston in 2013. The linked solid red circles represent the median values in [NO] bins. Note a log scale is used for the x-axis.

It was also found that at a given NO mixing ratio, a higher production rate of HO_x results in a higher O₃ production rate. Diurnal variations of the indicator of O₃ production sensitivity to NO_x and VOCs, L_N/Q, at eight individual locations where the P-3B conducted vertical spirals show that (1) at Deer Park, P(O₃) was mostly VOC sensitive for the entire day; (2) at Moody Tower and Channelview, P(O₃) was VOC sensitive or in the transition regime; (3) at Smith Point and Conroe, P(O₃) was mostly NO_x sensitive for the entire day; and (4) Galveston, West Houston, and Manvel Croix P(O₃) was VOC sensitive only in the early morning (Figure 5.11).

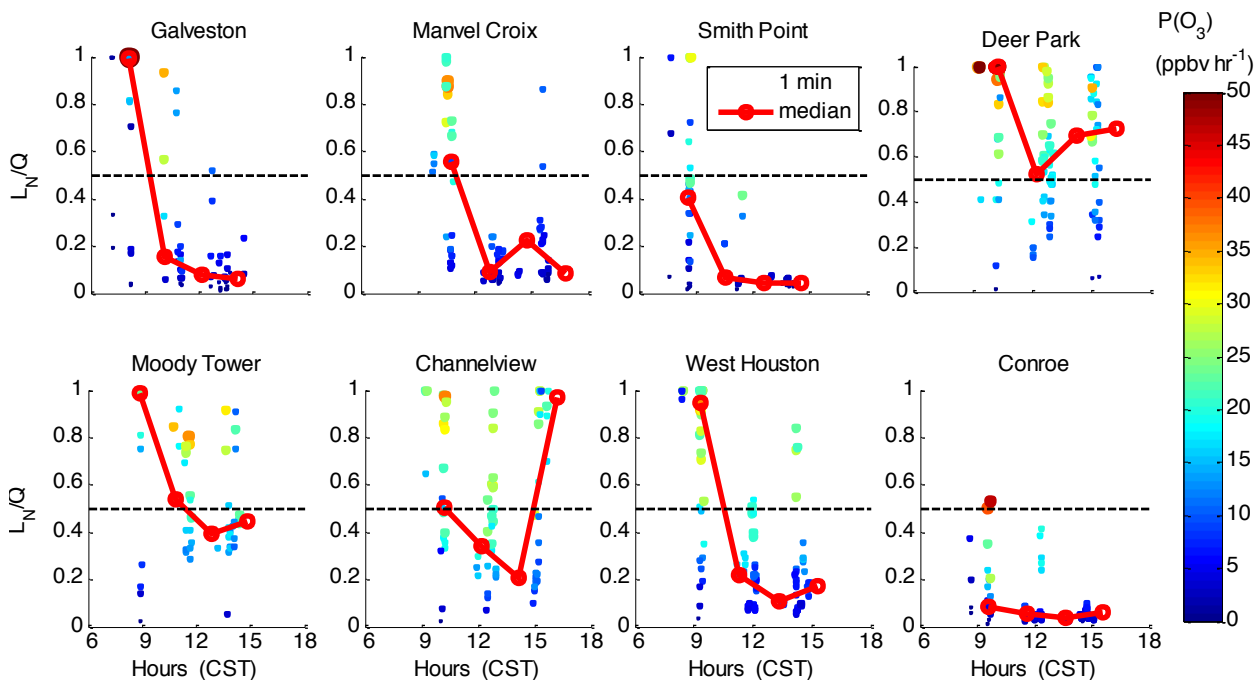


Figure 5.11. Diurnal variations of the indicator of O_3 production sensitivity to NO_x and VOCs, L_N/Q , at the individual spiral locations during DISCOVER-AQ in Houston in 2013. Individual points are 1-min data colored by $P(O_3)$ and the linked red circles represent the median values in hourly bins of $P(O_3)$. Data are limited with the pressure altitude less than 1000 m to approximately represent the boundary layer.

5.3.2 O_3 Production Efficiency

O_3 production efficiency (OPE) is defined as the number of molecules of oxidant O_x ($= O_3 + NO_2$) produced photochemically when a molecule of NO_x ($= NO + NO_2$) is oxidized. It conveys information about the conditions under which O_3 is formed and is an important parameter to consider when evaluating impacts from NO_x emission sources (Kleinman et al., 2002). The OPE can be determined by atmospheric observations, represented as the slope of a graph of O_x concentration vs. the concentration of NO_x oxidation products. The latter quantity is denoted as NO_z

and is commonly computed as the difference between NO_y (sum of all reactive-nitrogen compounds) and NO_x , i.e. $\text{NO}_z = \text{NO}_y - \text{NO}_x$.

Figure 5.12 shows the photochemical oxidant O_x as a function of NO_z during DISCOVER-AQ in Houston in 2013. The data were collected on September 25 and 26 (red) on a day with high ambient O_3 concentrations and recirculation due to a gulf breeze, and on seven other flight days, in blue. Note that the slopes obtained from these two data sets are essentially the same and an average OPE of ~ 8 is derived from the observations, meaning that 8 molecules of O_3 were produced when one molecule of NO_x was consumed.

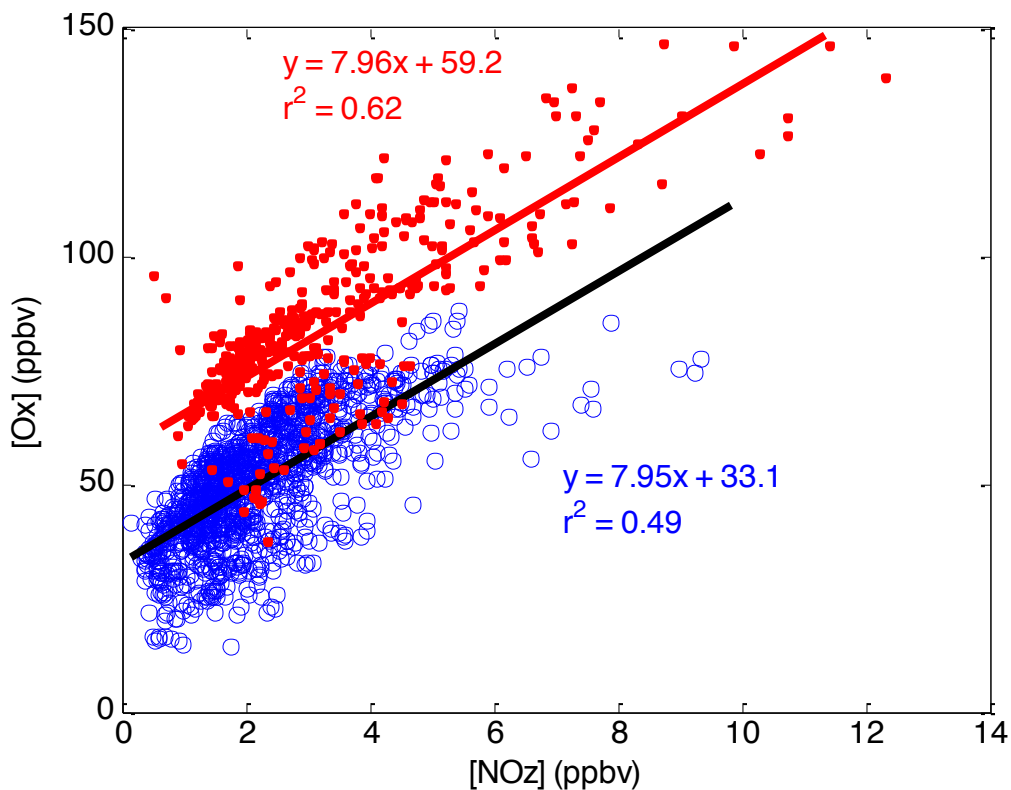


Figure 5.12 Photochemical oxidant, O_x ($=\text{O}_3+\text{NO}_2$) as a function of NO_z ($=\text{NO}_y-\text{NO}_x$) during DISCOVER-AQ in Houston in 2013. Red dots are the data collected on September 25 and 26, 2013 when high ambient O_3 concentrations were observed. Blue circles are the data collected during other flights (seven days of data). Data are

limited with the pressure altitude less than 1000 m to represent the concentrations in the boundary layer.

Even though higher O₃ concentrations were observed on September 25 and 26, the OPE on these two days is not different from those determined from other flights, indicating the O₃ event on these two days was not caused by a higher OPE, but mainly, by higher concentrations of O₃ precursors (and thus higher O₃ production rates) and background O₃ as indicated by the intercepts in the regression of the two data sets in Figure 5.12. The high O₃ observed on those days could also be due to influence of major primary VOC emissions from petrochemical facilities and recirculation by the Gulf Breeze (Mazzuca et al., 2017) as well as slower ventilation and lower boundary layer height and northerly transport from inland air pollution source regions and stagnation from the high-pressure system.

The OPE value of ~8 during DISCOVER-AQ in Houston in 2013 is greater than the average OPE value obtained during the Texas Air Quality Study in 2006 (TexAQS2006; OPE=5.9±1.2) (Neuman et al., 2009) and TexAQS2000 (OPE=5.4) (Ryerson et al., 2003). One possible reason for this increased OPE is the continuous reduction in NO_x emissions in Houston from 2000 to 2013 which pushed NO_x levels closer to 1 ppbv in 2013 (Figure S12), thus increased OPE, since OPE increases as NO_x decreases when the NO_x level is greater than ~1 ppbv (Figure 5.13).

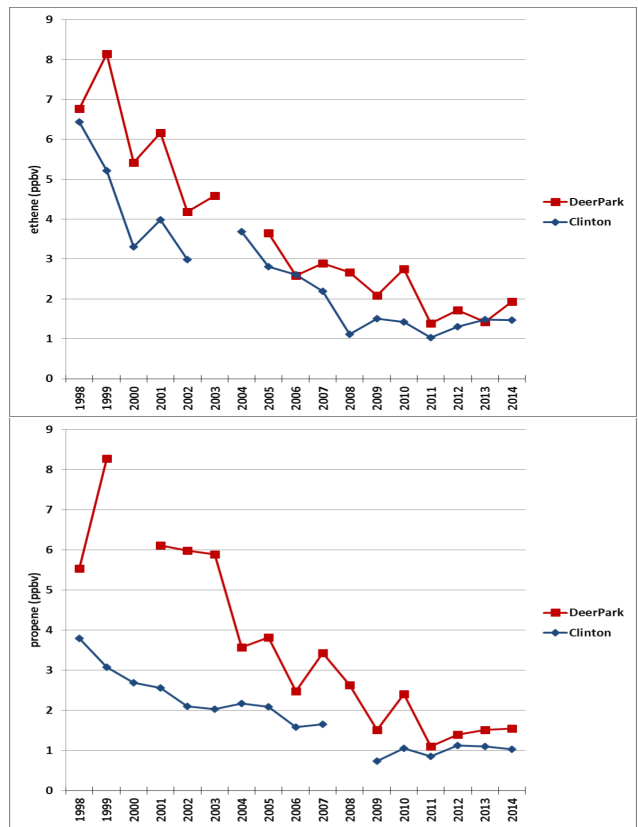
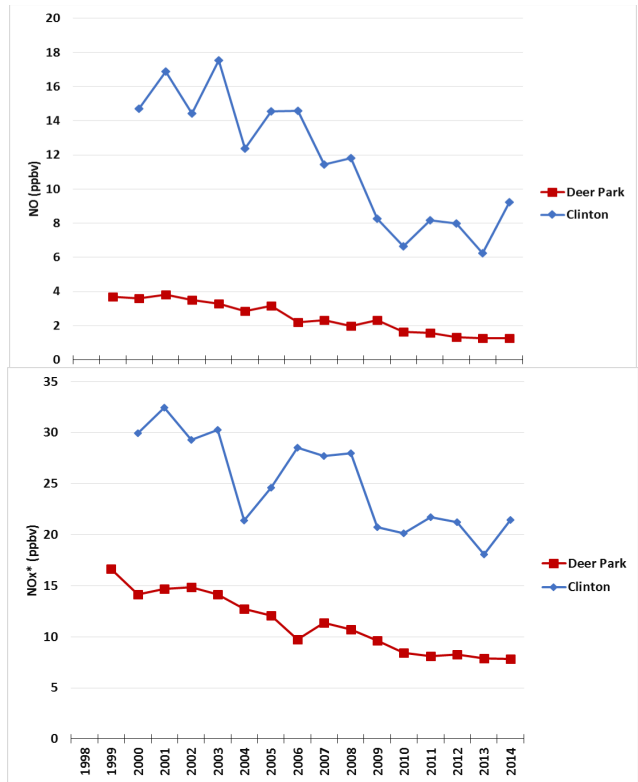


Figure S12. Time series of NO, NO_x, ethene and propene concentrations at the Deer Park and Clinton sites from 1998 to 2014. The Deer Park site is located southeast of the Ship Channel. The Clinton site is located on the northwestern end of the Ship Channel. Each data point represents an average of hourly samples collected between July 1 and November 30 for each year. Missing data points indicate that too few valid samples (< 70%) were collected during that year. NO and NO_x* data collected hourly using chemiluminescence sampler with molybdenum catalyst to convert NO_x* (not true NO_x because Mo catalyst converts other N species besides NO₂ to NO) to NO. VOC data collected over a 40-minute period each hour using automated gas chromatography with cryogenic pre-concentration.

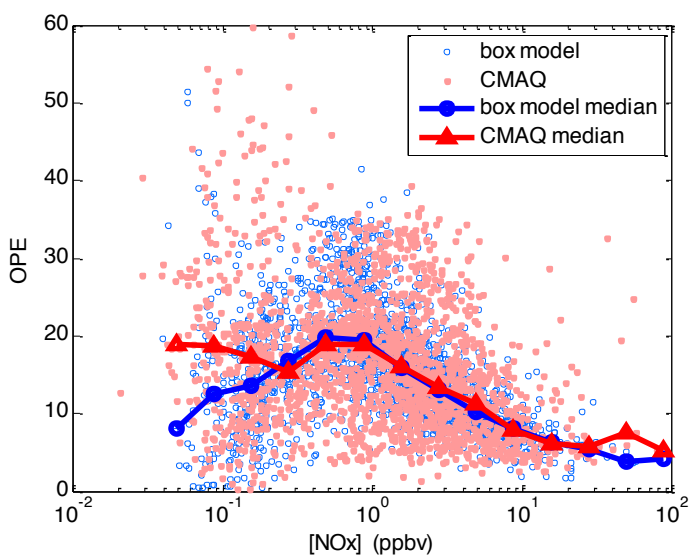


Figure 5.13 O₃ production efficiency (OPE) versus NO_x in the box model (blue circles) and CMAQ model (pink dots) results. The linked blue circles show the median OPE values binned by NO_x concentration in the box model, the linked red triangles show the median OPE values binned by NO_x concentration in the CMAQ model. OPE is calculated according to its definition as the net O₃ formation rate divided by of the formation rate of NO_z.

Houston area OPE values range from about a factor of 1.3 to 2 higher than the OPEs calculated from the DISCOVER-AQ 2011 study in Maryland, likely due to higher photochemical reactivity in Houston (OH reactivity of 1.2 s⁻¹ for MD and 3.3 s⁻¹ for TX; Figure S13).

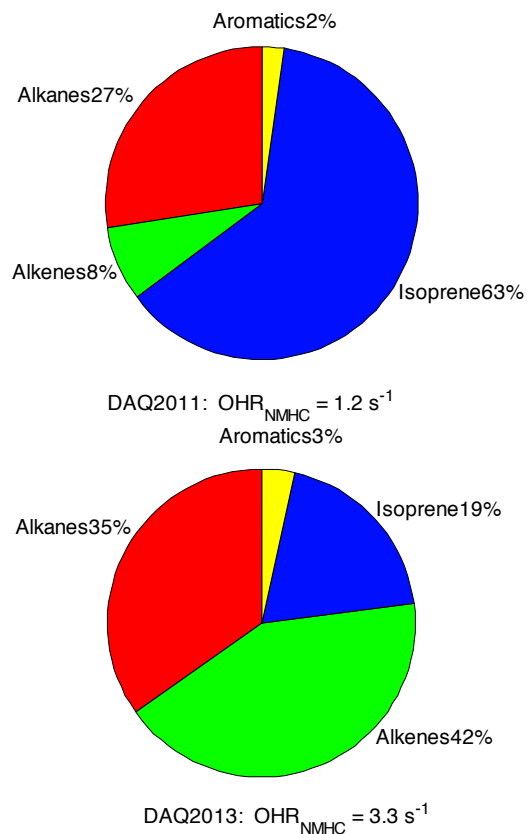


Figure S13. Distributions of OH reactivity due to non-methane hydrocarbons in DISCOVER-AQ 2011 in Maryland (top) and 2013 in Houston (bottom).

The 2011 Maryland OPEs ranged from 3.4 to 6.1 when all measured data below 1 km are used (Ren, X., unpublished data). An OPE of ~8 was calculated (He et al., 2013) for the 2011 Maryland DISCOVER-AQ campaign for measured data below the 850 hPa level during vertical spirals with a strong linear correlation ($r^2 > 0.8$) between O_x and NO_z . Additionally, OPEs of 7.7-9.7 were obtained from a ground site during the New England Air Quality Study (NEAQS) 2002 (Griffin et al., 2004).

When calculating OPE using observed O_x and NO_z , it is important to know whether there is substantial loss of nitric acid (HNO_3), since it can affect the OPE by

reducing the NO_z (Trainer et al., 1993; 2000; Neuman et al., 2009), thus biasing the OPE high. The derived OPE in Figure 5.12 is only valid when there is minimum loss of NO_z (especially HNO_3) from the source region to the point of observations. Neuman et al. (2009) found that $\Delta\text{CO}/\Delta\text{NO}_y$, i.e., the slope in a CO versus NO_y plot, is an indicator for distinguishing plumes with efficient O_3 formation from plumes with similarly high O_3 to NO_x oxidation products correlation slopes caused by variable mixing of aged polluted air that is depleted in HNO_3 . A typical $\Delta\text{CO}/\Delta\text{NO}_y$ ranges from ~ 40 in background air to ~ 4 -7 in fresh emission plumes in Houston (Neuman et al., 2009). The $\Delta\text{CO}/\Delta\text{NO}_y$ was examined at different times of the day on September 25 and 26. The results indicate that the $\Delta\text{CO}/\Delta\text{NO}_y$ was about 6.2 (Figure 5.14a) throughout the day with variation between 6.0 and 7.0 (Figure 5.14). This demonstrates that the observed O_3 formation was from fresh plumes and was not caused by variable mixing of aged polluted air depleted in HNO_3 .

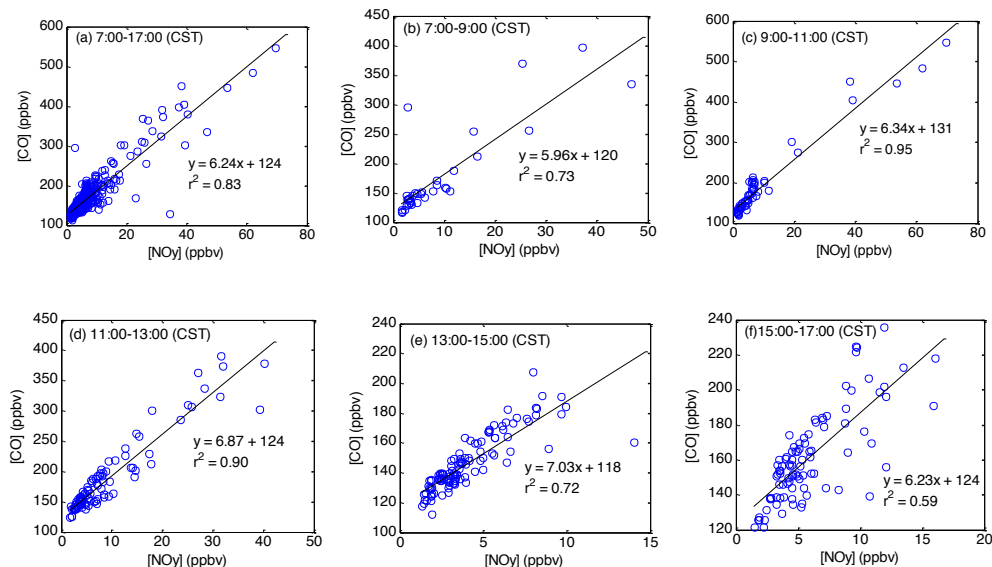


Figure 5.14 CO versus NO_y and linear regression on September 25 and 26 at different times of the day: (a) 07:00-17:00 (all data), (b) 07:00-09:00, (c) 09:00-11:00, (d) 11:00-13:00, (e) 13:00-15:00, and (f) 15:00-17:00 (CST).

Using both the box model and CMAQ model results, OPE can also be calculated according to its definition, i.e., the net O₃ formation rate divided by the formation rate of NO_z. Net P(O₃) was calculated using Eq. (1), while the NO_z formation rate is the sum of HNO₃ and organic nitrate formation rates. The agreement between the box model-derived and the CMAQ-derived OPEs is very good, with the mean OPEs of 14.8±7.4 in the box model and 16.6±8.1 in the CMAQ model. The dependence of OPE on NO_x is also similar for both the box and CMAQ models (Figure 5.13). On average, the maximum of OPE appears at a NO_x level around 1 ppbv. In general, if the NO_x level is below 1 ppbv, OPE increases as the NO_x level increases, while if the NO_x level is above 1 ppbv, OPE decreases as the NO_x level increases (Figure 5.13).

The OPE values calculated using the CMAQ and box model are greater than the values derived from the observations using the slope in the scatter plot of O_x versus NO_z in Figure 5.12. This is expected because in the calculation of OPE using the box and CMAQ model results, a few O₃ loss processes, such as O₃ dry deposition and horizontal/vertical dispersion, were not considered. This could result in higher calculated O₃ production rates using the model results.

Spatial variations of OPE demonstrate that except for a few hotspots over Downtown Houston and the Houston Ship Channel, most large OPEs appear away from the urban center, e.g., the northwest and southeast of the area, while in areas with high NO_x emissions close to the urban center, lower OPEs were generally observed (Figure 5.15). This is again consistent with the results in Figure 5.13 that the maximum of OPE appears at a NO_x level around 1 ppbv.

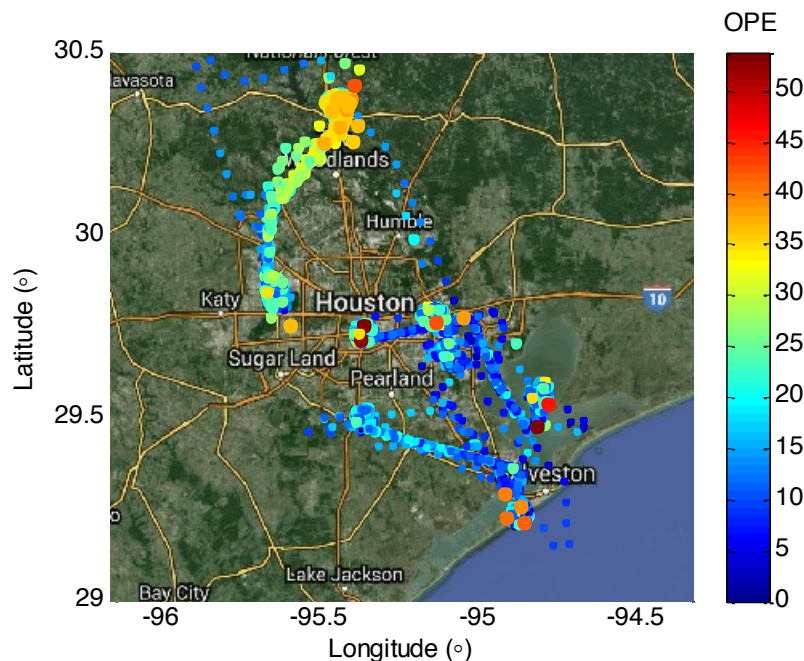


Figure 5.15 O₃ production efficiency (OPE) along the P-3B flight track during DISCOVER-AQ in Houston in 2013. OPE was calculated using the box model results as the ratio of net O₃ formation rate to the formation rate of NO_z.

5.4 Discussion and Conclusions

On average, O₃ production P(O₃), was about 20-30 ppbv hr⁻¹ in the morning and 5-10 ppbv hr⁻¹ in the afternoon during DISCOVER-AQ in Houston in 2013. The diurnal variation of P(O₃) shows a broad peak in the morning with significant P(O₃) in the afternoon obtained on ten flight days in September 2013. High P(O₃) mainly occurred with L_N/Q greater than 0.5, i.e., in the VOC sensitive regime. Since P(O₃) depends on NO_x levels and radical production rate, it increases as [NO] increases up to ~1 ppbv and then levels off with further increases of [NO]. At a given [NO], a higher production rate of HO_x results in a higher O₃ production rates. This finding has implications for the NO_x control strategies in order to achieve the O₃ control goal.

The DISCOVER-AQ campaign in Houston is unique because of its large spatial coverage and thus spatial variations of O₃ production and its sensitivity to NO_x and VOCs. Diurnal variations of P(O₃) at eight individual locations where the P-3B conducted vertical spirals show that the P(O₃) is on average more than 10 ppbv hr⁻¹ at locations with high NO_x and VOC emissions, such as Deer Park, Moody Tower, and Channelview, while at locations away from the urban center with lower emissions of O₃ precursors such as Galveston, Smith Point, and Conroe, the O₃ production rate is usually less than 10 ppbv hr⁻¹ on average. Hotspots of P(O₃) were observed over Downtown Houston and the Houston Ship Channel due to significant emissions in these areas.

O₃ production tended more towards VOC sensitive in the morning with high P(O₃) and in general, NO_x sensitive in the afternoon with some exceptions. It was found that during some afternoon time periods and locations, P(O₃) was VOC sensitive. The diurnal variation of L_N/Q indicates that P(O₃) was mainly VOC sensitive in the early morning and then transitioned towards the NO_x sensitive regime later in the day. High P(O₃) in the morning was mainly associated with VOC sensitivity due to high NO_x levels in the morning. Specifically, Deer Park was mostly VOC sensitive for the entire day, Moody Tower and Channelview were VOC sensitive or in the transition regime, and Smith Point and Conroe were mostly NO_x sensitive for the entire day.

Based on the measurements on the P-3B, O₃ production efficiency (OPE) was about 8 during DISCOVER-AQ 2013 in Houston. This OPE value is greater than the average OPE value (5.9±1.2) obtained during the Texas Air Quality Study in 2006

(TexAQS2006), likely due to the reduction in NO_x emissions in Houston between 2006 and 2013 that pushed NO_x levels closer to 1 ppbv in 2013 from higher NO_x levels in previous years. The results from this work strengthen our understanding of O₃ production; they indicate that controlling NO_x emissions will provide air quality benefits over the greater Houston metropolitan area in the long run, but in selected areas controlling VOC emissions will also be beneficial.

Chapter 6: Concluding Remarks and Future Work

6.1 – Concluding Remarks

The following overarching findings are provided to the scientific community by the completion of this thesis:

- 1) A characterization of mesoscale circulations, formed from temperature differences between the land and the water, and an understanding of the implications of these breezes on O₃ and PM concentration at coastal sites;
- 2) An improved understanding of the relationship between naturally occurring weather events and human-induced air pollution in areas of complex terrain and coastal configurations;
- 3) An investigation of different meteorological conditions and events as potential indicators of an O₃ episode or of O₃ episode termination;
- 4) A new analysis of O₃ photochemical production sensitivity to its precursors, NO_x and VOCs, in Houston, TX, an area impacted by differing emissions types and meteorological conditions, which may exacerbate or inhibit O₃ production.

While successful implementation of NO_x reductions and SIPs has markedly decreased O₃ in the U.S. (e.g., Sullivan et al., 2018), the risk of O₃-related ailments and mortality has not been eliminated. It is important to continue monitoring and researching causes, sources, and conditions favorable for high O₃ and PM pursuant to future policy refinements and cost-effective policy creation. To strengthen policies, in-depth research must be conducted to avoid uniform, blanket-approach and to adjust policies to effectively capture specific regions and meteorological situations. This dissertation addresses the diverse meteorological conditions and emissions that affect O₃ on a variety of time and spatial scales. Since observations and models are moving towards higher resolution, policies too should move towards higher resolution (local and city-level spatial scales and controlling emissions at the most effective times of day).

In this dissertation, I utilize the unprecedented data set from DISCOVER-AQ to examine meteorology-air pollution interactions occurring along the land-water interface, as well as in other areas of varying topography in the U.S. Prior to this analysis, the depth, frequency, and duration of bay breezes along the Chesapeake Bay were not sufficiently quantified or understood. From this work, we now have a richer image and understand that bay breezes can also be relatively small features that penetrate only a few kilometers inland, at times only affecting coastal sites and not locations farther inland. For example, a bay breeze affected the site prepared for the DISCOVER-AQ project at Edgewood, MD (Eagle Point, Aberdeen Proving Grounds), but did not affect the MDE site at Edgewood, less than 3 km farther inland. In addition to gaining information about how far inland some breezes penetrate, this

analysis also includes vertical profiles of bay breezes from a tethered balloon and P-3B aircraft, in which both the O₃ and meteorology profiles were characterized. This analysis showed that bay breezes can be much shallower than previously thought, with some having heights <100 m. Breezes that form as a result of the bay/land interface may be short-lived, but frequent meteorological features. It was found that there can be several short-lived events due to the breeze effectively acting to weaken the pressure gradient, which subsequently turns off the flow from the bay. The previous understanding centered on bay breezes as one large-scale, long-lived (+3 hour) event. In this new understanding, hours after a short-lived, spatially small event, a new breeze can form after sufficient additional daytime heating, creating a new thermal low over the land and leading to a new pressure gradient, thus initiating a cycle. While some of these breezes are short-lived (< 1hr) and spatially small (< 100m in depth and < 3km inland penetration), they can have significant impacts on surface O₃ (one case led to a 36 ppbv increase at the surface in ~30 minutes).

I conducted an in-depth investigation into a prime O₃ pollution event, where high concentrations of directly-emitted VOCs from petrochemical facilities and NO_x combined to produce high O₃ concentrations recirculated by gulf and bay breezes in the Houston, TX area. The recirculation during the Gulf of Mexico and Galveston Bay breezes led to sustained surface O₃ concentrations > 140 ppbv near Houston, TX, at Smith Point, for ~2 hours. This demonstrates the capacity for recirculation events to exacerbate air pollution and the potential for an air quality forecasting bust if these recirculation events are not well-forecasted or captured in weather and chemical models.

The land-water breeze case study in MD led to a climatology analysis and the development of an automated bay breeze identification algorithm (Chapter 3). The bay breeze detection algorithm provided necessary information for examining the O₃ concentration associated with different mesoscale meteorological events during a six-year period (2011-2016) at Edgewood, MD. A novel approach for the bay breeze identification algorithm was developed; it uses wind data to automate the determination of bay breezes rather than a strict criterion of thermodynamic variable responses used by previous hand analyses. The climatology reaffirmed previous research suggesting that bay/sea breezes can lead to high O₃ concentrations at coastal sites, but also demonstrated that the relationship between bay breezes and high O₃ diminishes as O₃ concentrations decrease due to NO_x emission controls. In addition, an analysis of the relationship between thunderstorms and O₃ suggests that days with thunderstorms often still have high O₃ concentrations, either before or after the thunderstorm, and longer-lived thunderstorms are more likely to terminate O₃ pollution episodes.

In an analysis of a case study from the July 2011 DISCOVER-AQ deployment in MD, a bay breeze-thunderstorm combination resulted in a high O₃ exceedance, regardless of temporary venting and mixing. Additionally, a case was analyzed during the July 2014 deployment of DISCOVER-AQ in CO, where upslope flow from Denver led to high O₃ and induced a thunderstorm, which resulted in the termination of an O₃ pollution event without O₃ recovering post-storm. Overall, days with thunderstorms were cleaner on average than days without thunderstorms during the CO deployment, whereas thunderstorms in MD had less of an effect on the O₃

pollution level, largely due to its small horizontal spatial extent and its short duration (~1 hr). It is important to understand how events, such as thunderstorms, may alter air pollution in different geographic regions to improve modeling and policy efforts. It was also shown that the WRF model can simulate the timing and location of a bay breeze and small-scale thunderstorms, with the use of LDA. At fine resolutions, this modeling technique can be a useful application for future chemical modeling.

I provided an analysis demonstrating that the sensitivity of O₃ production to its precursors, NO_x and VOCs, varies as a function of time and distance from the urban center in the Houston, TX metro area. For example, most of the sites analyzed were VOC-sensitive in the morning with high O₃ production rates, but transitioned to mostly NO_x-sensitive by afternoon. Other locations, however, were either VOC or NO_x sensitive for the entire day on average. One site near the urban center, Deer Park, was VOC-sensitive throughout the entire day, whereas sites downwind of or away from the urban center, Smith Point and Conroe, were NO_x sensitive throughout the day on average. This work shows that controlling NO_x will have a significant impact on reducing O₃ in the long run, but certain VOC-sensitive areas with large anthropogenic VOC sources can also benefit by having stricter controls on VOCs, especially if these emissions reductions are implemented during the most impactful time of day.

6.2 – Future Work

An analysis of the sensitivity of O₃ and PM production in coastal areas susceptible to a recirculation event can be useful. Land-water breezes advect air from

another air mass (higher water vapor, cooler, and shallower boundary layer) to the land. Therefore, differences in the O₃ production regime can occur, potentially changing the regulatory priorities during these events.

With BIA successfully identifying bay breezes at a site along the Chesapeake Bay, future studies may find this versatile algorithm useful in determining days with breezes due to the land-water interface in other areas (e.g., lake breezes at coastal locations along Illinois, Wisconsin, and Michigan and sound breezes in Connecticut and New York). By applying the algorithm to data, the relationship between land-water breezes and O₃ events and sources of predictability can be quantified. For example, by calculating the conditional probability of an O₃ exceedance given a sound breeze on the coast of Connecticut, this information can be used to determine how often a sound breeze day is also an O₃ standard violation day. In addition to quantifying the percent chance of an O₃ exceedance given a sound breeze, the algorithm can potentially be used with a forecast model to predict whether or not a sound breeze will occur. A statistical representation for whether a sound breeze will occur and the relationship of a sound breeze with O₃ can be useful in air quality forecasting for particular coastal areas.

Investigating the vertical mass flux in thunderstorms of varying types can assist in understanding whether a thunderstorm will terminate a pollution episode. Additionally, an understanding of the role that thunderstorms play in O₃ pollution in other areas other than Maryland, such as the Front Range in Colorado, would be useful. Fundamentally different dynamics in areas of complex topography may allow thunderstorms to play a different role in terminating O₃ pollution than those observed

in the MD area. This analysis will include separating storm types (e.g., pop-up mountain convection vs. DCVZ or frontal convection) similar to the MD analysis in Chapter 3.

Additional future work should include an analysis of how thermally-direct land-water breezes can affect levels of PM near coastal sites. Since humidity can lead to higher AOD and SSA, which in turn can result in faster photochemistry, a full understanding of these coastal interactions by use of the statistical model developed in Chapter 3 can be useful. Additionally, high resolution meteorological modeling that captures these mesoscale circulations and chemical modeling with multiphase chemistry would be of value to better understand recirculation of PM and its feedback mechanisms with O₃.

Bibliography

- Anderson, D. C., Loughner, C. P., Diskin, G., Weinheimer, A., Canty, T. P., Salawitch, R. J., ... Dickerson, R. R. (2014). Measured and modeled CO and NO_y in DISCOVER-AQ: An evaluation of emissions and chemistry over the eastern US. *Atmospheric Environment*, *96*, 78–87. <https://doi.org/10.1016/j.atmosenv.2014.07.004>
- Appel, K. W., Gilliam, R. C., Pleim, J. E., Pouliot, G. A., Wong, D. C., Hogrefe, C., ... Mathur, R. (2014). Improvements to the WRF-CMAQ modeling system for fine-scale air quality simulations. *EM: Air and Waste Management Association's Magazine for Environmental Managers*.
- Banta, R. M., Senff, C. J., Nielsen-Gammon, J., Darby, L. S., Ryerson, T. B., Alvarez, R. J., ... Trainer, M. (2005). A bad air day in Houston. *Bulletin of the American Meteorological Society*, *86*(5), 657–669. <https://doi.org/10.1175/BAMS-86-5-657>
- Bell, M. L., McDermott, A., Zeger, S. L., Samet, J. M., & Dominici, F. (2004). Ozone and short-term mortality in 95 US urban communities, 1987-2000. *Journal of the American Medical Association*, *292*(19), 2372–2378. <https://doi.org/10.1001/jama.292.19.2372>
- Beyersdorf, A. J., Ziemba, L. D., Chen, G., Corr, C. A., Crawford, J. H., Diskin, G. S., ... Anderson, B. E. (2016). The impacts of aerosol loading, composition, and water uptake on aerosol extinction variability in the Baltimore-Washington, D.C. region. *Atmospheric Chemistry and Physics*, *16*(2), 1003–1015. <https://doi.org/10.5194/acp-16-1003-2016>
- Bloomer, B. J., Stehr, J. W., Piety, C. A., Salawitch, R. J., & Dickerson, R. R. (2009). Observed relationships of ozone air pollution with temperature and emissions. *Geophysical Research Letters*, *36*(9). <https://doi.org/10.1029/2009GL037308>
- Burnett, R. T., Cakmak, S., Brook, J. R., & Krewski, D. (1997). The role of particulate size and chemistry in the association between summertime ambient air pollution and hospitalization for cardiorespiratory diseases. *Environmental Health Perspectives*, *105*(6), 614–620. <https://doi.org/10.1289/ehp.97105614>
- Burnett, R. T., Dales, R. E., Raizenne, M. E., Krewski, D., Summers, P. W., Roberts, G. R., ... Brook, J. (1994). Effects of low ambient levels of ozone and sulfates

on the frequency of respiratory admissions to Ontario hospitals. *Environmental Research*, 65(2), 172–194. <https://doi.org/10.1006/enrs.1994.1030>

- Byers, H. R., & Rodebush, H. R. (1948). Causes of Thunderstorms of the Florida Peninsula. *Journal of Meteorology*. [https://doi.org/10.1175/1520-0469\(1948\)005<0275:COTOTF>2.0.CO;2](https://doi.org/10.1175/1520-0469(1948)005<0275:COTOTF>2.0.CO;2)
- Canty, T. P., Hemberck, L., Vinciguerra, T. P., Anderson, D. C., Goldberg, D. L., Carpenter, S. F., ... Dickerson, R. R. (2015). Ozone and NO_x chemistry in the eastern US: Evaluation of CMAQ/CB05 with satellite (OMI) data. *Atmospheric Chemistry and Physics*, 15(19), 10965–10982. <https://doi.org/10.5194/acp-15-10965-2015>
- Chameides, W. L., Xingsheng, L., Xiaoyan, T., Xiuji, Z., Chao, L., Kiang, C. S., ... Giorgi, F. (1999). Is ozone pollution affecting crop yields in China? *Geophysical Research Letters*, 26(7), 867–870. <https://doi.org/10.1029/1999GL900068>
- Chatfield, R. B., & Esswein, R. F. (2012). Estimation of surface O₃ from lower-troposphere partial-column information: Vertical correlations and covariances in ozonesonde profiles. *Atmospheric Environment*, 61, 103–113. <https://doi.org/10.1016/j.atmosenv.2012.06.033>
- Chen, S., Ren, X., Mao, J., Chen, Z., Brune, W. H., Lefer, B., ... Crawford, J. H. (2010). A comparison of chemical mechanisms based on TRAMP-2006 field data. *Atmospheric Environment*, 44(33), 4116–4125. <https://doi.org/10.1016/j.atmosenv.2009.05.027>
- Darby, L. S. (2005). Cluster Analysis of Surface Winds in Houston, Texas, and the Impact of Wind Patterns on Ozone. *Journal of Applied Meteorology*, 44(12), 1788–1806. <https://doi.org/10.1175/JAM2320.1>
- Darby, L. S., McKeen, S. A., Senff, C. J., White, A. B., Banta, R. M., Post, M. J., ... Talbot, R. (2007). Ozone differences between near-coastal and offshore sites in New England: Role of meteorology. *Journal of Geophysical Research Atmospheres*, 112(16). <https://doi.org/10.1029/2007JD008446>
- Dickerson, R. R., Huffman, G. J., Luke, W. T., Nunnermacker, L. J., Pickering, K. E., Leslie, a C., ... Stedman, D. H. (1987). Thunderstorms: an important mechanism in the transport of air pollutants. *Science (New York, N.Y.)*, 235(4787), 460–465. <https://doi.org/10.1126/science.235.4787.460>
- Dickerson, R. R., Kondragunta, S., Stenchikov, G., Civerolo, K. L., Doddridge, B. G., & Holben, B. N. (1997). The impact of aerosols on solar ultraviolet radiation and photochemical smog. *Science*, 278(5339), 827–830. <https://doi.org/10.1126/science.278.5339.827>

- Eck, T. F., Holben, B. N., Reid, J. S., Arola, A., Ferrare, R. A., Hostetler, C. A., ... Sinyuk, A. (2014). Observations of rapid aerosol optical depth enhancements in the vicinity of polluted cumulus clouds. *Atmospheric Chemistry and Physics*, *14*(21), 11633–11656. <https://doi.org/10.5194/acp-14-11633-2014>
- EPA. (2006). Air Quality Criteria for Ozone and Related Photochemical Oxidants. *Molecular and Cellular Biochemistry*, *9*(3), 131–133. <https://doi.org/EPA/600/R-05/004aF>
- Evtyugina, M. G., Nunes, T., Pio, C., & Costa, C. S. (2006). Photochemical pollution under sea breeze conditions, during summer, at the Portuguese West Coast. *Atmospheric Environment*, *40*(33), 6277–6293. <https://doi.org/10.1016/j.atmosenv.2006.05.046>
- Evtyugina, M. G., Nunes, T., Pio, C., & Costa, C. S. (2006). Photochemical pollution under sea breeze conditions, during summer, at the Portuguese West Coast. *Atmospheric Environment*, *40*(33), 6277–6293. <https://doi.org/10.1016/j.atmosenv.2006.05.046>
- Fierro, A. O., Clark, A. J., Mansell, E. R., MacGorman, D. R., Dembek, S. R., & Ziegler, C. L. (2015). Impact of Storm-Scale Lightning Data Assimilation on WRF-ARW Precipitation Forecasts during the 2013 Warm Season over the Contiguous United States. *Monthly Weather Review*, *143*(3), 757–777. <https://doi.org/10.1175/MWR-D-14-00183.1>
- Fierro, A. O., Gao, J., Ziegler, C. L., Mansell, E. R., MacGorman, D. R., & Dembek, S. R. (2014). Evaluation of a Cloud-Scale Lightning Data Assimilation Technique and a 3DVAR Method for the Analysis and Short-Term Forecast of the 29 June 2012 Derecho Event. *Monthly Weather Review*, *142*(1), 183–202. <https://doi.org/10.1175/MWR-D-13-00142.1>
- Fierro, A. O., Mansell, E. R., Ziegler, C. L., & MacGorman, D. R. (2012). Application of a Lightning Data Assimilation Technique in the WRF-ARW Model at Cloud-Resolving Scales for the Tornado Outbreak of 24 May 2011. *Monthly Weather Review*, *140*(8), 2609–2627. <https://doi.org/10.1175/MWR-D-11-00299.1>
- Finlayson-Pitts, B. J., & Pitts, J. N. (1999). Chemistry of the Upper and Lower Atmosphere: Theory, Experiments, and Applications. *Chemistry of the Upper and Lower Atmosphere*, 969. <https://doi.org/10.1016/B978-0-12-257060-5.50027-7>
- Fishman, J., Bowman, K. W., Burrows, J. P., Richter, A., Chance, K. V., Edwards, D. P., ... Thompson, A. M. (2008). Remote sensing of tropospheric pollution from space. *Bulletin of the American Meteorological Society*. <https://doi.org/10.1175/2008BAMS2526.1>

- Fishman, J., Creilson, J. K., Parker, P. A., Ainsworth, E. A., Vining, G. G., Szarka, J., ... Xu, X. (2010). An investigation of widespread ozone damage to the soybean crop in the upper Midwest determined from ground-based and satellite measurements. *Atmospheric Environment*, *44*(18), 2248–2256. <https://doi.org/10.1016/j.atmosenv.2010.01.015>
- Flynn, C. M., Pickering, K. E., Crawford, J. H., Lamsal, L., Krotkov, N., Herman, J., ... Brent, L. (2014). Relationship between column-density and surface mixing ratio: Statistical analysis of O₃ and NO₂ data from the July 2011 Maryland DISCOVER-AQ mission. *Atmospheric Environment*, *92*, 429–441. <https://doi.org/10.1016/j.atmosenv.2014.04.041>
- Flynn, C. M., Pickering, K. E., Crawford, J. H., Weinheimer, A. J., Diskin, G., Thornhill, K. L., ... Strobe, S. A. (2016). Variability of O₃ and NO₂ profile shapes during DISCOVER-AQ: Implications for satellite observations and comparisons to model-simulated profiles. *Atmospheric Environment*, *147*, 133–156. <https://doi.org/10.1016/j.atmosenv.2016.09.068>
- Follette-Cook, M. B., Pickering, K. E., Crawford, J. H., Duncan, B. N., Loughner, C. P., Diskin, G. S., ... Weinheimer, A. J. (2015). Spatial and temporal variability of trace gas columns derived from WRF/Chem regional model output: Planning for geostationary observations of atmospheric composition. *Atmospheric Environment*, *118*, 28–44. <https://doi.org/10.1016/j.atmosenv.2015.07.024>
- Goldberg, D. L., Loughner, C. P., Tzortziou, M., Stehr, J. W., Pickering, K. E., Marufu, L. T., & Dickerson, R. R. (2014). Higher surface ozone concentrations over the Chesapeake Bay than over the adjacent land: Observations and models from the DISCOVER-AQ and CBODAQ campaigns. *Atmospheric Environment*, *84*, 9–19. <https://doi.org/10.1016/j.atmosenv.2013.11.008>
- Goldberg, D. L., Vinciguerra, T. P., Anderson, D. C., Hembeck, L., Canty, T. P., Ehrman, S. H., ... Dickerson, R. R. (2016). CAMx ozone source attribution in the eastern United States using guidance from observations during DISCOVER-AQ Maryland. *Geophysical Research Letters*, *43*(5), 2249–2258. <https://doi.org/10.1002/2015GL067332>
- Griffin, R. J., Johnson, C. A., Talbot, R. W., Mao, H., Russo, R. S., Zhou, Y., & Sive, B. C. (2004). Quantification of ozone formation metrics at Thompson Farm during the New England Air Quality Study (NEAQS) 2002. *Journal of Geophysical Research D: Atmospheres*, *109*(24), 1–14. <https://doi.org/10.1029/2004JD005344>
- He, H., Stehr, J. W., Hains, J. C., Krask, D. J., Doddridge, B. G., Vinnikov, K. Y., ... Dickerson, R. R. (2013). Trends in emissions and concentrations of air pollutants in the lower troposphere in the Baltimore/Washington airshed from 1997 to

2011. *Atmospheric Chemistry and Physics*, 13(15), 7859–7874.
<https://doi.org/10.5194/acp-13-7859-2013>
- He, H., Hemberck, L., Hosley, K. M., Canty, T. P., Salawitch, R. J., & Dickerson, R. R. (2013). High ozone concentrations on hot days: The role of electric power demand and NO_x emissions. *Geophysical Research Letters*, 40(19), 5291–5294.
<https://doi.org/10.1002/grl.50967>
- He, H., Loughner, C. P., Stehr, J. W., Arkinson, H. L., Brent, L. C., Follette-Cook, M. B., ... Dickerson, R. R. (2013). An elevated reservoir of air pollutants over the Mid-Atlantic States during the 2011 DISCOVER-AQ campaign: Airborne measurements and numerical simulations. *Atmospheric Environment*, 85, 18–30.
<https://doi.org/10.1016/j.atmosenv.2013.11.039>
- Hegarty, J., Mao, H., & Talbot, R. (2007). Synoptic controls on summertime surface ozone in the northeastern United States. *Journal of Geophysical Research Atmospheres*, 112(14). <https://doi.org/10.1029/2006JD008170>
- Hong, S.-Y., Noh, Y., & Dudhia, J. (2006). A New Vertical Diffusion Package with an Explicit Treatment of Entrainment Processes. *Monthly Weather Review*, 134(9), 2318–2341. <https://doi.org/10.1175/MWR3199.1>
- Hooke, W. H. (2014). *Living on the Real World: How Thinking and Acting Like Meteorologists Will Help Save the Planet*. American Meteorological Society. Retrieved from <https://books.google.com/books?id=7vd0mwEACAAJ>
- Hu, X. M., Nielsen-Gammon, J. W., & Zhang, F. (2010). Evaluation of three planetary boundary layer schemes in the WRF model. *Journal of Applied Meteorology and Climatology*, 49(9), 1831–1844.
<https://doi.org/10.1175/2010JAMC2432.1>
- Iacono, M. J., Delamere, J. S., Mlawer, E. J., Shephard, M. W., Clough, S. A., & Collins, W. D. (2008). Radiative forcing by long-lived greenhouse gases: Calculations with the AER radiative transfer models. *Journal of Geophysical Research Atmospheres*, 113(13). <https://doi.org/10.1029/2008JD009944>
- Jacob, D.J. (1999). Chapter 12. Ozone Pollution. *Introduction to Atmospheric Chemistry*, 3(2), 1999. <https://doi.org/10.1111/j.0954-6820.1949.tb11329.x>
- Jacob, D. J. (2000). Heterogeneous chemistry and tropospheric ozone. *Atmospheric Environment*. [https://doi.org/10.1016/S1352-2310\(99\)00462-8](https://doi.org/10.1016/S1352-2310(99)00462-8)
- Jacob, D. J., Logan, J. A., Gardner, G. M., Yevich, R. M., Spivakovsky, C. M., Wofsy, S. C., ... Prather, M. J. (1993). Factors regulating ozone over the United States and its export to the global atmosphere. *Journal of Geophysical Research*, 98(D8), 14817. <https://doi.org/10.1029/98JD01224>

- Jerrett, M., Burnett, R. T., Pope, C. A., Ito, K., Thurston, G., Krewski, D., ... Thun, M. (2009). Long-Term Ozone Exposure and Mortality. *New England Journal of Medicine*, 360(11), 1085–1095. <https://doi.org/10.1056/NEJMoa0803894>
- Kleinman, L. I., P. H. Daum, Y.-N. Lee, L. J. Nunnermacker, S. R. Springston, J. Weinstein-Lloyd, and J. Rudolph (2005a), A comparative study of ozone production in five U.S. metropolitan areas, *J. Geophys. Res.*, 110, D02301, doi: 10.1029/2004JD005096.
- Kleinman, L.I., 2005b. The dependence of tropospheric ozone production rate on ozone precursors. *Atmos. Environ.* 39, 575–586.
<https://doi.org/https://doi.org/10.1016/j.atmosenv.2004.08.047>
- Kleinman, L. I., Daum, P. H., Lee, Y. N., Nunnermacker, L. J., Springston, S. R., Weinstein-Lloyd, J., & Rudolph, J. (2002). Ozone production efficiency in an urban area. *Journal of Geophysical Research-Atmospheres*, 107(D23), 4733. <https://doi.org/Doi 10.1029/2002jd002529>
- Kleinman, L. I., Daum, P. H., Lee, Y. N., Nunnermacker, L. J., Springston, S. R., Weinstein-Lloyd, J., & Rudolph, J. (2001). Sensitivity of ozone production rate to ozone precursors. *Geophysical Research Letters*, 28(15), 2903–2906. <https://doi.org/10.1029/2000GL012597>
- Koren, V., Schaake, J., Mitchell, K., Duan, Q.-Y., Chen, F., & Baker, J. M. (1999). A parameterization of snowpack and frozen ground intended for NCEP weather and climate models. *Journal of Geophysical Research: Atmospheres*, 104(D16), 19569–19585. <https://doi.org/10.1029/1999JD900232>
- Krupa, S. V. (2003). Effects of atmospheric ammonia (NH₃) on terrestrial vegetation: A review. *Environmental Pollution*. [https://doi.org/10.1016/S0269-7491\(02\)00434-7](https://doi.org/10.1016/S0269-7491(02)00434-7)
- Laird, N. F., Kristovich, D. a. R., Rauber, R. M., Ochs, H. T., & Miller, L. J. (1995). The Cape Canaveral Sea and River Breezes: Kinematic Structure and Convective Initiation. *Monthly Weather Review*. [https://doi.org/10.1175/1520-0493\(1995\)123<2942:TCCSAR>2.0.CO;2](https://doi.org/10.1175/1520-0493(1995)123<2942:TCCSAR>2.0.CO;2)
- Lamsal, L. N., Duncan, B. N., Yoshida, Y., Krotkov, N. A., Pickering, K. E., Streets, D. G., & Lu, Z. (2015). U.S. NO₂ trends (2005-2013): EPA Air Quality System (AQS) data versus improved observations from the Ozone Monitoring Instrument (OMI). *Atmospheric Environment*, 110, 130–143. <https://doi.org/10.1016/j.atmosenv.2015.03.055>
- Landrigan, P. J., Fuller, R., Acosta, N. J. R., Adeyi, O., Arnold, R., Basu, N., ... Zhong, M. (2017). The Lancet Commission on pollution and health. *The Lancet*. [https://doi.org/10.1016/S0140-6736\(17\)32345-0](https://doi.org/10.1016/S0140-6736(17)32345-0)

- Langford, A. O., Senff, C. J., Banta, R. M., Hardesty, R. M., Alvarez, R. J., Sandberg, S. P., & Darby, L. S. (2009). Regional and local background ozone in Houston during Texas air quality study 2006. *Journal of Geophysical Research Atmospheres*, *114*(13). <https://doi.org/10.1029/2008JD011687>
- Langford, A. O., Tucker, S. C., Senff, C. J., Banta, R. M., Brewer, W. A., Alvarez, R. J., ... Williams, E. J. (2010). Convective venting and surface ozone in Houston during TexAQS 2006. *Journal of Geophysical Research Atmospheres*, *115*(16). <https://doi.org/10.1029/2009JD013301>
- Lei, W. (2004). Chemical characterization of ozone formation in the Houston-Galveston area: A chemical transport model study. *Journal of Geophysical Research*, *109*(D12), 1–15. <https://doi.org/10.1029/2003JD004219>
- Li, G., Zhang, R., Fan, J., & Tie, X. (2007). Impacts of biogenic emissions on photochemical ozone production in Houston, Texas. *Journal of Geophysical Research Atmospheres*, *112*(10). <https://doi.org/10.1029/2006JD007924>
- Li, Y., Pickering, K. E., Allen, D. J., Barth, M. C., Bela, M. M., Cummings, K. A., ... Biggerstaff, M. I. (2017). Evaluation of deep convective transport in storms from different convective regimes during the DC3 field campaign using WRF-Chem with lightning data assimilation. *Journal of Geophysical Research*, *122*(13), 7140–7163. <https://doi.org/10.1002/2017JD026461>
- Lim, J. O. J., Hong, S. Y., & Dudhia, J. (2004). The WRF-single-moment-microphysics scheme and its evaluation of the simulation of mesoscale convective systems. In *Bulletin of the American Meteorological Society* (pp. 2707–2710).
- Liu, X., Chance, K., Sioris, C. E., Spurr, R. J. D., Kurosu, T. P., Martin, R. V., & Newchurch, M. J. (2005). Ozone profile and tropospheric ozone retrievals from the Global Ozone Monitoring Experiment: Algorithm description and validation. *Journal of Geophysical Research D: Atmospheres*, *110*(20), 1–19. <https://doi.org/10.1029/2005JD006240>
- Loughner, C. P., Allen, D. J., Pickering, K. E., Zhang, D. L., Shou, Y. X., & Dickerson, R. R. (2011). Impact of fair-weather cumulus clouds and the Chesapeake Bay breeze on pollutant transport and transformation. *Atmospheric Environment*, *45*(24), 4060–4072. <https://doi.org/10.1016/j.atmosenv.2011.04.003>
- Loughner, C. P., Tzortziou, M., Follette-Cook, M., Pickering, K. E., Goldberg, D., Satam, C., ... Dickerson, R. R. (2014). Impact of bay-breeze circulations on surface air quality and boundary layer export. *Journal of Applied Meteorology and Climatology*, *53*(7), 1697–1713. <https://doi.org/10.1175/JAMC-D-13-0323.1>

- Mallet, V., & Sportisse, B. (2005). A comprehensive study of ozone sensitivity with respect to emissions over Europe with a chemistry-transport model. *Journal of Geophysical Research Atmospheres*, *110*(22), 1–15. <https://doi.org/10.1029/2005JD006234>
- Marchand, M. R., & Fuelberg, H. E. (2014). Assimilation of Lightning Data Using a Nudging Method Involving Low-Level Warming. *Monthly Weather Review*, *142*(12), 4850–4871. <https://doi.org/10.1175/MWR-D-14-00076.1>
- Martin, R. V. (2008). Satellite remote sensing of surface air quality. *Atmospheric Environment*. <https://doi.org/10.1016/j.atmosenv.2008.07.018>
- Martins, D. K., Stauffer, R. M., Thompson, A. M., Knepp, T. N., & Pippin, M. (2012). Surface ozone at a coastal suburban site in 2009 and 2010: Relationships to chemical and meteorological processes. *Journal of Geophysical Research Atmospheres*, *117*(5). <https://doi.org/10.1029/2011JD016828>
- Mazzuca, G. M., Pickering, K. E., Clark, R. D., Loughner, C. P., Fried, A., Stein Zweers, D. C., ... Dickerson, R. R. (2017). Use of tethered sonde and aircraft profiles to study the impact of mesoscale and microscale meteorology on air quality. *Atmospheric Environment*, *149*, 55–69. <https://doi.org/10.1016/j.atmosenv.2016.10.025>
- Mazzuca, G. M., Ren, X., Loughner, C. P., Estes, M., Crawford, J. H., Pickering, K. E., ... Dickerson, R. R. (2016). Ozone production and its sensitivity to NO_x and VOCs: Results from the DISCOVER-AQ field experiment, Houston 2013. *Atmospheric Chemistry and Physics*, *16*(22), 14463–14474. <https://doi.org/10.5194/acp-16-14463-2016>
- Mesinger, F., DiMego, G., Kalnay, E., Mitchell, K., Shafran, P. C., Ebisuzaki, W., ... Shi, W. (2006). North American regional reanalysis. *Bulletin of the American Meteorological Society*, *87*(3), 343–360. <https://doi.org/10.1175/BAMS-87-3-343>
- Miller, S. T. K. (2003). Sea breeze: Structure, forecasting, and impacts. *Reviews of Geophysics*, *41*(3), 1011. <https://doi.org/10.1029/2003RG000124>
- Molina, M. J., & Molina, L. T. (2004). Megacities and atmospheric pollution. *Journal of the Air and Waste Management Association*, *54*(6), 644–680. <https://doi.org/10.1080/10473289.2004.10470936>
- Neuman, J. A., Nowak, J. B., Zheng, W., Flocke, F., Ryerson, T. B., Trainer, M., ... Fehsenfeld, F. C. (2009). Relationship between photochemical ozone production and NO. *Journal of Geophysical Research*, *114*, 1–12. <https://doi.org/10.1029/2008JD011688>

- Ngan, F., & Byun, D. (2011). Classification of weather patterns and associated trajectories of high-ozone episodes in the Houston-Galveston-Brazoria area during the 2005/06 TexAQS-II. *Journal of Applied Meteorology and Climatology*, 50(3), 485–499. <https://doi.org/10.1175/2010JAMC2483.1>
- Weibring, P., Richter, D., Walega, J.G., A. F. (1993). First demonstration of a high performance difference frequency spectrometer on airborne platforms. *Applied Physics B Photophysics and Laser Chemistry*, 57(2), 131–139. <https://doi.org/10.1007/BF00425997>
- Pickering, K. E., Thompson, A. M., Scala, J. R., Tao, W.-K., Dickerson, R. R., & Simpson, J. (1992). Free tropospheric ozone production following entrainment of urban plumes into deep convection. *Journal of Geophysical Research: Atmospheres*, 97(D16), 17985–18000. <https://doi.org/10.1029/92JD01716>
- Rappenglück, B., Perna, R., Zhong, S., & Morris, G. A. (2008). An analysis of the vertical structure of the atmosphere and the upper-level meteorology and their impact on surface ozone levels in Houston, Texas. *Journal of Geophysical Research Atmospheres*, 113(17). <https://doi.org/10.1029/2007JD009745>
- Reddy, P. J., & Pfister, G. G. (2016). Meteorological factors contributing to the interannual variability of midsummer surface ozone in Colorado, Utah, and other western U.S. states. *Journal of Geophysical Research*, 121(5), 2434–2456. <https://doi.org/10.1002/2015JD023840>
- Ren, X., Van Duin, D., Cazorla, M., Chen, S., Mao, J., Zhang, L., Brune, W.H., Flynn, J.H., Grossberg, N., Lefer, B.L., Rappenglück, B., Wong, K.W., Tsai, C., Stutz, J., Dibb, J.E., Thomas Jobson, B., Luke, W.T., Kelley, P., 2013. Atmospheric oxidation chemistry and ozone production: Results from SHARP 2009 in Houston, Texas. *J. Geophys. Res. Atmos.* 118, 5770–5780. <https://doi.org/10.1002/jgrd.50342>
- Ring, A. M., Canty, T. P., Anderson, D. C., Vinciguerra, T. P., He, H., Goldberg, D. L., ... Salawitch, R. J. (2018). Evaluating commercial marine emissions and their role in air quality policy using observations and the CMAQ model. *Atmospheric Environment*, 173, 96–107. <https://doi.org/10.1016/j.atmosenv.2017.10.037>
- Seaman, N. L., & Michelson, S. A. (2000). Mesoscale Meteorological Structure of a High-Ozone Episode during the 1995 NARSTO-Northeast Study. *J. Appl. Meteorol.*, 39(3), 384–398. [https://doi.org/10.1175/1520-0450\(2000\)039<0384:MMSOAH>2.0.CO;2](https://doi.org/10.1175/1520-0450(2000)039<0384:MMSOAH>2.0.CO;2)
- Sillman, S. (1995). The use of NO_y, H₂O₂, and HNO₃ as indicators for ozone-NO_x - hydrocarbon sensitivity in urban locations. *Journal of Geophysical Research: Atmospheres*, 100(D7), 14175–14188. <https://doi.org/10.1029/94JD02953>

- Sillman, S., & Samson, P. J. (1995). Impact of temperature on oxidant photochemistry in urban, polluted rural and remote environments. *Journal of Geophysical Research*, *100*(D6), 11497. <https://doi.org/10.1029/94JD02146>
- Sillman, S., Vautard, R., Menut, L., & Kley, D. (2003). O₃-NO_x-VOC sensitivity and NO_x-VOC indicators in Paris: Results from models and Atmospheric Pollution Over the Paris Area (ESQUIF) measurements. *Journal of Geophysical Research*, *108*.
- Skamarock, W. C., & Klemp, J. B. (2008). A time-split nonhydrostatic atmospheric model for weather research and forecasting applications. *Journal of Computational Physics*, *227*(7), 3465–3485. <https://doi.org/10.1016/j.jcp.2007.01.037>
- Small, C., Nicholls, R.J., 2003. A global analysis of human settlement in coastal zones. *J. Coast. Res.* *19*, 584–599. <https://doi.org/10.2307/4299200>
- Stauffer, R. M., Thompson, A. M., Martins, D. K., Clark, R. D., Goldberg, D. L., Loughner, C. P., ... Tzortziou, M. A. (2015a). Bay breeze influence on surface ozone at Edgewood, MD during July 2011. *Journal of Atmospheric Chemistry*, *72*(3–4), 335–353. <https://doi.org/10.1007/s10874-012-9241-6>
- Stauffer, R. M., & Thompson, A. M. (2015b). Bay breeze climatology at two sites along the Chesapeake bay from 1986-2010: Implications for surface ozone. *Journal of Atmospheric Chemistry*, *72*(3–4), 355–372. <https://doi.org/10.1007/s10874-013-9260-y>
- Stein, A.F., Draxler, R.R., Rolph, G.D., Stunder, B.J.B., Cohen, M.D., Ngan, F., 2015. NOAA's HYSPLIT Atmospheric Transport and Dispersion Modeling System. *Bull. Am. Meteorol. Soc.* *96*, 2059–2077. <https://doi.org/10.1175/BAMS-D-14-00110.1>
- Sullivan, J. T., McGee, T. J., Langford, A. O., Alvarez, R. J., Senff, C. J., Reddy, P. J., ... Hoff, R. M. (2016). Quantifying the contribution of thermally driven recirculation to a high-ozone event along the Colorado Front Range using lidar. *Journal of Geophysical Research*, *121*(17), 10377–10390. <https://doi.org/10.1002/2016JD025229>
- Sullivan, T. J., Driscoll, C. T., Beier, C. M., Burtraw, D., Fernandez, I. J., Galloway, J. N., ... Watmough, S. A. (2018). Air pollution success stories in the United States: The value of long-term observations. *Environmental Science & Policy*, *84*, 69–73. <https://doi.org/10.1016/j.envsci.2018.02.016>
- Tang, X., Wang, Z., Zhu, J., Gbaguidi, A. E., Wu, Q., Li, J., & Zhu, T. (2010). Sensitivity of ozone to precursor emissions in urban Beijing with a Monte Carlo

scheme. *Atmospheric Environment*, 44(31), 3833–3842.
<https://doi.org/10.1016/j.atmosenv.2010.06.026>

Tewari, M., Chen, F., Wang, W., Dudhia, J., LeMone, M. A., Mitchell, K., ... Cuenca, R. H. (2004). Implementation and verification of the unified noah land surface model in the WRF model. In *Bulletin of the American Meteorological Society* (pp. 2165–2170). <https://doi.org/10.1007/s11269-013-0452-7>

Thielmann, A., Prévôt, A. S. H., & Staehelin, J. (2002). Sensitivity of ozone production derived from field measurements in the Italian Po basin. *Journal of Geophysical Research Atmospheres*, 107(22).
<https://doi.org/10.1029/2000JD000119>

Thompson, A.M., Pickering, K.E., Dickerson, R.R., Ellis, W.G., Jacob, D.J., Scala, J.R., Tao, W.-K., McNamara, D.P., Simpson, J. (1994). Convective transport over the central United States and its role in regional CO and ozone budgets. *Journal of Geophysical Research*, 99, pp. 18703-18711

Trainer, M., Parrish, D. D., Buhr, M. P., Norton, R. B., Fehsenfeld, F. C., Anlauf, K. G., ... Roychowdhury, U. K. (1993). Correlation of ozone with NO_y in photochemically aged air. *Journal of Geophysical Research: Atmospheres*, 98(D2), 2917–2925. <https://doi.org/10.1029/92JD01910>

Trainer, M., Parrish, D. D., Goldan, P. D., Roberts, J., & Fehsenfeld, F. C. (2000). Review of observation-based analysis of the regional factors influencing ozone concentrations. *Atmospheric Environment*. [https://doi.org/10.1016/S1352-2310\(99\)00459-8](https://doi.org/10.1016/S1352-2310(99)00459-8)

Vu, K. T., Dingle, J. H., Bahreini, R., Reddy, P. J., Apel, E. C., Campos, T. L., ... Flocke, F. (2016). Impacts of the Denver Cyclone on regional air quality and aerosol formation in the Colorado Front Range during FRAPPE 2014. *Atmospheric Chemistry and Physics*, 16(18), 12039–12058.
<https://doi.org/10.5194/acp-16-12039-2016>

Wallace, J. M., & Hobbs, P. V. (2006). *Atmospheric Science. Atmospheric Science*.
<https://doi.org/10.1016/B978-0-12-732951-2.50007-7>

Wentworth, G. R., Murphy, J. G., & Sills, D. M. L. (2015). Impact of lake breezes on ozone and nitrogen oxides in the Greater Toronto Area. *Atmospheric Environment*, 109, 52–60. <https://doi.org/10.1016/j.atmosenv.2015.03.002>

Yarwood, G. (2005). Updates to the Carbon Bond Chemical Mechanism: CB05. *Technical Report*, 1–246. <https://doi.org/10.1021/cr500486u>

Zaveri, R. A., Berkowitz, C. M., Kleinman, L. I., Springston, S. R., Doskey, P. V., Lonneman, W. A., & Spicer, C. W. (2003). Ozone production efficiency and

NO_x depletion in an urban plume: Interpretation of field observations and implications for evaluating O₃-NO_x-VOC sensitivity. *Journal of Geophysical Research: Atmospheres*, 108(D14), 4436. <https://doi.org/10.1029/2002JD003144>

Zhong, S., Leone, J. M., & Takle, E. S. (1991). Interaction of the sea breeze with a river breeze in an area of complex coastal heating. *Boundary-Layer Meteorology*, 56(1–2), 101–139. <https://doi.org/10.1007/BF00119964>